FABRICATION OF FUNCTIONAL SURFACES: PORPHYRIN-POLYOXOMETALATE FILMS AND POLYMER NANOLITHOGRAPHY

by

GIORGIO BAZZAN

A dissertation submitted to the Graduate Faculty in Chemistry in partial fulfillment

of the requirements for the degree of Doctor of Philosophy,

The City University of New York

2008

This manuscript has been read and accepted for the
Graduate Faculty in Chemistry in satisfaction of the dissertation
requirement for the degree of Doctor of Philosophy.

Dr. Charles Michael Drain

_____ _____

Date Chair of Examining Committee

Dr. Gerald Koeppl

_____ _____

Date Executive Officer

Dr. Alexander Couzis

Dr. Lynn C. Francesconi

Dr. Hiroshi Matsui

Supervisory Committee

THE CITY UNIVERSITY OF NEW YORK

Abstract

Fabrication of Functional Surfaces:

Porphyrin-Polyoxometalates Films and Polymer Nanolithography

by

Giorgio Bazzan

Adviser: Professor Charles Michael Drain

Many applications in catalysis, electrochemistry, electro-optics and sensors, require the preparation of ultra thin films or the formation of arrays of nanostructured features on surfaces. Strategies to create thin films using layer-by-layer methods use oppositely charged polymeric polyelectrolytes for both or at least one component to beneficially exploit multitopic electrostatic interactions between the deposited layers with opposite charges. In contrast, the electrostatic deposition of tetracationic 5,10,15,20-tetrakis(1-methyl-4-pyridinio)- porphyrin tetra(p-toluenesulfonate) ($TMPyP^{4+}$) with tetraanionic polyoxometalates such as $EuPW_{11}O_{39}^{4-}$ or $SiW_{12}O_{40}^{4-}$ onto charged substrates, such as mica, or polar substrates, such as glass and indium-tin oxide (ITO), demonstrates that the use of polymeric components is not *a priori* necessary. The use of molecules in sequential dipping approaches requires a careful balance in the interaction energies between the oppositely charged molecules, as demonstrated by the observation that a tetraanionic porphyrin such as 5,10,15,20-tetrakis(4-sulfonatophenyl)porphyrin does not form layers with $TMPyP^{4+}$. In the present case, these systems require several

rounds of dipping to obtain films of uniform coverage and durability. The thin films deposited onto glass, quartz, ITO, and mica have been characterized by UV-vis, fluorescence, cyclic voltammetry, and AFM microscopy. They are surprisingly robust, since they are not removed by sonication in either organic solvents or 100 mM NaCl.

A new technique to fabricate nano to micro scaled patterns of polymeric materials using a stamping method developed in our lab enables direct fabrication of architectures without employing advanced lithographic tooling or “wet” chemistry for pattern development. The polymer thermal-contact nanotransfer lithography produces nanometer thick polymer patterns on ceramic substrate using commercially available CD-R as stamps. The formation of patterns of functional photonic materials is accomplished by incorporating selected porphyrinoids into commodity polymers and using it in our polymer imprinting lithography technique to create patterns of the doped polymer.

Acknowledgments

The encouragement and support of many people have contributed to this dissertation.

First and foremost, I would like to extend thanks and appreciation to my mentor, Dr. Charles Michael Drain for his guidance, support, and for giving me the opportunity to work in a very stimulating multi-disciplinary project, which broadened my knowledge of chemistry and helped me mature as a scientist.

I owe special thanks to my doctoral committee: Drs. Alexander Couzis, Lynn Francesconi, and Hiroshi Matsui for their time and input over the years. I would like to give a special thanks to Dr. Francesconi for providing me with the polyoxometalates.

I would also like to express my gratitude to my dear colleagues and friends, Dr. Diana Samaroo and Dr. Gabriela Smeureanu, who both helped me a lot during these past few years. My warmest thanks to Ivana Radivojevic, Sebastian Thompson, Alessandro Varotto and Jacopo Samson whose friendship made my years at Hunter College particularly enjoyable.

I would also like to thank my family, especially my parents, Anna and Aldo, whose hard work, determination, and encouragement have been central in getting me to this point.

Lastly, I am especially grateful to my wife Kristine, who has been very supportive and helped me achieve this goal. You are my greatest reason to succeed.

Dedicated to my beloved wife Kristine

and to my parents Aldo and Anna

Dedicata alla mia amata moglie Kristine

e ai miei cari genitori Aldo e Anna

Table of Contents

List of Tables

List of Figures

List of Abbreviations

AFM ..... Atomic force microscopy

CD ..... Compact disc

CME ..... Chemically modified electrode

CV ..... Cyclic voltammetry

DVD ..... Digital video disc

ITO ..... Indium-tin oxide

LB ..... Langmuir-Blodgett

NIL ..... Nano imprinting lithography

NLO ..... Non linear optics

NMR ..... Nuclear magnetic resonance

OLED ..... Organic light-emitting diode

PDMS ..... Polydimethylsiloxane

POM ..... Polyoxometalate

Por ..... Porphyrin

SEM ..... Scanning electron microscopy

TCPP ..... 5,10,15,20-tetrakis-(4-carboxyphenyl)-porphyrin

TFT ..... Thin film transistor

$TMPyP^{4+}$ ..... 5,10,15,20-tetrakis(1-methyl-4-pyridinio)-porphyrin

$TPPS^{4-}$ ..... 5,10,15,20-tetrakis(4-sulfonatophenyl)-porphyrin

T_g ..... Glass transition temperature

μCP ..... Micro contact printing

Chapter 1

OVERVIEW ON SELF-ASSEMBLY AND SELF-ORGANIZATION

1.1 Introduction

The advantages and disadvantages of self-assembled/organized, supramolecular systems* as components of materials and/or devices are well delineated.[1-12] The synthesis of the molecular components is oftentimes straightforward with good yields, and the formation of complex, multicomponent systems by self-assembly can also proceed in remarkably high yields. The disadvantages of self-assembled systems largely stem from the complex equilibria inherent to supramolecular entities that make both characterization and material/device stability keystone issues in real-world applications. However, the principles and strategies for the *de novo* design of multicomponent supramolecular systems that self-assemble into solid-state materials such as crystals, or self-organize into predictably sized aggregates such as nanoparticles, are far less understood. Furthermore, the complex interactions of these materials with support/substrate surfaces have just recently become a topic of interest.

For self-assembled materials in devices one may consider four levels of structural organization.[13] (1) The primary structure is that of the molecular components, for which we have exquisite control. (2) The secondary structure is that of the supramolecule, and

* Though there is leeway, for the purposes of this thesis the following definitions are used. Nanoscaled = < 200 nm; self-assembly = the formation of a discrete supramolecular entity wherein there is no tolerance for error since a different supramolecular system results from errors; self-organization = the formation of a non-discrete supramolecular system, such as a multimer or a monolayer, wherein there is a threshold below which errors are non-critical.

while there remains much to be discovered, supramolecular synthesis is a mature field. (3) The tertiary structure pertains to how the supramolecular systems self-assemble or self-organize into solid-state materials, and predicting the tertiary structure of both molecular and supramolecular systems remains a major challenge, but some progress has been made in the last few years especially in terms of what is often called crystal engineering. (4) The quaternary structure describes how solid-state supramolecular systems self-assemble and/or self-organize onto surfaces as components of materials and devices – and may include the interconnections between the macroscopic and nanoscaled realms. This last level of structural order is important because the complex interactions between supporting substrate surfaces and the molecules, supramolecules, and supramolecular materials can significantly alter the structure, therefore the function. The nature of the electronic interactions between surfaces and molecules (adsorbed or covalently attached) is of major importance and the subject of much theoretical and experimental study. From another standpoint, the surface can be considered an additional design parameter to exploit in the design, assembly/organization and function of these materials.[14-17]

The porphyrinoids [porphyrins (Por), phthalocyanines (Pc), porphyrazines (Pz), and corroles (Cor)] are exemplary molecules to construct supramolecular photonic materials because of their remarkable stability in view of their diverse photophysical and chemical properties.[14-22] The photonic properties such as: excited state lifetimes, redox potentials, catalytic activities, magnetism, optical cross sections, etc. can be systematically varied both by the metalation with nearly every metal in the periodic table, and by the substituents on the macrocycle. The structural or architectural organization of

the chromophores in a material, as well as other environmental factors such as solvent or matrix, has a profound influence on the functionality of photonic materials. The importance of both the supramolecular structure and the matrix are notably typified by the photosynthetic reaction centers and antenna complexes, wherein the former serves as a conduit for electrons and the latter a conduit of energy. Though these are self-assembled and self-organized systems, as there are no covalent bonds between chromophores and there is evidence that some antenna complexes do not need a protein scaffold, both can have quantum yields near unity. It has been demonstrated that materials composed of porphyrinoids can be very robust to real-world conditions[3-5] such as elevated temperatures, and the presence of dioxygen and/or water, and that they are quite versatile tectons that afford rich variations in supramolecular topologies.

The number of reports on the self-organization and self-assembly of porphyrinoids has grown nearly exponentially[15] since the late 1980s, with the report of the formation of a photogated transistor that functioned via an ion-chain composed of transiently formed porphyrin cations self-organized by electrostatic interactions with hydrophobic anions.[12] Numerous supramolecular systems[20-30] using electrostatics,[11,12] hydrogen bonding,[20-22] metal ion coordination,[20-29] and reversible covalent bonds such as disulfides have been reported and the subject has been well reviewed.[14,15,23,24] The formation of 3-dimensional crystal lattices of porphyrins by designed supramolecular chemistry has also been reviewed.[23,24] The reason for this wide interest in the supramolecular chemistry porphyrins and their analogues arise from the aforementioned photonic properties, the robustness of the chromophores, and the supramolecular design flexibility. Potential applications include catalysts, sensors, molecular electronics,

molecular sieves, and solar energy conversion – all of which have been demonstrated to various degrees – that have superior properties or new functions compared to the individual, non-supramolecular components.[28,31-41]

1.2 Self-Assembled Porphyrin Arrays

The self-assembly of porphyrins using specific intermolecular interactions[2] has been reviewed.[14,15,23,24] Hydrogen-bonding provides a variety of recognition motifs and is reversible, thus potentially affording good yields of supramolecular arrays, but simple recognition motifs with 3-4 H-bonds are unlikely to be suitable for deposition of discrete arrays on surfaces because the intermolecular interactions are too weak to maintain the nanoarchitecture as solvent evaporates. Coordination chemistry has the advantages of more robust but reversible bonds, and the metal ion linkers can dictate a variety of geometries and provide further functionality. Therefore, self-assembly via coordination chemistry is widely studied in terms of photonic materials. There are well over 30 possible different geometric topologies that metalloporphyrins can afford,[15] and combined with the various topologies of the transition metals, the possible porphyrinic arrays are limited only by imagination. Secondly, hard-soft metal-ligand interactions can be exploited to accomplish multistep assembly of more complex supramolecular systems held together by different metal ions.[15] Note that in designing photonic materials, the heavy atom effect must be considered.

1.3 Self-Organized Porphyrinic Materials

Secondary, non-specific intermolecular interactions[2] such as pi-stacking, van der Waals, and electrostatic interactions of all kinds can be used to self-organize the supramolecular porphyrin arrays in the solid state.[42-44] These secondary interactions tend to be non-specific and non-directional, so tend to result in self-organized aggregates such as porphyrin nanoparticles, columnar stacks, nanocrystals, and films. Therefore, in order to investigate the commingled roles of supramolecular structure, dynamics, and stability as well as the effects of peripheral substitution on the surface organization of supramolecular arrays, dodecyloxy groups have been appended onto the peripheral phenyl groups of the tetrameric array (Figure 1.1).

1.4 Organization of Self-Assembled Arrays on Surfaces

One recent example illustrates the manifold factors that influence supramolecular materials morphology, and present a proof-of-concept example on the quaternary organization of these materials on surfaces. The orientation of porphyrins on surfaces is determined by factors such as the nature of the peripheral substituents, R, and their position on the macrocycle. For example, small substituents on the 4-position of tetraaryl porphyrins favor π-stacking, whereas those on 2 or 3 positions inhibit significant π-stacking and generally weaken surface-porphyrin interactions.[17,29]

The role of peripheral groups in the self-organization of self-assembled multiporphyrinic arrays on surfaces was examined for Pt(II)-linked trapezoidal tetrameric porphyrin arrays with peripheral *tert*-butylphenyl or dodecyloxyphenyl functionalities.[16]

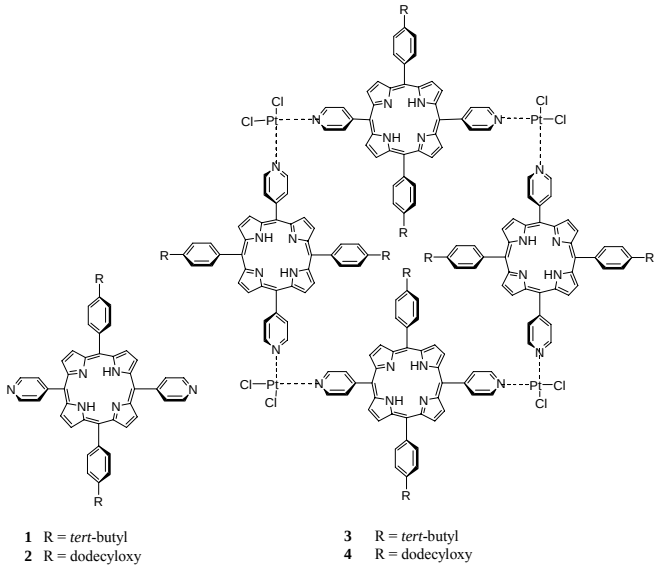

Figure 1.1 Porphyrin building blocks and self-assembled array **3, 4** (Adapted from Ref.16).

AFM investigations reveal that the supramolecular architecture of the Pt(II) assembled trapezoids remain intact when cast on glass and that the orientation and length of peripheral alkyl substituents influence the resulting structures on surfaces. The *tert*-butylphenyl substituted porphyrin arrays form small aggregates which organize in a vertical direction via π-stacking interactions among the macrocycles. In contrast, tetrameric porphyrin arrays with dodecyloxyphenyl groups form a continuous film via van der Waals interactions between the peripheral hydrocarbon chains. By appending peripheral dodecyloxyphenyl groups to porphyrin building blocks, the strategies were both to minimize conformational flexibility compared to simple self-assembled dimers[20-25] and to increase inter-array interactions via the self-organizing properties of long chain hydrocarbons to yield organized films on surfaces.

^{1}H NMR data suggest that there is some flexibility in the supramolecular structure of the trapezoidal tetramers and steric energy minimization calculations (MM2) indicate arrangements schematically depicted in Figure 1.2.

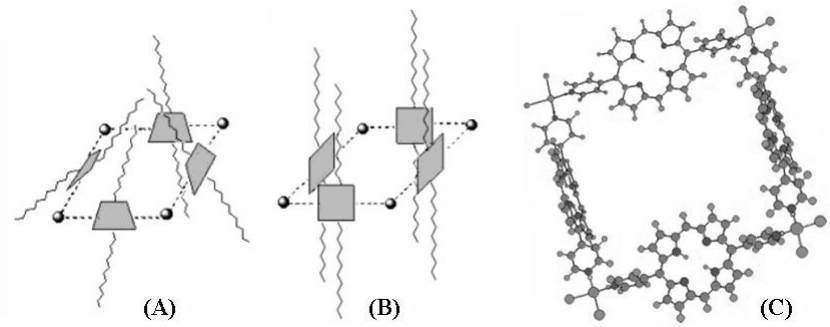

Figure 1.2 Models of possible arrangements of the porphyrins in tetramer **4** (Adapted from Ref. 16).

Using this model, the distance from side to side (porphyrin face to porphyrin face) of the tetramer is approximately 1.8 nm, and the diagonal distance between opposite platinum atoms is approximately 2.6 nm. A similar structure was proposed for tetramers of porphyrin with Re(II) corners.[27,28] The square pyramidal arrangement shown in Figure 1.2A has four identical porphyrins with pyridyl, pyrrole and phenyl protons facing into or away from the center of the structure.

1.5 Surface Organization of Tetrameric Porphyrin Arrays

When samples were prepared by solvent evaporation via drop deposition, a variety of surface morphologies are observed that are largely a consequence of the

concentration of the solution. Representative surface structures of **3** and **4** assayed by AFM are shown in Figures 1.3 and 1.4. Array **3** forms discrete nanoclusters or porphyrin stacks of various heights on glass surfaces. The aggregates are organized randomly across the surface, and it is clear that the porphyrin stacks do not merge and are separated by distances of at least 50 nm. These are observed over a supramolecular concentration range from 1 to ~50 μM. Cursor measurements indicate that the columnar stacks have variable heights, ranging from 1.5 to 18 nm. Thus, for the surface organization of the tert-butylphenyl tetramer **3**, the π-π stacking interactions in solution direct the assembly into columnar structures. With surface deposition, the porphyrin planes maximize the interactions with the substrate.

In contrast, the dodecyloxyphenyl functionalized porphyrin supramolecule **4** forms films of different morphologies on glass depending on the concentration of the deposition solution. At low <10 μM concentrations, this array forms small islands of variable horizontal dimensions (50 – 700 nm) and heights that range between 5 and 20 nm. At higher concentrations, ~100 μM, array **4** forms continuous 10 nm thick films (Figure 1.3), and intermediate concentrations form films with large circular defects. At still greater concentrations, ~200 μM, nanocrystalline domains are observed.[16]

The tetramers are packed closely in random arrangements, touching neighboring clusters to form a densely aggregated structure. Within the films, the individual supramolecular clusters are nearly spherical with a uniform geometry and size (Figure 1.3). Nanoshaving was used to measure the thickness of the film (Figure 1.3B and 1.3C).[30] These results indicate that the dispersion interactions among the peripheral long alkyl chains on tetramer **4** affect both the supramolecular structure and the self-

organization of the supermolecule on surfaces. The dodecyloxy groups significantly enhance the horizontal intermolecular interactions during surface deposition, and columnar stacks are not observed in solution or on surfaces.

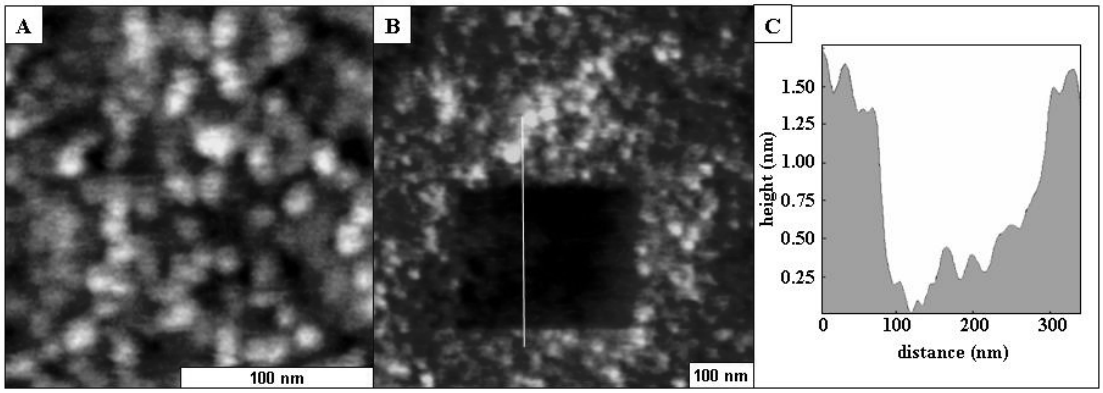

Figure 1.3 AFM image of the continuous film formed from supramolecular porphyrin array **4** with dodecyloxyphenyl substituents on glass. (A) Close-up view in ethanol; (B) hole fabricated in the same porphyrin film; and (C) representative line profile for the nanopattern (Adapted from Ref. 16).

The proposed intermolecular interactions in which the sides of the porphyrin trapezoids assemble in a side-on arrangement on the surface are represented schematically in Figure 1.4. This ensures the maximal interaction between the hydrocarbon chains in and between arrays of **4**, minimizes interactions with the hydrophilic surface, and allows one porphyrin face and two $PtCl_2$ units to interact with the surface. We find that the organization of these arrays depends on the surface energetics, *vide infra*.

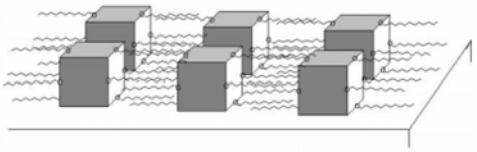

Figure 1.4 Surface organization of **4** due to horizontal interactions between supramolecular arrays (Adapted from Ref. 16).

1.6 Quaternary Organization: Patterning Porphyrin Arrays on Surfaces

The ability to incorporate self-assembled materials into devices requires that the materials be organized on surfaces in predefined patterns. There are a variety of means to accomplish this task including both bottom-up and top-down strategies. Using widely available PDMS stamps is a way to pattern the arrays of **4** on surfaces rapidly and reproducibly. The dodecyloxy groups make array **4** highly soluble compared to most porphyrins and porphyrinic arrays, and this can be exploited as part of the quaternary organization of the materials (Figure 1.5). Though the films are not yet perfect, double deposition and/or annealing the system may provide the route to patterns of high quality thin films of these arrays.

The peripheral R groups dictate not only solubility of the multiporphyrin array but also play crucial role in the self-organization of the tetramers on surfaces and influence the surface binding energetics. Therefore, for surface patterning of porphyrin assemblies, we focused on the deposition and properties of tetramer **4**. To prepare patterned

microstructures of the porphyrin arrays, a clean PDMS stamp was placed onto a Au substrate. Next, a drop (5 μL) of porphyrin solution (2.4 x 10^{-6} M of the Pt(II)-linked dodecyloxy array in toluene) was introduced at the end of the channels, and guided to selected areas of the substrate by capillary action, (Figure 1.5) as previously described for protein solutions using microfluidic networks.[45] After drying, the PDMS stamp was removed, and the samples were imaged in air (Figures 1.5B and 1.5C).[46]

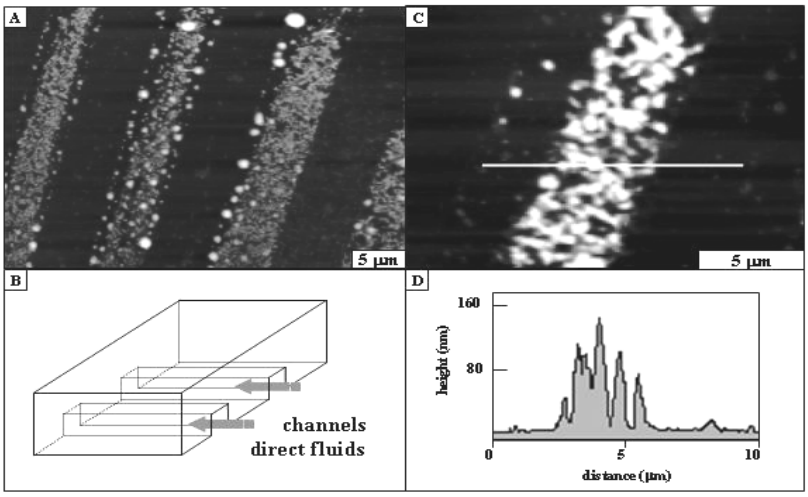

Figure 1.5 Microprinting of dodecyloxy array **4** on Au. (A) Channels of nanoparticles were prepared by placing a PDMS stamp against the surface. Solutions are pulled into the channels via capillary action. (B) AFM topograph of 5 μm lines of porphyrin spaced 5 μm apart. (C) Zoom-in view of a single channel; (D) cursor for line trace in B. From Ref. 46.

The heights of the microstructures ranged from 40 to 160 nm along the lengths of the microstructures, depending on the shape of the channels and the uniformity of deposition (Figure 1.5D). This lithographic approach is a rapid and practical means to chemically pattern substrates for microscopy characterizations.

Organizing porphyrin materials on surfaces provides a means of generating potential device structures and for controlling the dimensions and density of materials by confinement in narrow (microns) channels of PDMS. Pt(II)-linked dodecyloxy material have been patterned on Au and glass surfaces using microfluidic channels formed with polydimethyl siloxane (PDMS). Using this approach, patterned arrays can be formed over large areas which conform to the dimensions of the PDMS mold. Figure 5B demonstrates the patterning of the Pt(II)-linked dodecyloxy material over large areas of a Au surface. In this example, the microchannels were 5 μm wide. The flow of the solution through the channels is found to be semi-continuous with patterns extending beyond 50 microns. This suggests that at higher concentrations, the lateral interactions of the side chains as well as significant π stacking can promote organization into larger structures, potentially with liquid crystalline behavior.[18,19,25] Other stamping methods will likely yield similar results.[47]

1.7 Summary

The hierarchical structural organization of porphyrins – from molecules to supramolecules to nanoscaled aggregates to patterns on surfaces – has been studied. The physical chemical properties and the architecture of the supramolecular array are important design criteria for the deposition of these materials on surfaces; however,

supramolecular dynamics and/or conformation flexibility are also factors that determine the final structure and morphology on surfaces. Just as importantly, the surface properties can be exploited as a means to control both tertiary and quaternary structure. The formation of hierarchical structures using both specific and nonspecific interactions may or may not be cooperative, but imparts a high degree of stability and control of size not found in most supramolecular systems.[29] The ability to synthesize many porphyrins in good yields[48,49] and the variety of functions of porphyrinic systems on surfaces warrants further investigations into applications as nanoscaled photonic materials.

Nanostructures formed on surfaces

For many supramolecular systems self-assembly and self-organization take place in solution, and if the nanostructure is robust it can be subsequently deposited onto surfaces. In contrast, there is a growing literature on the use of surface energetics and the dynamics of solvent evaporation to form 10–500 nm structures. From one perspective, these latter studies explore the nanoscaled supramolecular materials chemistry of what the paint and coatings industry has known to be important for many decades—that the rate of solvent evaporation, the intermolecular forces between the dyes/pigments/solvents/additives, and the nature of the surface dictate the morphology of the solid materials and the quality of the film. One examples is the layer-by-layer deposition of electrolytes. In the layer-by-layer method, a substrate with a net charge (electronically or by an adsorbed or covalently attached species) is dipped into a solution containing an oppositely charged species. The system is dipped into alternate solutions of cationic and anionic species to form nominally multilayered structures or aggregates of

controllable size. Polyelectrolytes form films that are remarkably stable. This latter method is akin to the electrostatic coating of conductive materials wherein the substrate is charged and a solution containing oppositely charged ions is sprayed on (there are other variations of this process, e.g., the use of a charged nozzle). The layer-by-layer method has been used to create nanometer-scaled films of porphyrins through several strategies.

1.8 Chapter 1 References

(1) Ball, P. *Nature* **2001**, *409*, 413-416.

(2) Alivisatos, A. P.; Barbara, P. F.; Castleman, A. W.; Chang, J.; Dixon, D. A.; Klein, M. L.; McLendon, G. L.; Miller, J. S.; Ratner, M. A.; Rossky, P. J.; Stupp, S. I.; Thompson, M. E. *Adv. Mater.* **1998**, *10*, 1297-1336.

(3) Fox, M. A. *Acc. Chem. Res.* **1999**, *32*, 201-207.

(4) Aviram, A.; Ratner, M. *Ann. N.Y. Acad. Sci.* **1998**, *852*, 1-21.

(5) Reed, M. A. *MRS Bull.* **2001**, *26*, 113-120.

(6) Lehn, J.-M. *Angew. Chem.* **1990**, *102*, 1347-1362.

(7) Lehn, J.-M. *Angew. Chem. Int. Ed.* **1990**, *29*, 1304-1319.

(8) Lindsey, J. S. *New J. Chem.* **1991**, *15*, 153-180.

(9) Stang, P. J.; Olenyuk, B. *Acc. Chem. Res.* **1997**, *30*, 502-518.

(10) Krische, M. J.; Lehn, J.-M.; Melendez, R. E.; Carr, A. J.; Linton, B. R.; Hamilton, A. D.; Zimmerman, S. C.; Corbin, P. S.; Kato, T.; Fujita, M. *Molecular Self-Assembly Organic versus Inorganic Approaches*; Springer-Verlag Berlin Heidelberg, 2000; Vol. 96.

(11) Drain, C. M.; Mauzerall, D. *Bioelectrochem. Bioenerg.* **1990**, *24*, 263-266.

(12) Drain, C. M.; Christensen, B.; Mauzerall, D. C. *Proc. Natl. Acad. Sci., USA* **1989**, *86*, 6959-6962.

(13) Drain, C. M. *Proc. Natl. Acad. Sci., USA* **2002**, *99*, 5178-5182.

(14) Drain, C. M.; Smeureanu, G.; Batteas, J.; Patel, S. In *Encyclopedia of Nanoscience and Nanotechnology*; Schwartz, J. A., Contescu, C. I., Putyera, K., Eds.; Marcel Dekker, Inc.: New York, 2004; Vol. 5, p 3481-3502.

(15) Drain, C. M.; Chen., X. In *Encyclopedia of Nanoscience & Nanotechnology*; Nalwa, H. S., Ed.; American Scientific Press: New York, 2004; Vol. 9, p 593-616.

(16) Milic, T.; Garno, J. C.; Smeureanu, G.; Batteas, J. D.; C. M. Drain *Langmuir* **2004**, *20*, 3974-3983.

(17) Milic, T. N.; Chi, N.; Yablon, D. G.; Flynn, G. W.; Batteas, J. D.; Drain, C. M. *Angew. Chem., Int. Ed.* **2002**, *41*, 2117-2119.

(18) Bruce, D. W.; Wali, M. A.; Wang, Q. M. *Chem. Commun.* **1994**, 2089-2090.

(19) Wang, Q. M.; Bruce, D. W. *Angew. Chem. Int. Ed. Engl.* **1997**, *36*, 150-152.

(20) Drain, C. M.; Lehn, J.-M. *Chem. Commun.* **1994**, 2313-2315 (correction 1995, p503).

(21) Drain, C. M.; Russel, K. C.; Lehn, J.-M. *Chem. Commun.* **1996**, 337-338.

(22) Drain, C. M.; Fischer, R.; Nolen, E.; Lehn, J. M. *Chem. Commun.* **1993**, 243-245.

(23) Drain, C. M.; Hupp, J. T.; Suslick, K. S.; Wasielewski, M. R.; Chen, X. *J. Porph. Phthal.* **2002**, *6*, 241-256.

(24) Shmilovits, M.; Diskin-Posner, Y.; Vinodu, M.; Goldberg, I. *Crystal Growth & Design* **2003**, *3*, 855-863.

(25) Latterini, L.; Blossey, R.; Hofkens, J.; Vanoppen, P.; De Schryver, F. C.; Rowan, A. E.; Nolte, R. J. M. *Langmuir* **1999**, *15*, 3582-3588.

(26) Drain, C. M.; Nifiatis, F.; Vasenko, A.; Batteas, J. D. *Angew. Chem. Int. Ed.* **1998**, *37*, 2344-2347.

(27) Slone, R. V.; Hupp, J. T. *Inorg. Chem.* **1997**, *36*, 5422-5423.

(28) Merlau, M. L.; Mejia, M. d. P.; Nguyen, S. T.; Hupp, J. T. *Angew. Chem. Int. Ed.* **2001**, *40*, 4239-4242.

(29) Drain, C. M.; Batteas, J. D.; Flynn, G. W.; Milic, T.; Chi, N.; Yablon, D. G.; Sommers, H. *Proc. Natl. Acad. Sci., USA* **2002**, *99*, 6498-6502.

(30) Liu, G.-Y.; Xu, S.; Qian, Y. *Acc. Chem. Res.* **2000**, *33*, 457-466.

(31) Gong, X.; Milic, T.; Xu, C.; Batteas, J. D.; Drain, C. M. *J. Am. Chem. Soc.* **2002**, *124*, 14290-14291.

(32) Fujita, M.; Kwon, Y. J.; Washizu, S.; Ogura, K. *J. Am. Chem. Soc.* **1994**, *116*, 1151-1152.

(33) Slone, R. V.; Hupp, J. T.; Stern, C. L.; Albrecht-Schmitt, T. E. *Inorg. Chem.* **1996**, *35*, 4096-4097.

(34) Linton, B.; Hamilton, A. D. *Chem. Rev.* **1997**, *97*, 1669-1680.

(35) Yuan, H.; Thomas, L.; Woo, L. K. *Inorg. Chem.* **1995**, *35*, 2808-2817.

(36) Stang, P. J.; Fan, J.; Olenyuk, B. *Chem. Commun.* **1997**, 1453-1454.

(37) Hunter, C. A.; Sanders, J. K. M. *J. Am. Chem. Soc.* **1990**, *112*, 5525-5534.

(38) Chou, J. H.; Nalwa, H. S.; Kosal, M. E.; Rakow, N. A.; Suslick, K. S. *Applications of Porphyrins and Metalloporphyrins to Materials Chemistry*; Academic Press: New York, 2000; Vol. 6.

(39) Chambron, J.-C.; Heitz, V.; Sauvage, J.-P. In *The Porphyrin Handbook*; Kadish, K. M., Smith, K. M., Guilard, R., Eds.; Academic Press: New York, 2000; Vol. 6, p 1-42.

(40) Dagani, R. In *C & E News* 1998; Vol. 76 p1-32.

(41) Qi, L.; Colfen, H.; Antonietti, M. *Nano Lett.* **2001**, *1*, 61-65.

(42) Maiti, N. C.; Mazumdar, S.; Periasamy, N. *J. Phys. Chem. B* **1998**, *102*, 1528-1538.

(43) Kano, K.; Minamizono, H.; Kitae, T.; Negi, S. *J. Phys. Chem. A* **1997**, *101*, 6118-6124.

(44) Purrello, R.; Monsu' Scolaro, L.; Bellacchio, E.; Gurrieri, S.; Romeo, A. *Inorg. Chem.* **1998**, *37*, 3647-3648.

(45) Delamarche, E.; Bernard, A.; Schmid, H.; Bietsch, A.; Michel, B.; Biebuyck, H. *J. Am. Chem. Soc.* **1998**, *120*, 500-508.

(46) Xu, C.; Bazzan, G.; Garno, J. C.; Batteas, J. D.; Drain, C. M. In *ACS Symp. Ser. 928*; Schubert, U. S., Newkome, G. R., Manners, I., Eds.; American Chemical Society: 2006, p 168-183.

(47) Helt, J. M.; Drain, C. M.; Batteas, J. D. *J. Am. Chem. Soc.* **2004**, *136*, 628-634.

(48) Lindsey, J. S. In *The Porphyrin Handbook*; Kadish, K. M., Smith, K. M., Guilard, R., Eds.; Academic Press: New York, 2000; Vol. 1, p 45-118.

(49) Drain, C. M.; Gong, X. *Chem. Commun.* **1997**, 2117-2118.

Chapter 2

ELECTROSTATIC SELF-ORGANIZATION OF ROBUST PORPHYRIN-POLYOXOMETALATE FILMS

2.1 Introduction

Fabrication of robust thin films by layer-by-layer methods is accomplished by sequentially exposing a substrate to solutions containing oppositely charged polyelectrolytes, and the topic is well-reviewed.[1,2] Polymeric polyelectrolytes are used to provide robust interactions between oppositely charged layers, wherein the detailed architecture of the self-organized material depends on the specific and nonspecific intermolecular interactions. These interactions are dominated by the electrostatics, but dispersion forces can play an important role as well. Oftentimes there is a significant degree of interdigitation of the oppositely charged polymers in the layers. The polyelectrolytes can be organic polymers, biopolymers, or inorganic materials. There are also some examples of materials made by layer-by-layer methods wherein one component is a small, charged molecule and the other is a charged polymer. There are a plethora of applications and potential applications of thin films fabricated by layer-by-layer methods, including photonics, coatings, and sensors.[3-6]

Porphyrins and metalloporphyrins are functional molecules that are used for a variety of applications and devices such as sensors, luminescent devices, catalysts, solar energy harvesting systems, photonic materials, and therapeutics.[7-10] These applications are affected by the diverse photophysical and electrochemical properties of the

porphyrins and the ability to fine-tune these properties via the choice of chelated metal ion and by the exocyclic substituents on the macrocycle. Some applications, such as nonlinear optical materials, require that the choromophores reside in precise self-assembled supramolecular architectures. Other applications, such as thin films for sensors and solar energy harvesting, require efficient, controlled self-organization on surfaces and may not require the same degree of order. The synthesis of complex asymmetric porphyrins bearing hydrogen-bonding motifs[11-14] or exocyclic ligands such as pyridyl groups[15,16] has yielded a variety of self-assembled arrays with defined geometries. Much has been learned about supramolecular chemistry and about the photophysical properties of self-assembled porphyrinic arrays, but the efficient commercially viable synthesis of these designer chromophores remains a keystone issue that is a strong disincentive for most commercial applications. This synthetic barrier necessitates the development of supramolecular strategies to self-organize porphyrinic materials based on easy-to-prepare symmetric macrocycles.[17-19] Self-assembly into specific supramolecular architectures requires shape and intermolecular chemical complementarities, whereas self-organization into less ordered materials can often be accomplished with nonspecific intermolecular interactions. The plane of the porphyrin macrocycle is ca. 1 nm (between hydrogens on opposing pyrroles), ca. 0.5 nm thick, and the distance between the para hydrogen atoms on opposing meso-phenyl groups is ca. 1.8 nm.

In many ways, polyoxometalates (POMs) are the inorganic equivalent of a porphyrin.[20,21] POMs are discrete metal oxide clusters that are ca. 1 nm in diameter and can have a variety of compositions, yet they are easy to prepare in large scales. Because POMs have a rich electrochemistry that can be modulated by the incorporation of a wide

variety of metal ions in specific defect sites, and can be photochemically active, they can serve as the active component of catalysts and sensors. There are several commercial applications of POMs, and they are widely used as discrete molecular models of defects in oxide surfaces.[21]

Since the diverse chemical and physical properties of porphyrins and POMs[22,23] are in many ways complementary rather than overlapping, it is somewhat surprising that there are only a few reports on the activity of materials containing both types of molecule. A composite organic/inorganic material formed by association of metalloporphyrins and POMs showed more efficient catalytic properties than the corresponding metalloporphyrins alone.[24] Crystal structures using specifically designed intermolecular interactions or wherein POMs are encapsulated into porphyrin framework solids were reported[25] To our knowledge, there are no studies detailing the supramolecular organization of thin films of porphyrin/POM composite materials.

The potential applications of layers of porphyrinoids have been established in a number of reports.[8] Multilayers of porphyrins have been assembled by coordination chemistry using exocyclic ligands on the macrocycle that are designed to interact with specific metal ions.[26-28] Thin films were prepared by Wrighton et al. using metalloporphyrins coordinated to four cationic Ru bipyridine moieties as one layer and a tetra anionic porphyrin bearing sulfate groups as the complementary component.[29] Constructs using phthalocyanines have also been reported.[30,31] Porphyrins have been combined with derivatives of C_{60}, inorganic nanoparticles, and polyphenylenevinylene to create photonic films.[32-34] Films of porphyrins have been made using polymers as complementary layers,[35] or cationic porphyrins have been placed between titania

nanosheets using LB methods to create photoactive materials.[36] The deposition of cationic porphyrins and anionic POMs on modified glassy carbon electrodes produces organic-inorganic hybrid films[37-39] that display electrocatalytic activity for the reduction of O_2 to peroxide or for hydrogen evolution from acidic water.[37] Films containing POMs and phthalocyanine show a third-order nonlinear optical response.[40] Most of these films are characterized by their chemical, electrochemical, or photophysical functions, but there is paucity of structural or organizational information because these are generally not highly ordered materials.

Herein we report the electrostatic formation of thin films by sequentially dipping a substrate into solutions of small, oppositely charged porphyrin and POM molecules. Tetracationic 5,10,15,20-tetrakis(1'-methyl-4'-pyridinio)porphyrin tetra(*p*-toluenesulfonate) ($TMPyP^{4+}$) and the zinc complex ($ZnTMPyP^{4+}$) with acetate counterions are electrostatically matched by the tetraanionic polyoxometalates of the potassium salt of $EuPW_{11}O_{39}^{4-}$ and $SiW_{12}O_{40}^{4-}$ with hydrogen counterions (Figure 2.1). Though there is a reasonably linear addition of material for each dipping cycle, each cycle does not form a complete layer, which is consistent with previous observations,[37-39] and this is likely true for other electrostatically assembled films made from small molecules. Thus, the term "layer-by-layer" for Por-POM films formed by sequential dipping into solutions of Por and POM is somewhat misleading. After a minimum number of dipping cycles, the films are remarkably robust, since they are removed neither by sonication in organic solvents nor by sonication in 100 mM NaCl. These films are fabricated using readily available compounds.

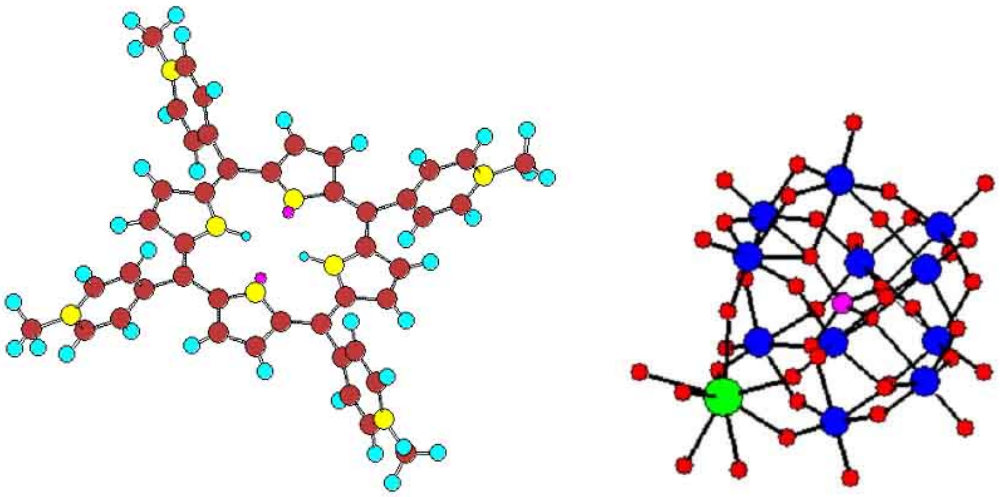

Figure 2.1 Left 5,10,15,20-tetrakis(1'-methyl-4'-pyridinio)porphyrin tetra(*p*-toluenesulfonate) ($TMPyP^{4+}$) (H = light blue, N = Yellow, C=brown), and right: polyoxometalate (POM) $EuPW_{11}O_{39}K_4$ (O = red, W = blue, Eu = green, P = pink) where the counter ios are left out for clarity.

2.2 Experimental Procedure

Materials. All reagents and solvents were of analytical grade and used without further purification. The water was passed through a Barnstead NANOPure water purification system and filtered using a Nalgene PTEF 0.2 μm filter. The 5,10,15,20-tetrakis(1'-methyl-4'-pyridinio)porphyrin tetra(*p*-toluenesulfonate) ($TMPyP^{4+}$), silicotungstic acid hydrate ($SiW_{12}O_{40}^{4-}$), and meso-tetraphenylporphyrin sulfonate ($TPPS^{4-}$) were purchased from Aldrich.

Zn(II)$TMPyP^{4+}$ was prepared as follows. 5,10,15,20-tetrapyridylporphyrin was refluxed with zinc acetate in dichloromethane/methanol (6:1)for 3 h. The resulting crystals were purified by a water/dichloromethane extraction, whereupon the dried

crystals were then dissolved in a dichloromethane/methanol mixture (50:1) with an excess of methyl iodide and left stirring at room temperature overnight. The recovered purple microcrystals are soluble in water and characterized by the UV-visible spectrum and mass spectrometry.[41]

$EuPW_{11}O_{39}^{4-}$ was prepared according to literature procedures.[42] The mica (muscovite form) was purchased from SPI supplies and freshly cleaved using Scotch tape before use. The indium-tin oxide (ITO) coated slides (70-100 ohm resistance) were purchased from Aldrich, glass slides were purchased from Fisher, and quartz slides were purchased from SPI supplies. The glass, ITO, and quartz substrates were cleaned in an ozone cleaner for 30 min, rinsed with copious amounts of NanoPure water, dried, and used within 0.5 h. The nanolithographic methods to place patterns of polymer insulated gold nanowires on mica were reported previously.[43]

Physical Measurements. A Varian Cary Bio-3 spectrophotometer was used for UV-visible spectroscopy, in double-beam mode. Steady-state fluorescence spectra were taken on a Fluorolog-3, with excitation at the maximum UV-visible absorbance (Soret band). Atomic force microscope (AFM) measurements were made with a Nanoscope III Multi-mode (Veeco Metrology, Sunnyvale, CA). Images were acquired in air using commercial silicon tips (MikroMasch USA, Portland, OR) in both contact mode (CSC21/AlBS lever A & B) and tapping mode (NSC15/AlBS) with a typical tip curvature radius of less than 10 nm. CSC21-A typical force constant 0.12 N/m, resonant frequency = 12 kHz; CSC21-B, force constant = 2.0 N/m, resonance frequency = 0.2 kHz; NSC15, force constant = 40N/m, resonance frequency = 325 kHz). The z scale was calibrated using commercial calibration grids (MikroMasch USA, Portland, OR).

Nanoshaving data were obtained with a minimum of three nanoshaving experiments per sample for a minimum of two samples.

Fabrication of Multilayer Films.

Films were prepared at room temperature by soaking the solid substrate (mica, glass, quartz, ITO) in a 0.5 mM aqueous solution of porphyrin for 1 min, followed by dipping the substrate three times in unbuffered NANOPure water to remove the excess, nonbound porphyrin solution from the substrate. Subsequently, a layer of polyoxometalates was added by soaking the substrate for 1 minute in a 0.5 mM aqueous solution of polyoxometalates and rinsed three times by dipping in NANOPure water (Figure 2.4). The procedure was repeated until the desired film thickness was obtained. The amount of the material deposited is affected by the drying procedure. After each rinsing, the samples were dried by keeping the substrate vertical and blowing a gentle stream of nitrogen gas at a ca. 45° angle to drive the drops of solution on the surface off the lower part of the substrate. The films on the glass side of the ITO substrate were physically removed by gently wiping with a cotton Q-tip moistened with H_2O, followed by a Q-tip moistened with ethanol. Material is deposited on both sides of the glass, quartz, and mica substrates, and since removal of the material from one side may be incomplete, the samples were used as made. Thus, the UV-visible spectral data (Figures A2.2, A2.4, A2.5 A2.6, A2.9, A2.11), the fluorescence (Figures 2.6, 2.7), and the photos (Figure 2.8) represents the material deposited on both sides of these substrates. To compare the amount of material on one side of these substrates to the ITO, the absorbance values for glass, quartz, and mica in Figure 2.5 are divided by two.

2.3 Results and Discussion

Solution Phase Interactions

Solution-phase experiments were done to garner information on the interactions between the two components, but the hierarchical organization of the molecular components in the films is likely quite different from the structures in the solution. UV-visible spectra of 10 μM solutions of $TMPyP^{4+}$ titrated with $EuPW_{11}O_{39}^{4-}$ or $SiW_{12}O_{40}^{4-}$ in water show well-resolved isosbestic points until 1 equivalent of the POM has been added to the aqueous solution (Figure 2.2). This indicates that the two molecules interact in water due to strong electrostatic interactions to form an ion pair that does not precipitate for several hours. The 422 nm Soret slightly blue shifts by 2 nm, and 518.5 nm Q band slightly red shifts by 3 nm as the POM is titrated into the porphyrin solution. However, when more than 1 equiv of the POM is added to the porphyrin solution, e.g., an excess of 0.2 equiv, there is a change in the electronic spectrum manifested by a deviation from the isosbestic points and the formation of a brown precipitate over ca. 1 hour. Under these conditions, the association constant for the 1:1 complex is about 10^4 L M^{-1}, but this can only be considered an estimate since further aggregation leading to precipitation is occurring. Solutions containing a 2:3 porphyrin:POM ratio have significantly different UV-visible spectra, indicating further aggregation prior to the rapid precipitation. The fluorescence intensity of the porphyrin decreases linearly, reaching ca. 70% of the initial value when 1 equivalent of the POM is added (Figure 2.3). The quenching can be due to electron or energy transfer to the POM species and/or due to the heavy atom effect and enhanced intersystem crossing to the triplet state.

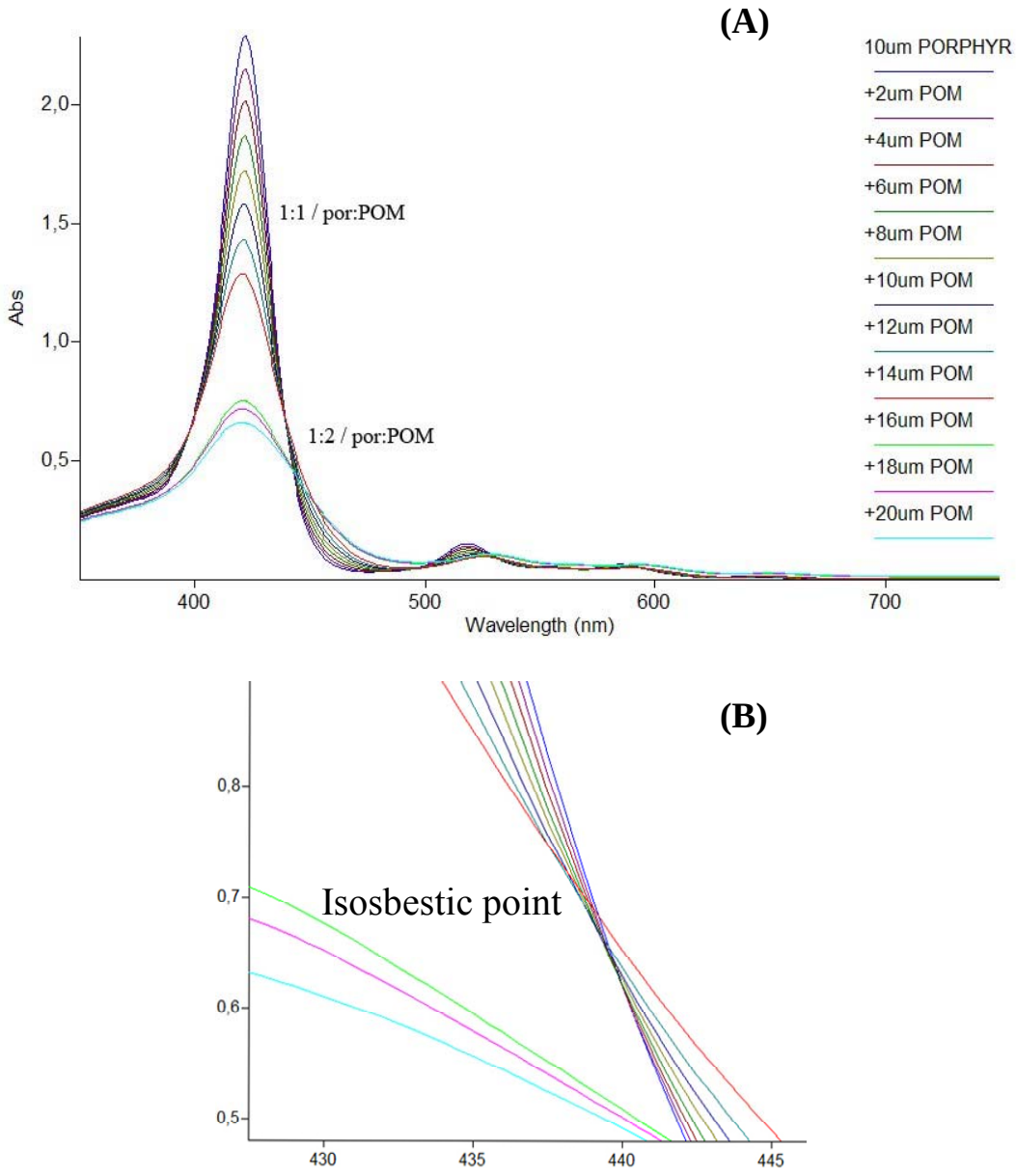

Figure 2.2 (A) UV-visible spectra of the titration of $EuPW_{11}O_{39}^{4-}$ into a 10 μM solution of $TMPyP^{4+}$ in water. The lower plot **(B)** shows the isosbestic point where the red line represents a 20% excess of the POM. Two other isosbestic points are observed at 495 nm and 530 nm.

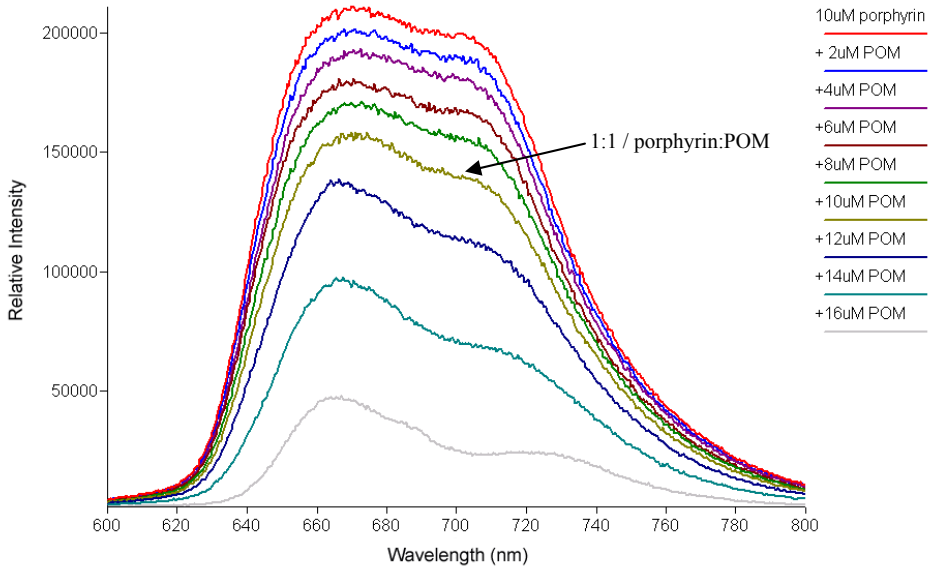

Figure 2.3 Fluorescence spectra of the titration of $EuPW_{11}O_{39}^{4-}$ into a 10 μM solution of $TMPyP^{4+}$ in water. λ_{exc} = 422 nm (Soret band).

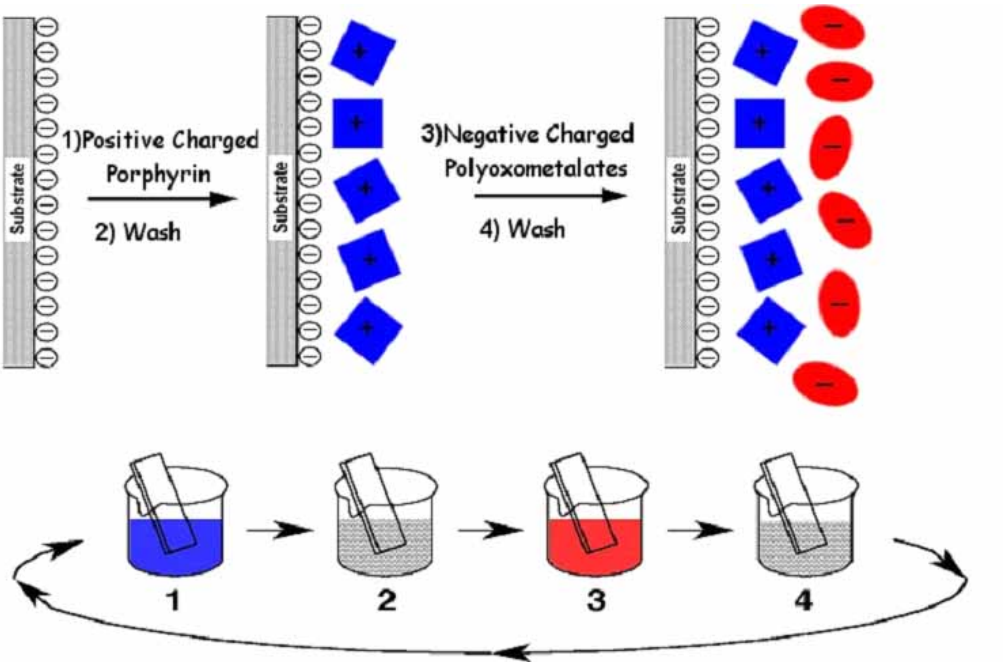

Figure 2.4 Schematic of the Layer-by-Layer process for porphyrin-polyoxometalates deposition. Modeled after Decker, G. *Science* **1997,** *277*, 1232.

The last is likely the predominant pathway, because neither the characteristic porphyrin radical anion or cation electronic bands nor photosensitization of Eu luminescence is observed. The characteristic blue color of the reduced POM is also not observed upon illumination with a 50 W halogen lamp in the presence of 2-propanol.[44]

Film

UV-Visible Characterization. The film growth can be monitored by UV-visible spectroscopy as each deposition of POM or porphyrin is added (Appendix). The 434 nm Soret absorption peak of the porphyrin in the multilayer film shows a red shift of approximately 12 nm and a significant broadening of the absorption bands compared to the spectra in solution. The red shift and broadening of the optical spectra of the films are likely ascribed to porphyrin-POM aggregates, as observed to a lesser extent in the solution spectra, and to the absorption of the chromophores onto surfaces as previously observed.[45] Significant porphyrin-porphyrin interactions are not indicated because the well-known spectral signatures for J and H aggregates of these chromophores are not observed. Also, the lack of observable energy transfer in experiments with the zinc and free base derivative in alternating layers contraindicates significant electronic communication between chromophores. UV-visible spectra show that very little of the porphyrin is removed during the deposition of the POM (Appendix).

The O to W charge-transfer band of the POM is at ca. 250 nm, so deposition of these films onto quartz substrates allows one to monitor the increasing absorbance due to the addition of the POMs. Since the porphyrin pyridyl groups also absorb in this region, a plot of the absorbance at 255 nm is a convolution of the two molecular components, but it

remains linear (appendix Fig. A2.9). There are no significant shifts in the UV-visible spectra for the POM in the films compared to solution.

The plot of the absorbance as a function of the number of layers for the deposition on different substrates shows the influence of the substrate on the multilayer film formation (Figure 2.5). Because the surface energetics change during the first few dipping cycles due to screening of surface energy/charge, the initial part of the plots are not *a priori* linear, but the deposition process does not yield enough data to accurately fit a nonlinear curve. The second part of these plots should be linear since this represents the regime where the surface energy/charge no longer changes. Thus, we broke the curves into two linear parts to more accurately assess and compare the different systems. Our hypothesis is that the initial part of these curves is affected more by the surface properties, and the second linear portion depends more on the compounds used to make the films. See the detailed discussion by Koenig and Martel on plots of optical spectral intensities versus deposition in layer-by-layer systems.[46] The initial slopes and the number of deposition cycles in the first region of the plots depend on the magnitude of the surface charge/energy. While the charge density (lattice charge) of mica is well known (2.1 negative charges/nm^2),[47] the glass charge density depends on the type of glass and the method of cleaning, but in general, the number of negative sites on mica is considerably greater than the number of charged sites on glass,[48] which is greater than that on ITO. The surface energies of the three different substrates are quite different; for mica at room temperature in air, this is 375 mJ/m^2 and the value is 180 mJ/m^2 in a water vapor atmosphere,[49] while for glass it is 82.5 mJ/m^2 [50] and for ITO after ultrasonic degreasing the surface energy is 56 mJ/m^2.[51]

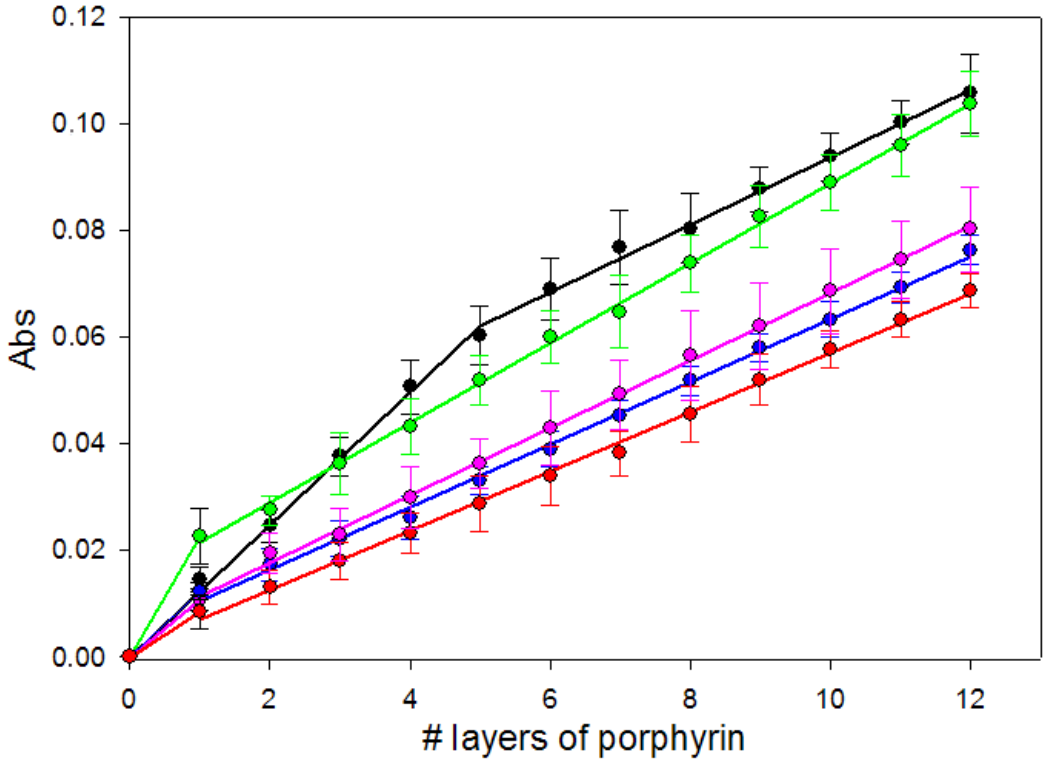

Figure 2.5 Absorbance at the Soret band (434 nm) is plotted as a function of the number of layers for the deposition on different substrates and using different porphyrins. Deposition of $TMPyP^{4+}$ and $EuPW_{11}O_{39}^{4-}$ on mica (black), on glass (blue), and on ITO (red). Deposition of $ZnTMPyP^{4+}$ and $EuPW_{11}O_{39}^{4-}$ on ITO (green) and alternating between porphyrins $TMPyP^{4+}$/$EuPW_{11}O_{39}^{4-}$/ $ZnTMPyP^{4+}$ on ITO (pink). The plot for the deposition on quartz is not shown for clarity since it is nearly the same as that on glass (see Appendix). In the case of the glass and mica the measured absorption is divided by two to account for the deposition of material on both sides of these substrates. Error bars represent ± 1 standard deviation from the mean.

Note that the magnitude of the slopes of the initial lines in Figure 2.5 are in the same order: mica > glass > ITO. On mica, we estimate that the surface density of the initially deposited $TMPyP^{4+}$ from one dipping cycle is ca. 1 porphyrin per 5 nm^2 using the extinction coefficient of the Soret band of 2.3 x 10^5 $M^{-1}cm^{-1}$ and assuming that the macrocycles lay flat on the surface. The initial surface density is less on the other

substrates. Thus on mica, four or five deposition cycles are required to reach the point where the surface energetics are screened, while on glass and ITO it takes one or two deposition cycles.

The second line for the mica (slope 0.0063) data represents the remaining layers and the slope is similar to those of glass (0.0059), quartz (0.0060), and ITO (0.0056), indicating that the surfaces are essentially similar. The greater error for the mica data compared to ITO and glass is likely due to imperfections and greater variation in the baseline due to the multiple planes in the mica. Atomic force microscopy (AFM) of the ITO surface shows that it is not atomically smooth and has a surface RMS (root means square) roughness of 1.5 nm on 1 μm^2 scans (glass RMS = 0.74 nm, mica RMS = 0.29 nm). Thus, the increased surface area and perhaps the deposition of more material in the valleys may effect the deposition. Annealing the films at 120° C up to 24 h does not result in any change of the film morphology or thickness. For the $SiW_{12}O_{40}^{4-}/TMPyP^{4+}$ system, the slope of the lines is similar, even after 60 deposition cycles on ITO and 30 deposition cycles on glass.

The molar absorptivities of the Soret band of $Zn(II)TMPyP^{4+}$ ($\varepsilon = 2.04 \times 10^5\ M^{-1}\ cm^{-1}$)[41] is ca. 10% less than the free base $TMPyP^{4+}$ ($\varepsilon = 2.26 \times 10^5\ M^{-1}\ cm^{-1}$),[52] so the UV spectra indicate that when $Zn(II)TMPyP^{4+}$ is used, more material is initially deposited on ITO compared to the free base (Figure 2.5). When the porphyrin layers alternate between the free base and the metalloporphyrin derivatives, the amount of material deposited is in between those of the individual compounds. The Zn(II) ion in the porphyrin has no propensity to bind oxygen ligands, and there is no evidence of free base protonation; thus, the increased slope may be due to small electrostatic or solubility differences of the

metalloporphyrin compared to the free base. The deposition of $TMPyP^{4+}$ using $SiW_{12}O_{40}^{4-}$ as the counterion material on glass produced films that are similar to those obtained using $TMPyP^{4+}$/ $EuPW_{11}O_{39}^{4-}$ on the same substrate, but with a greater amount of material deposited in each cycle, as judged by the slope of the Soret absorption band maximum versus deposition cycle (0.010). This confirms that the net charge and size of the porphyrin and POM are important determinants of film formation.

Fluorescence Properties of the Films

The fluorescence analysis of film formation (Figure 2.6) shows that the $TMPyP^{4+}$ fluorescence (λ_{ext}=432 nm, porphyrin Soret) is slightly quenched when deposited on quartz due to anisotropy. The fluorescence is further quenched by the deposition of the POM due to the heavy atom effect from the tungsten in the POM. The fluorescence intensity reaches a steady ca. 20% of the initial value after four deposition cycles (Figure 2.7), which is when the films reach a consistent composition (vide infra). This demonstrates that the porphyrin-POM material has inherent fluorescence properties. The fluorescence properties of the films suggest that not all porphyrins have POMs directly stacked on the top of the macrocycle, which would likely completely quench the fluorescence by heavy atom effects, so there is a fraction of porphyrins wherein the POMs are held away from the porphyrin by the pyridinium groups. Because of the pyridinium groups are orthogonal to the macrocycle, this architectural arrangement less effectively quenches the fluorescence by the heavy atoms in the POM.[15,16]

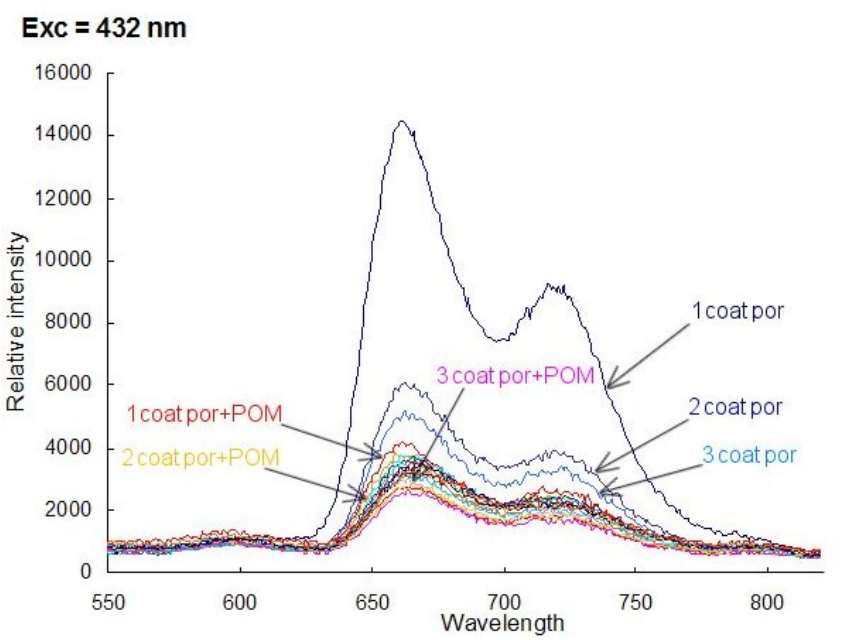

Figure 2.6 The fluorescence spectra of $TMPyP^{4+}$ as a function of deposition cycle on quartz, excitation at 432 nm.

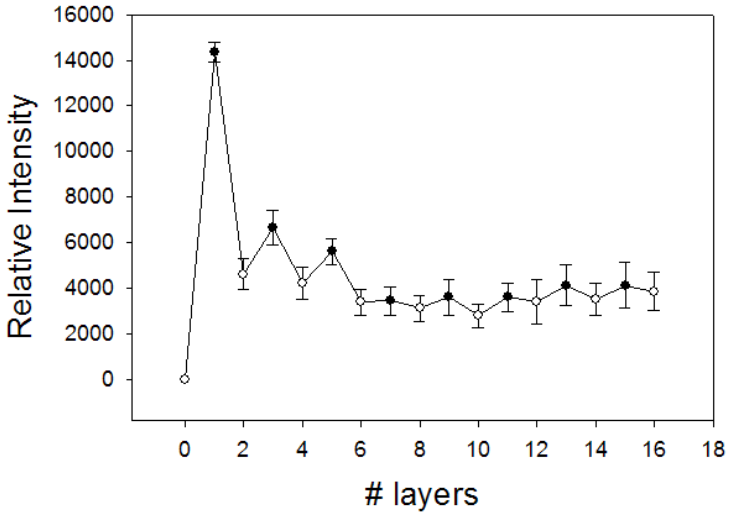

Figure 2.7 The fluorescence intensity of the strong emission band at 660 nm of $TMPyP^{4+}$ is plotted as a function of deposition cycle, where the closed circle represent spectra taken after porphyrin deposition and the open circles spectra after $EuPW_{11}O_{39}^{4-}$ deposition on a quartz substrate. Error bars represent ± 1 standard deviation from the mean.

Metalloporphyins

Consistent with the reduced fluorescence of zinc porphyrins relative to the corresponding free bases, the fluorescence of films made by 12 dipping cycles on ITO with $ZnTMPyP^{4+}$ is ca. 20% of the films formed from the free base. In order to probe the degree of energy transfer between porphyrins in these materials, both the free base $TMPyP^{4+}$ and the metalated $ZnTMPyP^{4+}$ were alternately used in the deposition cycles, i.e., $TMPyP^{4+}$/EuPOM/$ZnTMPyP^{4+}$. It is well-established that supramolecular constructs containing both zinc and free base porphyrins can exhibit energy transfer from the metalloporphyrins to the free base macrocycles, which is often demonstrated by observing an increase in the free base fluorescence when the metalloporphyrin is selectively excited.[15,16] Fluorescence studies of these films on glass show that both the free base and the zinc porphyrin fluoresce, but there is little observable indication of energy transfer from the zinc complex to the free base. This likely means that the porphyrins are generally not close enough, or electronically coupled via the POM, to allow efficient energy transfer. An alternative explanation, that the POMs quench the excited state of the porphyrins by rapid electron transfer or energy reactions, is not indicated by these steady-state experiments for the same reasons they are not observed in the solution-phase studies (*vide supra*).

Oppositely Charged Porphyrins

Mixtures of $TMPyP^{4+}$ and $TPPS^{4-}$ porphyrins and similar derivatives have been extensively studied in terms of the formation of a plethora of aggregate structures.[8,9] We find that sequential dipping of a substrate into aqueous solutions of $TMPyP^{4+}$ and $TPPS^{4-}$ does not result in multilayer films and no subsequent materials are deposited after the

first dipping cycle. This is in contrast to films made with tetrapyridylporphryin appended with four cationic ruthenium complexes[29,30] and $TPPS^{4-}$, and electrostatically assembled porphyrin/phthalocyanine films.[31] Though $TPPS^{4-}$ bears the same number of negative charges and is of similar size as the polyoxometalates, it is likely that the $TMPyP^{4+}$ and the $TPPS^{4-}$ interact so strongly that the ion pair formed has little affinity for the substrate. The interactions between these oppositely charged species are further stabilized by hydrophobic interactions between the aromatic macrocycles. This demonstrates that there must be a careful balance between the intermolecular interactions, the molecular interactions with surfaces, and geometries of the component molecules.

Stability

The stability of the POM-porphyrin films in toluene, water, and 0.1 M NaCl was investigated. The films formed from 12 deposition cycles on the three different substrates were immersed in toluene, water, and 0.1 M NaCl. UV-visible spectra were taken of samples soaked in the solvent after 1 h, 24 h, and 24 h followed by 1 min of sonication (Figure 2.8). The UV-visible spectra of the films do not show significant absorption decreases after treatment in these solvents (<10%), and this is confirmed by the optical spectra of the soaking solutions. One might expect that the salt ions screen the charges on the molecules and therefore, decrease the interaction energies between the component molecules and between the film and the surface. Thus, the electrostatically self-organized films are remarkably robust to solvent induced disassembly or delamination. The films are stable independent of the type of substrate used. Sonication does not seem to accelerate the delamination process, but the film can be mechanically removed by wiping with a solvent soaked Q-tip.

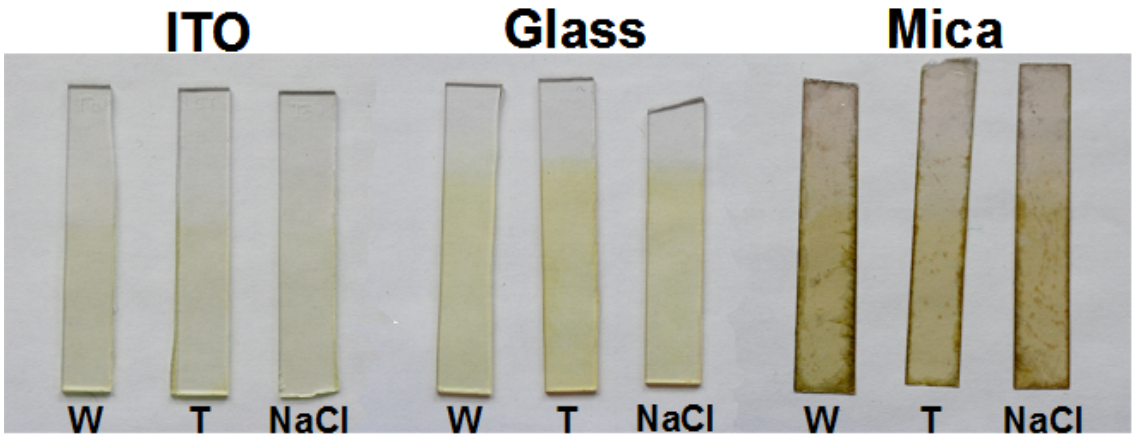

Figure 2.8 Stability of the films formed by 12 deposition cycles of $TMPyP^{4+}$ and $EuPW_{11}O_{39}^{4-}$ on ITO, glass and mica. The samples shown are after being soaked for 24 hours followed by 1 min sonication in water (W), toluene (T) and 100 mM NaCl.

Film Morphology

The film morphology and thickness were analyzed by AFM using both tapping and contact mode. For example, tapping mode images of the films after eight deposition cycles on mica (Figure 2.9) show a uniform coverage of the surface that has a granular look with a RMS roughness of 2.6 nm. The RMS varies somewhat with the number deposition process (4 cycles = 1.8 nm, 12 cycles= 1.6 nm) on 1 μm^2 scans.

Contact mode AFM studies on films from eight deposition cycles on mica reveal that some of the topmost material can be moved by the scanning probe tip, even with the minimum force between the tip (CSC21-A) and the surface. We refer to this part of the film as the *mobile layer*. To determine the total thickness of the film a small square section was nanoshaved using contact mode AFM.

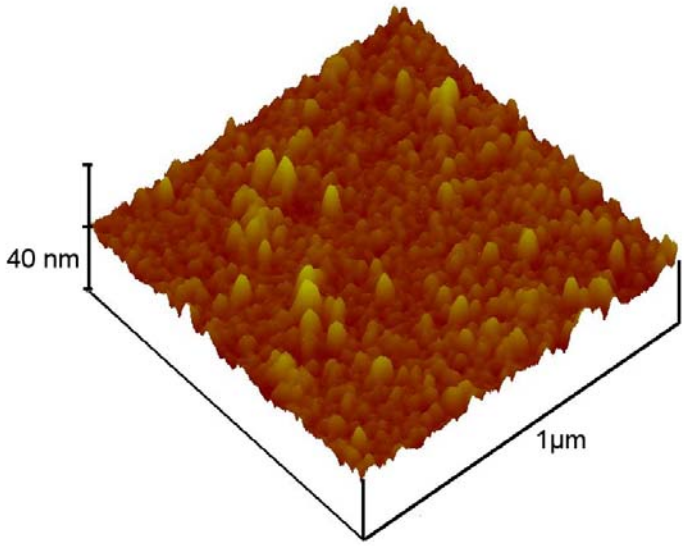

Figure 2.9 Tapping mode images of the films after eight deposition cycles of $TMPyP^{4+}$ and $EuPW_{11}O_{39}^{4-}$ on mica shows a uniform coverage of the surface that has a granular morphology with a root mean square roughness of 2.6 nm.

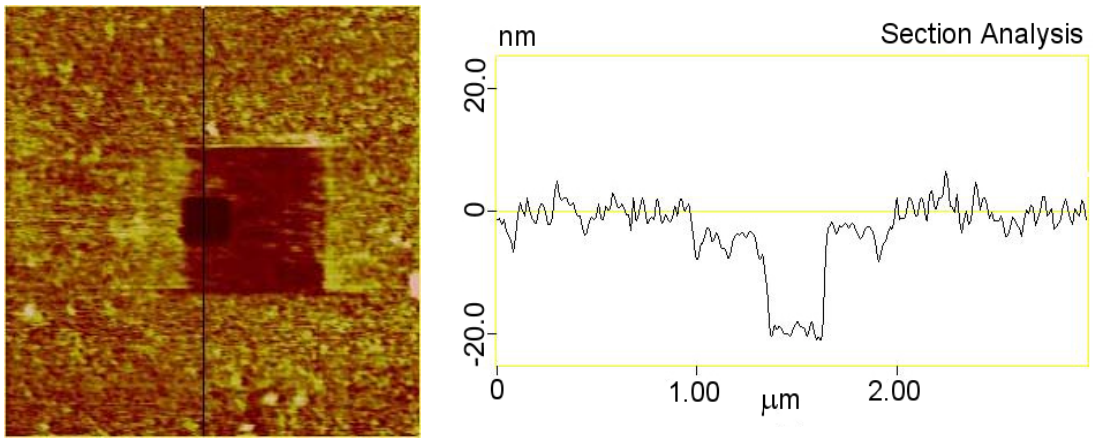

Figure 2.10 AFM analysis of a film formed after eight deposition cycles of $TMPyP^{4+}$ and $EuPW_{11}O_{39}^{4-}$ on mica show that there are two components of the film, a top ca. 7 nm mobile layer and a bottom ca. 15 nm non-mobile layer.

These nanoshaving experiments (Figure 2.10) indicate that the film on mica has a total film thickness of 23 ± 3 nm consisting of a lower *non-mobile* layer of 15 ± 3 nm and an upper mobile layer (thickness 7 ± 2 nm). Table 2.1 summarizes the thicknesses of the films after different numbers of deposition cycles were determined by nanoshaving experiments. The film prepared with 12 deposition cycles shows a total thickness of approximately 29 nm, but no significant mobile layer. The initial layers can be characterized by AFM on mica substrates, but not

on ITO or glass because of the surface roughness. We propose that on mica the first few depositions result in an underlying non-mobile layer until the surface energy is effectively screened by the film. Above this, the mobile layer represents a part of the film that is neither densely packed nor strongly interacting with the surface, and may be ca. 7 nm aggregates. Additional deposition cycles increase the thickness of the upper, mobile part of the film and fill in the defects to makes it more compact (Figure 2.11). Thus, a robust film emerges after 12 deposition cycles. This also explains the difference in roughness between the samples with eight and 12 layers, and is consistent with the UV-visible data.

AFM analysis shows that the morphologies of films resulting from 12 deposition cycles on glass and ITO are similar to those on mica. However, nanoshaving experiments (using a small contact mode cantilever followed by imaging using a tapping mode tip) reveal a film thickness of 9.5 ± 2 nm on glass and 8 ± 2 nm on ITO. The films on glass and ITO are ca. 3-fold thinner than the corresponding 29 nm films on mica, but the UV-visible data indicate that the amount of material deposited on glass and ITO is only ca. half of that of the films on mica.

Tale 2.1 AFM Analvsis of Film Thickness on Mica

	4 deposition cycles	8 deposition cycles	12 deposition cycles
total depth	14 ± 2 nm	23 ± 3 nm	29 ± 3 nm
mobile film	7 ± 2 nm	7 ± 2 nm	none
non-mobile film	7 ± 2 nm	15 ± 3 nm	29 ± 3 nm

Table 2.1. The total thickness of the film deposited on mica increases nonlinearly as indicated by the electronic spectra. The mobile and non-mobile layers were assayed by AFM and nanoshaving experiments. The latter used a cantilever with a higher force constant (CSC21-B).

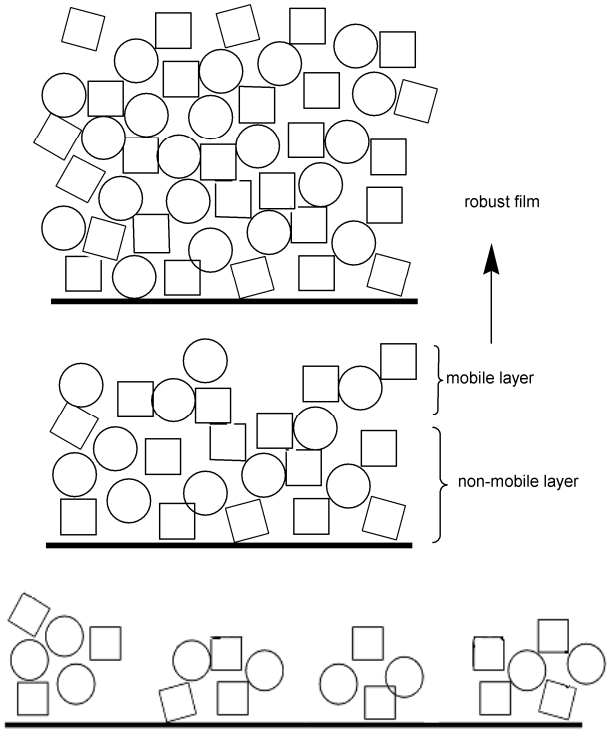

Figure 2.11 Schematic representation of the films formed from the first few deposition cycles with the possible formation of porphyrin/POM aggregates (bottom). After few more deposition cycles (middle) there is a non-mobile layer that depends on the surface energies of the substrate, and an incomplete mobile layer. Further deposition cycles then allows the formation of a more densely packed robust films (top).

The discrepancy between measured film thicknesses and the optical data is attributed to denser packing of porphryins and POMs on the glass and ITO substrates, to the wider variations in the surface roughness, and to errors in the measurements. UV-visible measurements of the mica films are hampered by light refraction on mica planes and micrometer imperfections on the surface.

Patterns of Porphyrin-POM Films

The use of thin films of photonic materials often requires the formation of patterns of the material on appropriate surfaces. We recently reported a new nanolithographic method that yields polymer insulated gold nanowires on a variety of ceramic substrates.[43] Stamped arrays of gold nanowires insulated with polycarbonate on mica provides an ideal platform to further organize the porphyrin-POM film into patterns, because these molecules have high affinities for the mica substrate and low affinities for the polycarbonate polymer. Thus, the sequential dipping of a mica substrate bearing a pattern of gold nanowires encapsulated in polycarbonate into the POM and porphyrin solutions results in a thin film residing on the exposed mica. AFM analysis of these photonic films (Figure 2.12) reveals that they are somewhat thicker than the films on bare mica, likely due to the accumulation of materials in the valleys of the pattern.

2.4 Conclusions

The sequential dipping of a variety of ceramic substrates into aqueous solutions of a tetracationic porphyrin and tetra anionic POM results in remarkably stable nanoscaled films. There are a minimum number of layers needed to fabricate robust films, which depends on the surface energetics of the substrate, but films are readily deposited onto

glass, quartz, and ITO in addition to a charged mica surface. Both the nanolithographic method and the electrostatic formation of the thin films described herein demonstrate that control of surface energetics can be beneficially used in the fabrication of nanomaterials. The film thickness or optical density can be exquisitely controlled by the number of deposition cycles. The chemical properties of the two molecular components, the substrate, and the balance of the intermolecular and molecule-surface interactions dictate the ability to form these films in analogy to the widely studied layer-by-layer methods. The functionality of these films can be modulated by the metal ions in either the porphyrin or lacunary POMs. These thin films are remain luminescent, and can be patterned by dipping substrates bearing nanoscaled arrays of polymers for which the water-soluble molecules have little affinity.

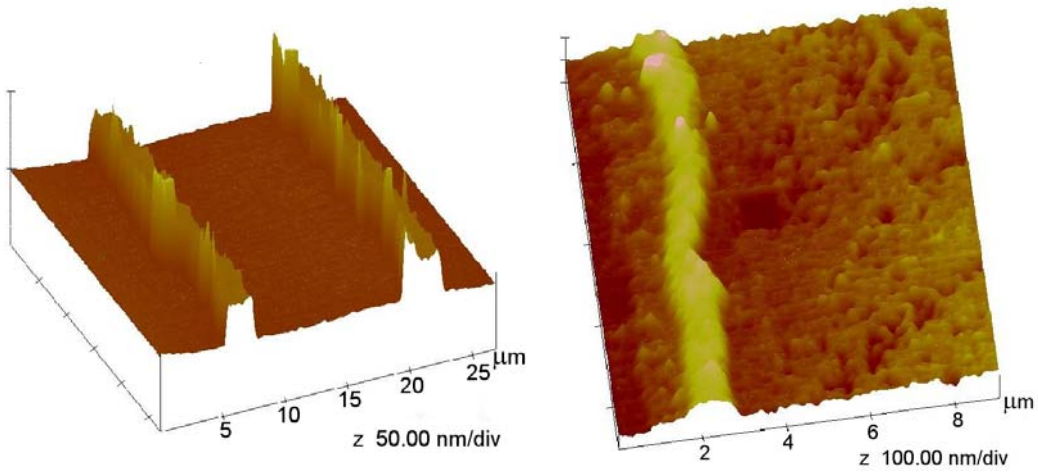

Figure 2.12 Left: contact mode AFM topography of mica patterned with gold nanowires encapsulated in polycarbonate. Right: contact mode AFM topography of a different part of the substrate after eight deposition cycles of $TMPyP^{4+}$ and $EuPW_{11}O_{39}^{4-}$ shows that the thin film resides on the exposed mica, and nanoshaving experiments indicates a thickness of ca. 40 nm.

2.5 Appendix

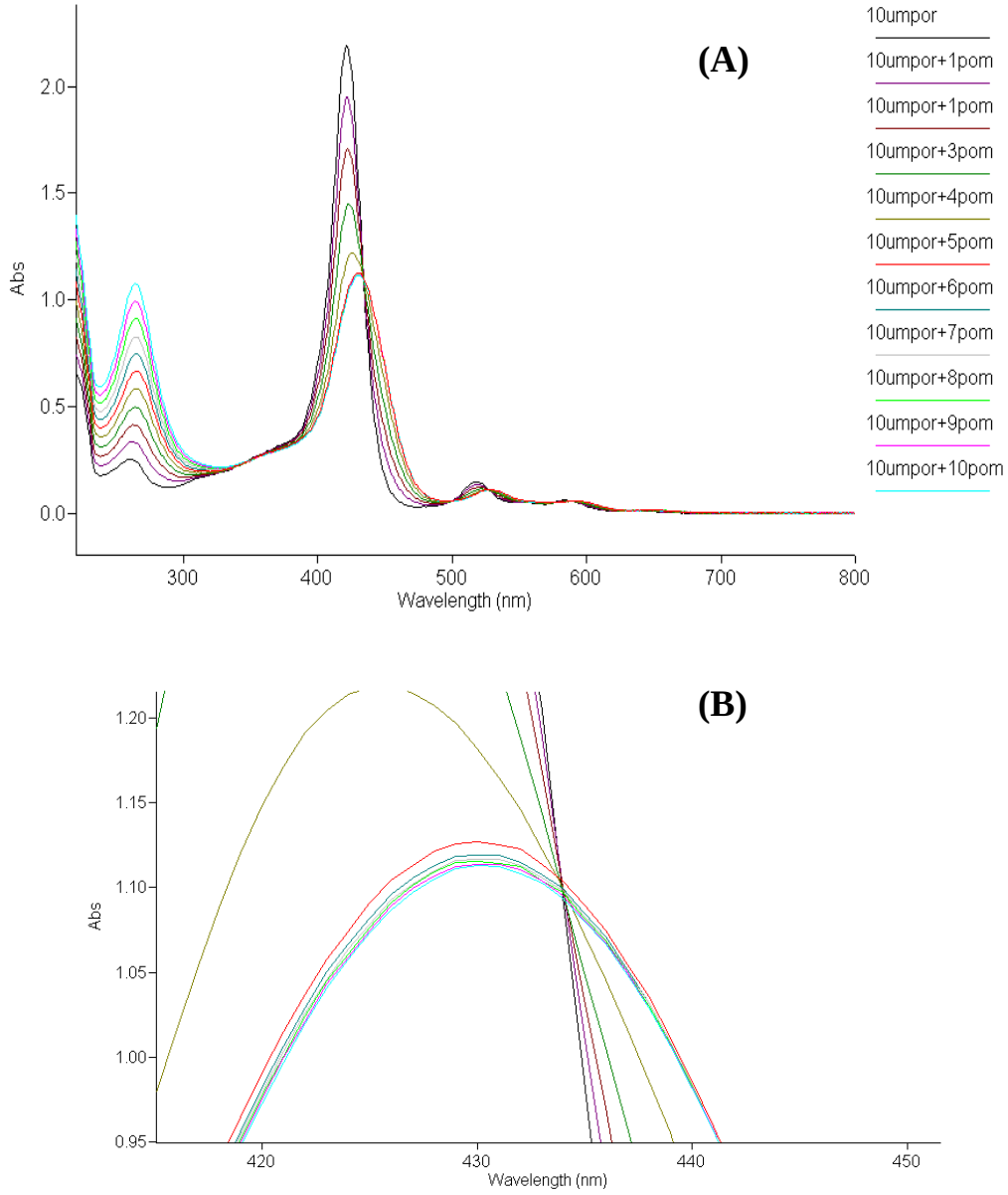

Figure A2.1 (A) UV-visible spectra of the titration of $SiW_{12}O_{40}^{4-}$ into a 10 μM solution of $TMPyP^{4+}$ in water. The lower plot **(B)** shows the isosbestic point where the light blue line represents a 20% excess of the POM. Two other isosbestic points are observed at 495 nm and 530 nm.

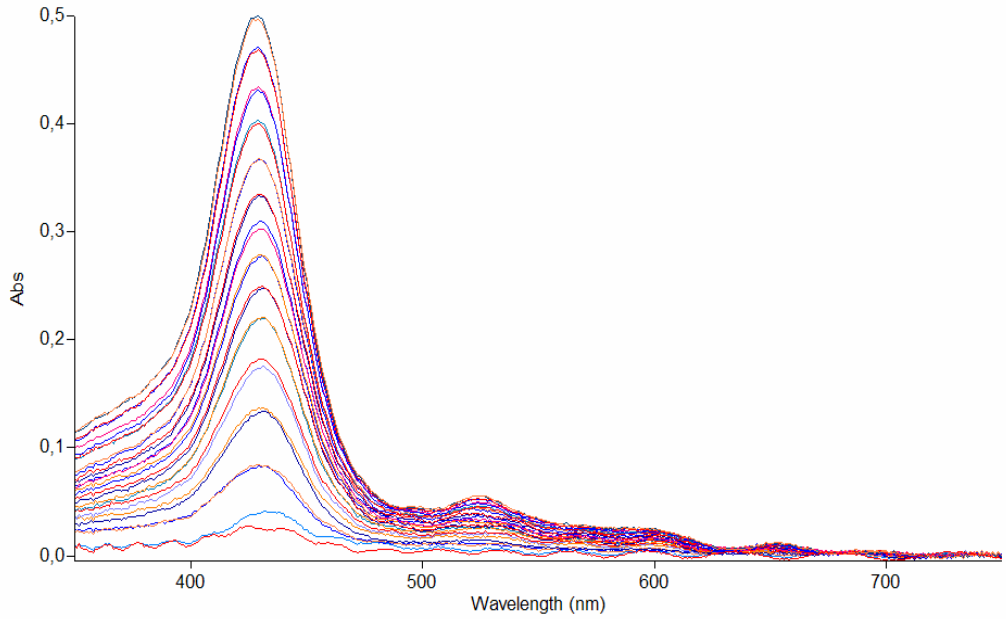

Figure A2.2 Layer-by-layer formation of $EuPW_{11}O_{39}^{4-}$ / $TMPyP^{4+}$ matrix on mica. The blue lines — represent the spectra after porphyrin deposition and the red lines — after POM deposition.

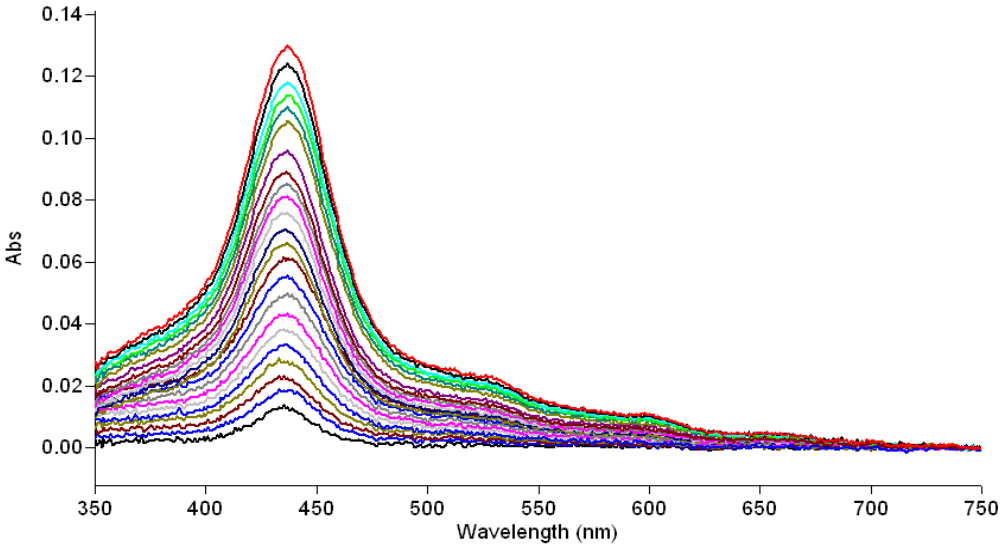

Figure A2.3 Layer-by-layer formation of $EuPW_{11}O_{39}^{4-}$ / $TMPyP^{4+}$ matrix on ITO, UV-vis spectra recorded after porphyrin deposition (24 deposition cycles).

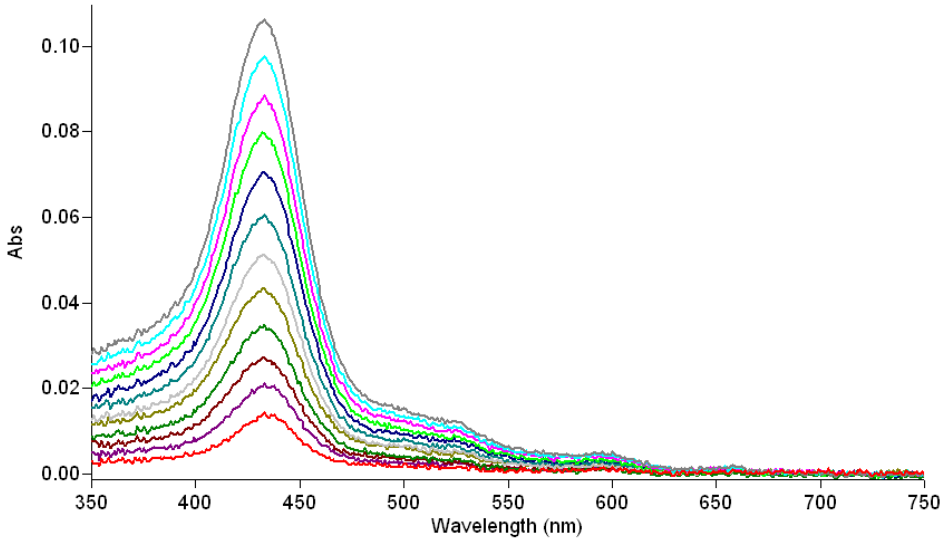

Figure A2.4 Layer-by-layer formation of $EuPW_{11}O_{39}^{4-}$ / $TMPyP^{4+}$ matrix on glass, UV-vis spectra recorded after porphyrin deposition (12 deposition cycles).

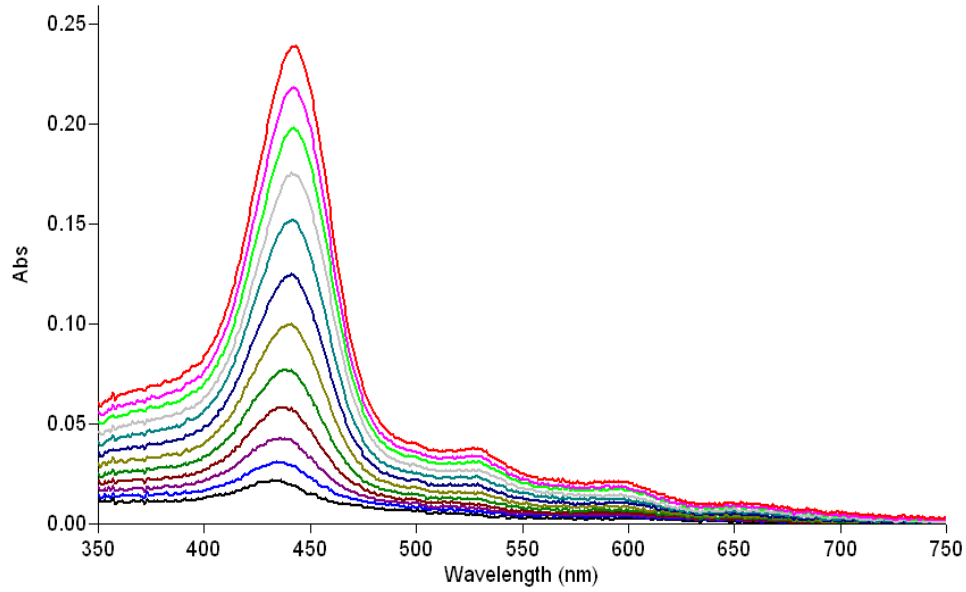

Figure A2.5 Layer-by-layer formation of $SiW_{12}O_{40}^{4-}$ / $TMPyP^{4+}$ matrix on glass, UV-vis spectra recorded after porphyrin deposition (12 deposition cycles).

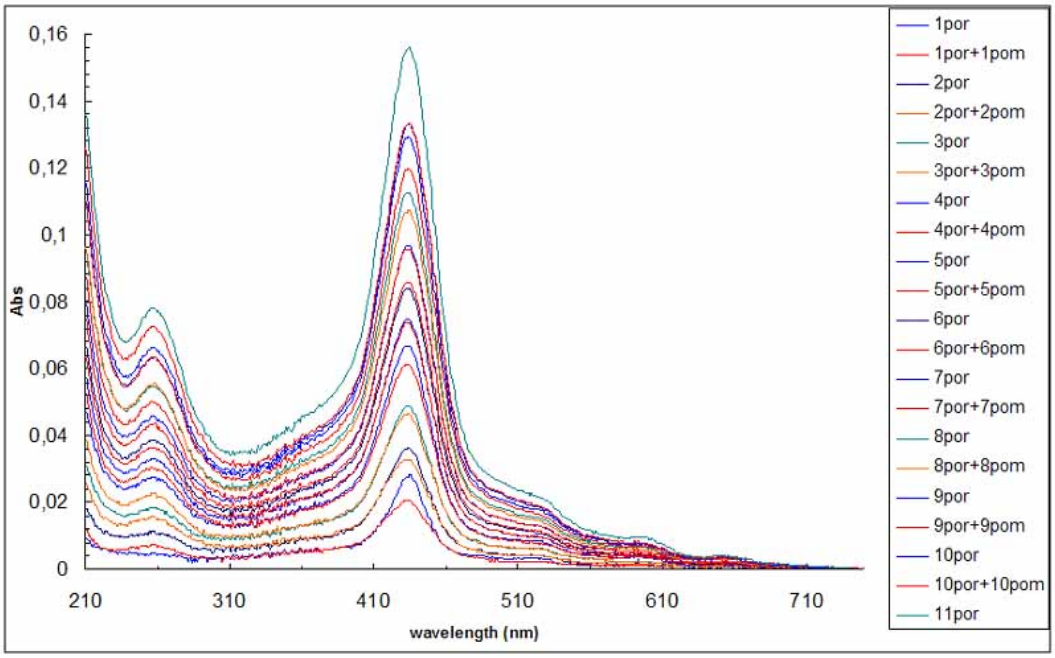

Figure A2.6 Layer-by-layer formation of $EuPW_{11}O_{39}^{4-}$ / $TMPyP^{4+}$ matrix on quartz showing the increasing absorbance due to the POM. The peak at 250 nm comes from the oxygen-to-tungsten charge transfer transition of the POM convolved with a band from the pyridyl groups on the porphyrin.

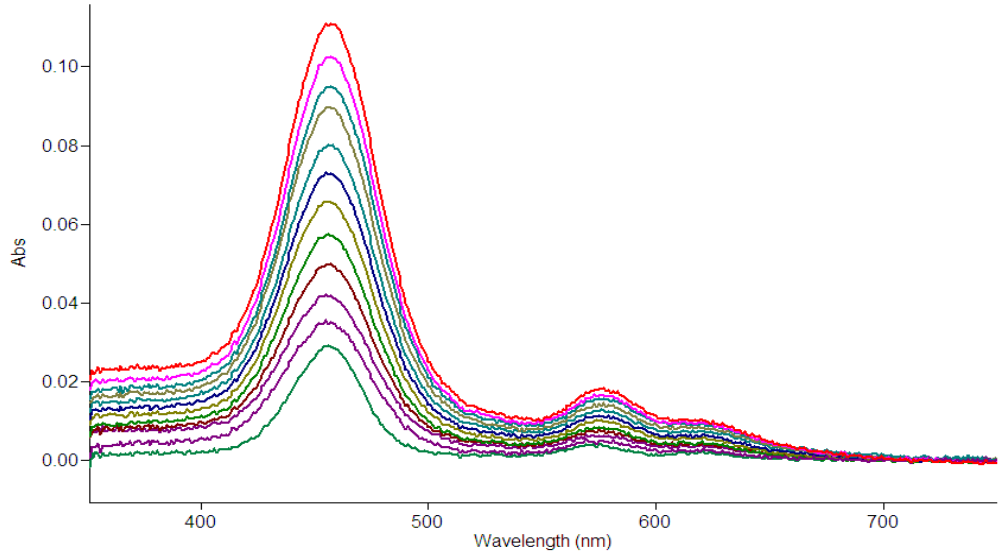

Figure A2.7 Layer-by-layer formation of $EuPW_{11}O_{39}^{4-}$ / $ZnTMPyP^{4+}$ matrix on ITO, UV-vis spectra recorded after porphyrin deposition (12 deposition cycles).

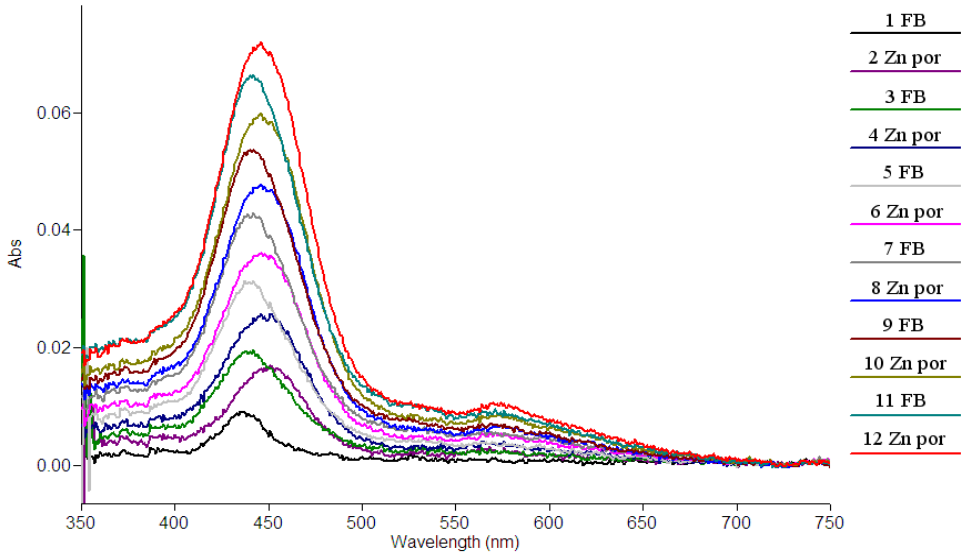

Figure A2.8 Layer-by-layer formation of $TMPyP^{4+}$ / $EuPW_{11}O_{39}^{4-}$ / $ZnTMPyP^{4+}$ matrix on ITO, UV-vis spectra recorded after porphyrin deposition (12 deposition cycles). Obtained by alternating using free base (odd deposition Cycles) and Zn porphyrin (even deposition cycles).

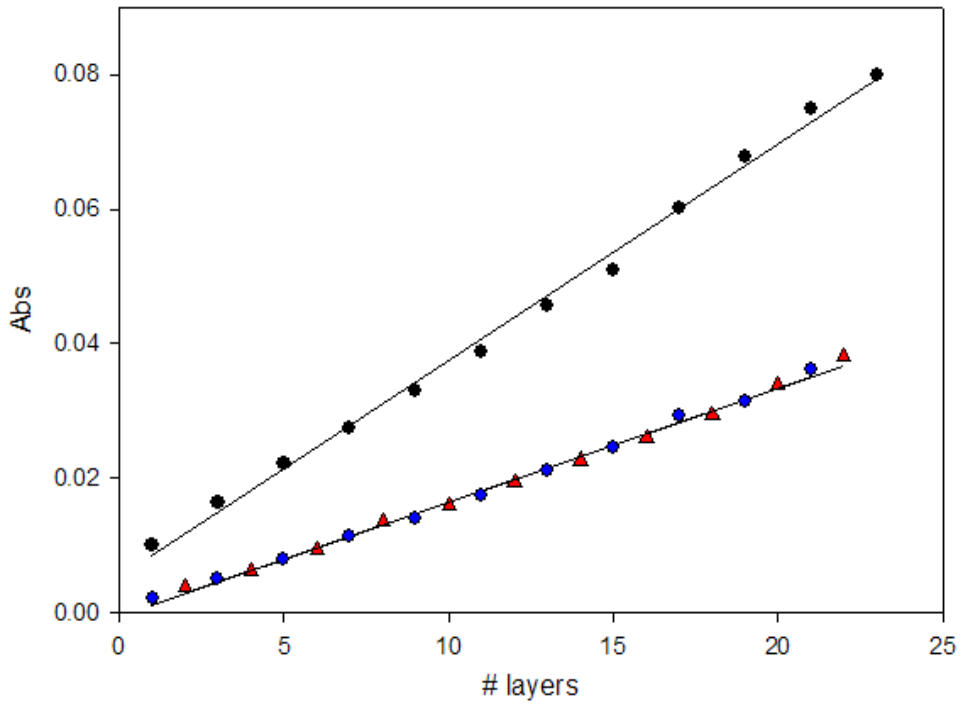

Figure A2.9 Absorbance at the Soret band (434 nm, black circles) is plotted as a function of the number of deposition cycles on quartz using $TMPyP^{4+}$ and $EuPW_{11}O_{39}^{4-}$. Quartz substrates allow the 255 POM band to be monitored, which overlaps with a porphyrin aromatic band, (●)Absorbance at 255 nm after porphyrin deposition; (▲)Absorbance at 255nm after POM deposition.

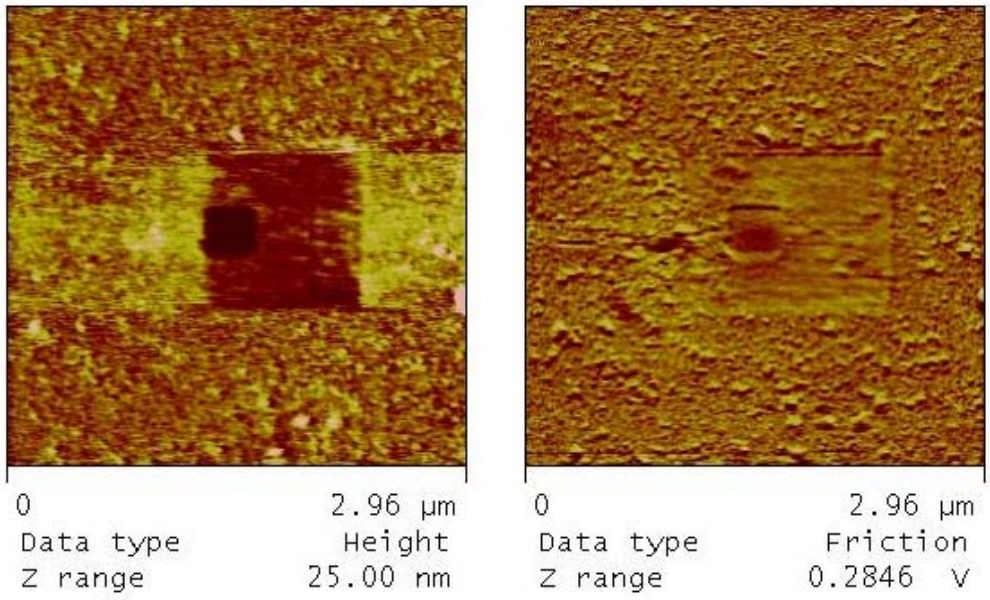

Figure A2.10 AFM analysis of a film formed after eight deposition cycles of $TMPyP^{4+}$ and $EuPW_{11}O_{39}^{4-}$ on mica show that there are two components of the film, a top ca. 7 nm mobile layer and a bottom ca. 15 nm non-mobile layer. The friction image right shows that the two layers are compositionally the same.

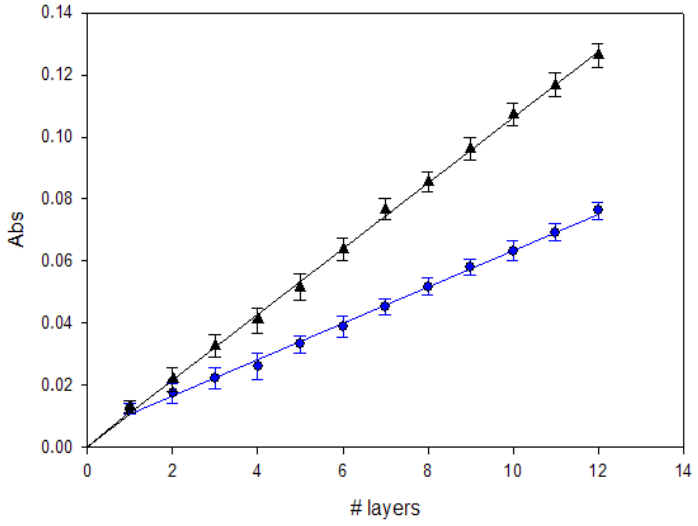

Figure A2.11 Using different POMs for the deposition process affects the amount of material deposited but not the linear increase ● $TMPyP^{4+}/EuPW_{11}O_{39}^{4-}$ ▲ $TMPyP^{4+}/SiW_{12}O_{40}^{4-}$ (both on glass substrates).

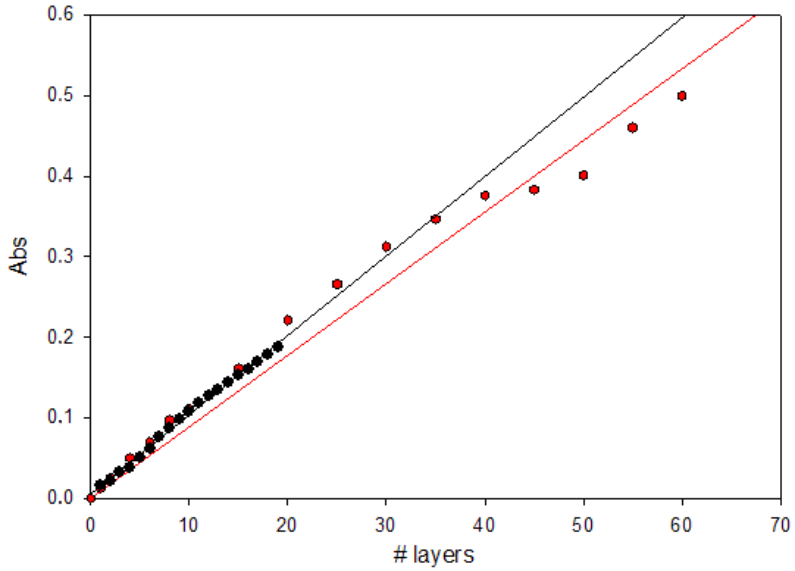

Figure A2.12 After the formation of a consistent film (4 layers on glass and ITO, 12 layers on mica) there is a linear increase in the optical density of the nanoscaled films with number of dipping cycles. ● 20 layers of $TMPyP^{4+}/SiW_{12}O_{40}^{4-}$ on glass, ● 60 layer of $TMPyP^{4+}/SiW_{12}O_{40}^{4-}$ on ITO.

Figure A2.13 4.5 cm^2 of mica with a film formed by eight deposition cycles shows no desorption.in 1 mL of H_2O after 20 days.

2.6 Chapter 2 References

(1) Izquierdo, A.; Ono, S. S.; Voegel, J. C.; Schaaf, P.; Decher, G. *Langmuir* **2005**, *21*, 7558-7567.

(2) Schlenoff, J. B.; Dubas, S. T. *Macromolecules* **2001**, *34*, 592-598.

(3) Maruccio, G.; Cingolania, R.; Rinaldia, R. *J. Mater. Chem.* **2004**, *14*, 542-554.

(4) Wei Zhao, J.-J. X. H.-Y. C. *Electroanalysis* **2006**, *18*, 1737-1748.

(5) Ozin, G. A.; Arsenault, A. C. *Nanochemistry - A Chemical Approach to Nanomaterials*; Royal Society of Chemistry: London, 2005.

(6) Ariga, K.; Hill, J. P.; Ji, Q. *Phys. Chem. Chem. Phys.* **2007**, 2319-2340.

(7) Drain, C. M.; Chen., X. In *Encyclopedia of Nanoscience & Nanotechnology*; Nalwa, H. S., Ed.; American Scientific Press: New York, 2004; Vol. 9, pp 593-616.

(8) Drain, C. M.; Smeureanu, G.; Batteas, J.; Patel, S. In *Dekker Encyclopedia of Nanoscience and Nanotechnology*; Schwartz, J. A., Contescu, C. I., Putyera, K., Eds.; Marcel Dekker, Inc.: New York, 2004; Vol. 5, pp 3481-3502.

(9) Drain, C. M.; Bazzan, G.; Milic, T.; Vinodu, M.; Goeltz, J. C. *Isr. J. Chem.* **2005**, *45*, 255-269.

(10) Drain, C. M.; Goldberg, I.; Sylvain, I.; Falber, A. *Top. Cur. Chem.* **2005**, *245*, 55-88.

(11) Drain, C. M.; Fischer, R.; Nolen, E.; Lehn, J. M. *Chem. Commun.* **1993**, 243-245.

(12) Drain, C. M.; Kirmaier, C.; Medforth, C. J.; Nurco, D. J.; Smith, K. M.; Holten, D. *J. Phys. Chem.* **1996**, *100*, 11984-11993.

(13) Drain, C. M.; Shi, X.; Milic, T.; Nifiatis, F. *Chem. Commun.* **2001**, 287-288 (Adendum 1418).

(14) Shi, X.; Barkigia, K. M.; Fajer, J.; Drain C. M. *J. Org. Chem.* **2001**, *66*, 6513-6522.

(15) Drain, C. M.; Nifiatis, F.; Vasenko, A.; Batteas, J. D. *Angew. Chem., Int. Ed.* **1998**, *37*, 2344-2347.

(16) Drain, C. M.; Lehn, J.-M. *Chem. Commun.* **1994**, 2313-2315 (correction 1995, p503).

(17) Drain, C. M.; Christensen, B.; Mauzerall, D. C. *Proc. Natl. Acad. Sci., U.S.A.* **1989**, *86*, 6959-6962.

(18) Drain, C. M.; Mauzerall, D. C. *Biophys. J.* **1992**, *63*, 1544-1555.

(19) Drain, C. M.; Mauzerall, D. C. *Biophys. J.* **1992**, *63*, 1556-1563.

(20) Yamase, T. *Chem. Rev.* **1998**, *98*, 307-326.

(21) Katsoulis, D. E. *Chem. Rev.* **1998**, *98*, 359-388.

(22) Geletii, Y. V.; Hill, C. L.; Atalla, R. H.; Weinstock, I. A. *J. Am. Chem. Soc.* **2006**, *128*, 17033-17042.

(23) Fang, X.; Hill, C. L. *Angew. Chem. Int. Ed* **2007**, *46*, 3877-3880.

(24) Santos, I. C. M. S.; Rebelo, S. L. H.; Balula, M. S. S.; Martins, R. R. L.; Pereira, M. M. M. S.; Simoes, M. M. Q.; Neves, M. G. P. M. S.; Cavaleiro, J. A. S.; Cavaleiro, A. M. V. *J. Molecular Catalysis A: Chemical* **2005**, *231*, 35-45.

(25) Hagrman, D.; Hagrman, P. J.; Zubieta, J. *Angew. Chem., Int. Ed.* **1999**, *38*, 3165-3168.

(26) Qian, D. J.; Nakamura, C.; Miyake, J. *Chem. Commun.* **2001**, *22*, 2312-2313.

(27) Massari, A. M.; Gurney, R. W.; Wightman, M. D.; Huang, C.-H. K.; Nguyen, S. T.; Hupp, J. T. *Polyhedron* **2003**, *22*, 3065-3072.

(28) Lee, S. J.; Hupp, J. T. *Coord. Chem. Rev.***2006**, *250*, 1710-1723.

(29) Araki, K.; Wagner, M. J.; Wrighton, M. S. *Langmuir* **1996**, *12*, 5393-5398.

(30) Mayer, I.; Nakamura, M.; Toma, H. E.; Araki, K. *Electrochim. Acta* **2006**, *52*, 263-271.

(31) Sun, Y.; Zhang, X.; Sun, C.; Wang, Z.; Shen, J.; Wang, D.; Li, T. *Chem. Commun.* **1996**, 2379-2380.

(32) Jiang, L.; Chang, Q.; Ouyang, Q.; Liu, H.; Wang, Y.; Zhang, X.; Song, Y.; Li, Y. *Che.l Phys.* **2006**, *324*, 556-562.

(33) Jiang, L.; Lu, F.; Li, H.; Chang, Q.; Li, Y.; Liu, H.; Wang, S.; Song, Y.; Cui, G.; Wang, N.; He, X.; Zhu, D. *J. Phys. Chem. B.* **2005**, *109*, 6311-6315.

(34) Huang, M.; Shao, Y.; Sun, X.; Chen, H.; Liu, B.; Dong, S. *Langmuir* **2005**, *21*, 323-329.

(35) Han, B. H.; Manners, I.; Winnik, M. A. *Chem. Mater.* **2005**, *17*, 3160-3171.

(36) Akatsuka, K.; Ebina, Y.; Muramatsu, M.; Sato, T.; Hester, H.; Kumaresan, D.; Schmehl, R. H.; Sasaki, T.; Haga, M. *Langmuir* **2007**, *23*, 6730-6736.

(37) Shen, Y.; Liu, J.; Jiang, J.; Liu, B.; Dong, S. *J. Phys. Chem. B.* **2003**, *107*, 9744-9748.

(38) Shen, Y.; Liu, J.; Jiang, J.; Liu, B.; Dong, S. *Electroanalysis* **2002**, *14*, 1557-1553.

(39) Martel, D.; Gross, M. *J. Solid State Electrochemistry* **2007**, *11*, 421-429.

(40) Xu, L.; Wang, E.; Li, Z.; Kurth, D. G.; Du, X.; Zhang, H.; Qin, C. *New J. Chem.* **2002**, *26*, 782-786.

(41) Pasternack, R. F.; Francesconi, L.; Raff, D.; Spiro, E. *Inorg. Chem.* **1973**, *12*, 2606-2610.

(42) Zhang, C.; Howell, R. C.; Scotland, K. B.; Perez, F. G.; Todaro, L.; Francesconi, L. C. *Inorg. Chem.* **2004**, *43*, 7691-7701.

(43) Helt, J. M.; Drain, C. M.; Bazzan, G. *J. Am. Chem. Soc.* **2006**, *128*, 9371-9377.

(44) Troupis, A.; Hiskia, A.; Papaconstantinou, E. *Applied Catalysis B: Environmental* **2003**, *42*, 305-315.

(45) Milic, T.; Garno, J. C.; Batteas, J. D.; Smeureanu, G; Drain, C. M. *Langmuir* **2004**, *20*, 3974-3983.

(46) Koenig, J.-F.; Martel, D. *Thin Solid Films* **2007**, in press (corrected proof doi:10.1016/j.tsf.2007.07.137).

(47) Rojas, O. J.; Ernstsson, M.; Neuman, R. D.; Claesson, P. M. *J. Phys. Chem. B* **2000**, *104*, 10032-10042.

(48) Radeva, R.; Radeva, T. *Physical Chemistry of Polyelectrolytes;* Marcel Dekker: New York, 2001; Vol. 99.

(49) Ostrovskaya, L.; Perevertailo, V.; Ralchenko, V.; Dementjev, A.; Loginova, O. *Diamond Relat. Mate.* **2002**, *11*, 845-850.

(50) Smay, G. L. *J. Am. Ceram. Soc.* **1988**, *71*, C-217-C-219.

(51) Zhong, Z.; Zhong, Y.; Liu, C.; Yin, S.; Zhang, W.; Shi, D. *Phys. Stat. Sol. (A)* **2003**, *198*, 197-203.

(52) Pasternack, R. F.; Huber, P. R.; Boyd, P.; Engasser, G.; Francesconi, L.; Gibbs, E.; Fasella, P.; Cerio Venturo, G.; Hinds, L. deC. *J. Am. Chem. Soc.* **1972**, *94*, 4511-4517.

Chapter 3

ELECTROCHEMICAL STUDIES OF THE PORPHYRIN-POLYOXOMETALATE FILMS

3.1 Introduction

The porphyrin-polyoxometalates organic-inorganic hybrid films described in chapter two were characterized by cyclic voltammetry (CV). Though preliminary CV data was reported in the Langmuir paper,[1] the data indicated that there were several interesting features that were worth pursuing and that seem to be glossed over in the literature of these types of films.

Organic-inorganic hybrid materials are of great interest in the field of material chemistry as these materials can exhibit synergistic electrical, optical, and catalytic properties.[2] The layer-by-layer method is a good approach for a direct and low-cost fabrication of nanostructured films in which synergy between diverse materials may be accomplished.

Chemically-modified electrodes (CME), in which a thin film of a selected chemical is bonded or coated onto the electrode surface, are used in a wide spectrum of basic electrochemical investigations and for the design of various electrochemical devices such as sensors and energy conversion systems. A vast reviewed literature is available on this subject.[3] The ionic self-assembly technique is a common way to fabricate multilayered film CME, based on the electro- and photo-active building block.[4]

Metalloporphyrins are very versatile catalysts for several electrochemical reactions.[5] Using electrostatic self-assembly, chemically-modified electrodes with porphyrin have been prepared by combining porphyrins with polyelectrolytes, oppositely charged porphyrins, titania nanosheets, and other compounds.[6-8]

Electrodes modified with polyoxometalates have recently attracted increasing attention because of their good stability and catalytic activity. POM-containing multilayer films can be advantageous in heterogeneous and electro catalysis because they have many specific advantages over other chemically modified electrodes. These advantages include the ability to fabricate a three-dimensional layered distribution of electrocatalyst by an easy method that allows precise control of the amount of attached electrocatalyst, thereby optimizing materials usage.

Typical methods to prepare these chemically modified electrodes have been addressed in a review of the electrochemical properties of POMs.[9] The three main methods commonly used to immobilize POMs onto electrode surfaces are: (1) adsorption on electrode surface by dip coating,[10] (2) immobilization of POM as a dopant in a conductive polymer matrix,[11] (3) electrochemical deposition directly on the electrode.[12] The electrodeposition produces largely porous granular films, and the absorption on surfaces leads to the immobilization of the material only at the level of sub-monolayer to monolayer coverage.[13] The entrapment into polymer matrix produces stable films, but in some cases the polymer environment affects the electrochemical behavior of the immobilized heteropolyanions.[11,14]

Recently a layer-by-layer strategy has been successfully used to modify electrode surfaces based on electrostatic interactions between anionic POM and cationic

compounds or polymer.[15-17] Among these there are two examples of deposition of cationic porphyrins and anionic POM on modified glassy carbon electrode.[18,19] These electrodes display electrocatalytic activity for the reduction of O_2 to peroxide and for hydrogen evolution from acidic water. These two systems were prepared by derivitization of the glassy carbon electrode with 4-aminobenzoic acid, and the material was deposited by cyclic potential sweeps of the electrode inside the solution of the ions to be deposited.

Herein we demonstrate that porphyrin/POM modified electrodes can be easily prepared just by dipping the electrode in the solutions of the oppositely charged materials without any previous preparation of the electrode surface.

3.2 Experimental Procedure

Materials. All reagents and solvents were of analytical grade and used without further purification. The water was passed through a Barnstead NANOPure Water Purification System. The 5,10,15,20-tetrakis(1'-methyl-4'-pyridinio)porphyrin tetra(*p*-toluenesulfonate) ($TMPyP^{4+}$) and silicotungstic acid hydrate ($SiW_{12}O_{40}^{4-}$) (Fig. 3.1) were purchased from Aldrich.

Cyclic voltammetry were performed with a BAS CV-50W electrochemical analyzer in a conventional three-electrode electrochemical cell, using ITO (0.6 mm^2) as the working electrode, a platinum wire as the auxiliary electrode, and Ag/AgCl/KCl (3mol/L) as the reference electrode. NaCl 0.1 (mol/L) in ultrapure water was used as electrolyte a two different pH values, pH=3 (adjust by addition of H_2SO_4 0.5 M) and 0.1 (mol/L) acetate buffer (pH=4) . Scan rate 0.1 V/s.

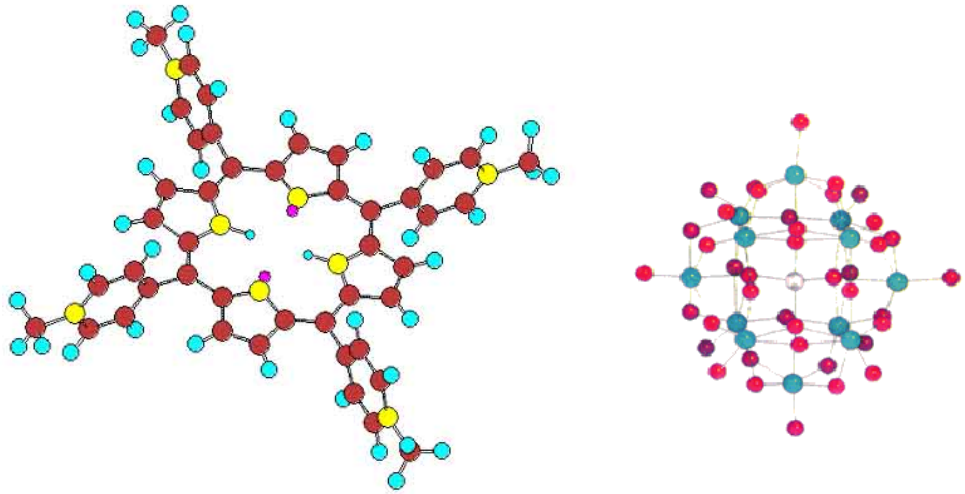

Figure 3.1 Left 5,10,15,20-tetrakis(1'-methyl-4'-pyridinio)porphyrin tetra(*p*-toluenesulfonate) ($TMPyP^{4+}$) (H = light blue, N = Yellow, C=brown), and right: polyoxometalate (POM) $H_4SiW_{12}O_{40}$ (O = red, W = blue, Si = gray) where the counter ions are left out for clarity.

All the solutions were degassed thoroughly with pure nitrogen and kept under a positive pressure of this gas during experimentation. The ITO substrate was cleaned using a UV/ozone cleaning system, rinsed with ultrapure water, sonicated in ethanol for 10 min. and dried by blowing a steam of nitrogen gas over the surface.

Films were prepared at room temperature by soaking the ITO substrate in a 0.5 mM aqueous solution of porphyrin for 1 min, followed by dipping the substrate three times in unbuffered NANOPure water to remove the excess, non-bound porphyrin

solution from the substrate. Subsequently, a layer of polyoxometalates was added by soaking the substrate for 1 minute in a 0.5 mM aqueous solution of polyoxometalates, rinsed three times by dipping in NANOPure water. The procedure was repeated until the desired film thickness was obtained. The films on the glass side of the ITO substrates were left in place.

3.3 Results and Discussion

Solution Analysis

Electrochemical characteristic of $TMPyP^{4+}$ have been reported in detail using Hg and ITO electrodes.[20] The reduction in acidic solution is pH dependent but overall involves the addition of 6 electrons. Above pH 2 (between pH 2 and 6) two peaks are observed, there is a first quasi reversible reduction step that involves the reduction of the porphyrin free base to the chlorin free base:

$$P(0)H_2 + 2e^- + 2H^+ \rightleftharpoons P(-II)H_4 \qquad \text{pH dependent (60 mV/pH)}$$

A potentials more negative than -0.65 V vs Ag/AgCl a complicated irreversible four electron reduction occurs which generate instable porphyrinigen cations (Fig. 3.2).

The electrochemical response of the $H_4SiW_{12}O_{40}$ in aqueous medium has been extensively studied. In acid solution using a glassy carbon working electrode the CV shows 5 reductions waves with an approximate electron ratio of 1:1:2:8:12. The first three reductions are reversible while the last two are irreversible and accompanied by chemical reactions of the complex.[9]

$SiW_{12}O_{40}^{4-} + e^- \rightleftharpoons SiW_{12}O_{40}^{5-}$

$SiW_{12}O_{40}^{5-} + e^- \rightleftharpoons SiW_{12}O_{40}^{6-}$

$SiW_{12}O_{40}^{6-} + 2e^- + 2H^+ \rightleftharpoons H_2SiW_{12}O_{40}^{6-}$

In the potential window suitable for the porphyrin (-0.6 V / +0.6 V) there are two reversible reductions that are essentially unaltered for $1 < pH < 5$ (Fig. 3.3).

Prior to the electrochemical study of the layer-by-layer deposition process, we analyzed the behavior in aqueous solutions (pH=3) of $TMPyP^{4+}$ and $SiW_{12}O_{40}^{4-}$ using ITO as the working electrode. The CV curves at pH 3 confirmed that the ITO surface has a small effect on the reduction potentials measured compared to the literature and set the scan limit of our cyclic voltammetry to -0.55 V vs. Ag/AgCl.

Film Analysis

Cyclic voltammetry can be used to monitor the deposition process and to characterize the electrochemical behavior of the film. Compared to the solution electrochemistry, the film exhibits less well resolved redox peaks for the two POM reduction. This is indicative of surface-confined redox processes.[21] There is a broad reduction peak at -0.3 V and when the potential reverses three oxidation peaks are observed, the first two for the POM and the last for the porphyrin. To assure identical and reproducible data, the CV curves shown (Fig. 3.4 and Fig. 3.5) are the fifth after a preliminary set of polarization cycles. The electrochemical data previously reported on Por-POM films also report the CV after several cycles (data not shown in those papers).[22]

The CV curves in Figure 3.4 are recorded with POM as outermost layer and after eight deposition cycles to assure complete surface coverage and film robustness (see previous chapter). Peak currents represent the surface concentration of POM and porphyrin loaded on the electrode, and as expected, these increase gradually with the number of deposition cycles indicating that a consistent amount of porphyrin and polyoxometalate are deposited with each deposition cycle. Similar CV curves are obtained when the porphyrin is the outermost layer (Fig. 3.5) but with a slightly different electrochemical behavior (see later description).

Figures 3.6 and 3.7 show the data from the first four potential scan cycles with the POM and porphyrin as the last deposited material, respectively, on the eight layer films. The cyclic voltammograms are quite different, exhibiting mainly a decrease of the cathodic peak and of the anodic peak relative to the porphyrin oxidation (near 0 V vs Ag/AgCl). The more intense reduction of the cathodic peak compared to the anodic peak suggests: (A) an irreversible reduction reaction of the porphyrinic material (in spite of the fact that the porphyrin is stable in the potential window examined), (B) a deabsorption of some porphyrinic material from the film after the reduction process, (C) a reorganization of the film since 8 deposition cycles were shown to form films with two domains, a lower non-mobile domain and an upper mobile domain. The latter deabsorption process is less likely because UV-visible analysis of the electrolyte solution after 15 deposition cycles and consequently many potential scans does not shows the presence of porphyrin in solution, moreover the films in 0.1M NaCl are quite stable (see chapter 2).

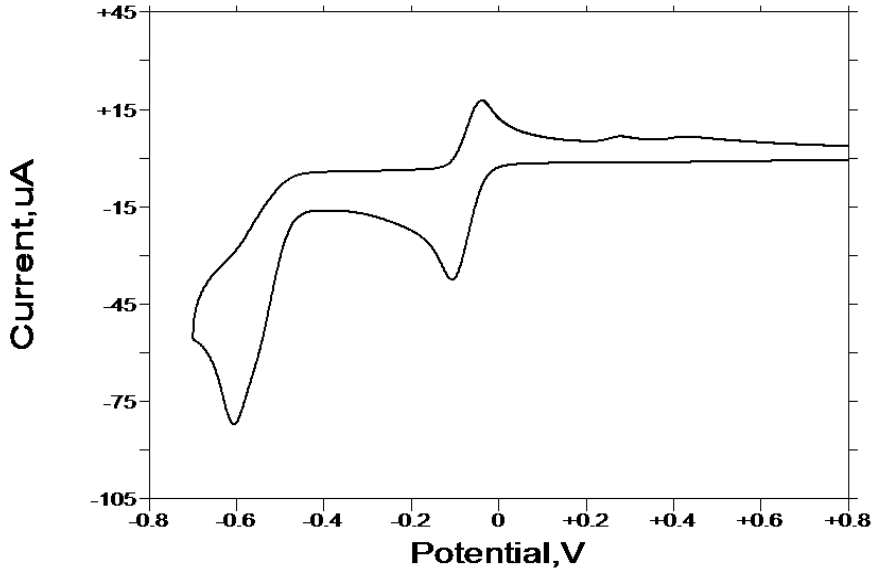

Figure 3.2 Cyclic voltammogram of a $TMePyP^{4+}$ solution. ITO (0.6 mm^2) as the working electrode, platinum wire as counter electrode and Ag/AgCl/KCl (3mol/L) reference electrode. Unbuffered NaCl 0.1 (mol/L) in ultrapure water, pH=3 (adjust by addition of H_2SO_4 0.5 M). Scan rate 0.1 V/s. (Potential vs. Ag/AgCl).

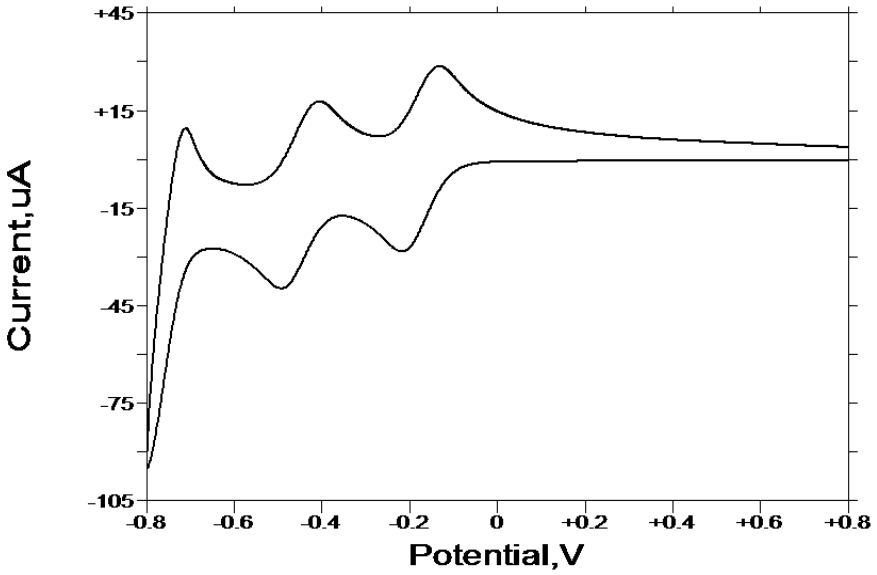

Figure 3.3 Cyclic voltammogram of a $SiW_{12}O_{40}^{4-}$ solution. ITO (0.6 mm^2) as the working electrode, platinum wire as counter electrode and Ag/AgCl/KCl (3mol/L) reference electrode. Unbuffered NaCl 0.1 (mol/L) in ultrapure water, pH=3 (adjust by addition of H_2SO_4 0.5 M). Scan rate 0.1 V/s. (Potential vs. Ag/AgCl).

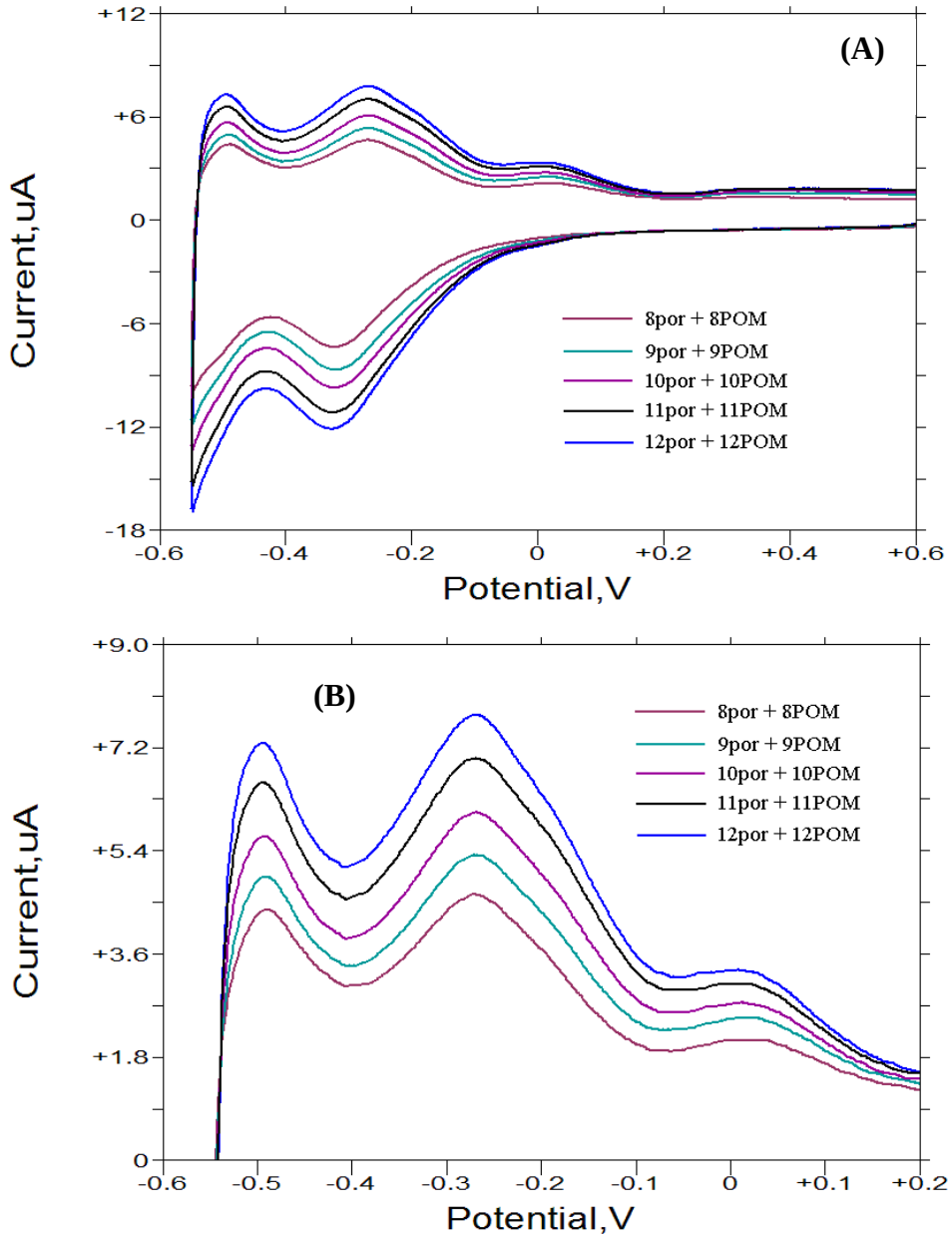

Figure 3.4 (A) Cyclic voltammetry of a film built on ITO using $TMePyP^{4+}$ and $SiW_{12}O_{40}^{4-}$ with different number of bilayers (8 to 12). Each CV was recorded with the POM as the outermost layer. To assure identical and reproducible data, the CV curves shown are the fifth after a preliminary set of polarization cycles. The current in the cyclic voltammograms increases regularly with an increase in the number of bilayers, confirming that a consistent amount of $SiW_{12}O_{40}^{4-}$ and $TMePyP^{4+}$ is deposited at each deposition cycle. **(B)** Detail of the oxidation peaks. (Potential vs. Ag/AgCl).

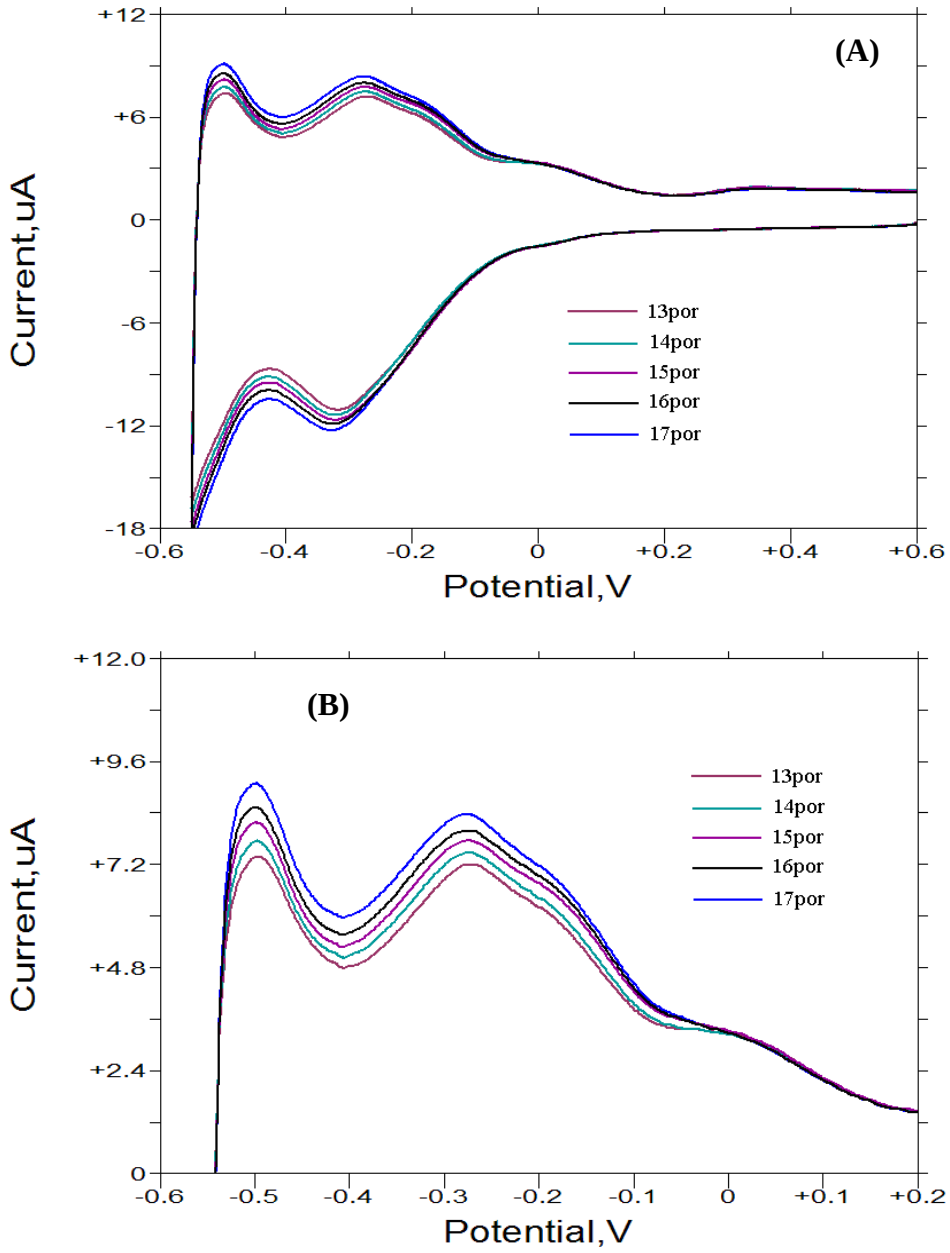

Figure 3.5 (A) Cyclic voltammetry of the same films as in Fig. 3.4 (film built on ITO using $TMePyP^{4+}$ and $SiW_{12}O_{40}^{4-}$), but each CV was recorded with the porphyrin as the outermost layer for deposition cycles 13 to 17. To assure identical and reproducible data, the CV curves shown are the fifth after a preliminary set of polarization cycles. The current in the cyclic voltammograms increases regularly with an increase in the number of bilayers, confirming that a consistent amount of $SiW_{12}O_{40}^{4-}$ and $TMePyP^{4+}$ is deposited at each deposition cycle. **(B)** Details of the oxidation peaks. (Potential vs. Ag/AgCl).

The decrease in the peak height stops after the first four potential scan cycles, indicating that not all hybrid material present on the film undergo the above changes but most likely, only the external part of the film (corresponding to the mobile layer). The changes in the first few CV are observed for both POM and Por as the last deposited compound because as shown in chapter 2 each deposition process does not form a complete layer, leaving some of both materials exposed.[1,22]

However, the film growth during the deposition process is dependent on the composition of the outermost layer, Figure 3.4 and Figure 3.5. Note that the magnitude of the current is significantly less when the porphyrin is the last deposited material compare to when the POM is added last. For layers 13-17 when the porphyrin is added last the current increases from 7.0 μA to 8.6 μA, while for the same film with the POM added last in layers 8-12, the current increases from 4.5 μA to 7.5 μA. So there is a 40% decrease in the current for the additional layers with the porphyrin adsorbed last The differences in the observed current versus layer slopes and magnitude of the currents for the films with porphyrin adsorbed last versus the POM adsorbed last can be for several reasons.

(1) The POM can serve to protect the porphyrin from desorption or decomposition. This may be indicated by the decrease in the porphyrin peak in the first four CV scans (*vide infra*). UV-vis spectra of the solution after the initial four CV scans do not detect any porphyrin but the solutions may be too dilute.

(2) The observed differences in slope and reduced current could correlate with the presence of the mobile layer in deposition cycles 8-12, and the absence of the mobile layer in subsequent deposition cycles 13-17 (see previous chapter). The

films with mobile layers may be more active because they likely have a greater effective electrode surface (i.e. the electrolyte may permeate further into the film), which would result in a greater observed current.

(3) The CV currents also depend on the energetics and electrostatics of the surface, and there are likely some differences in the surface properties when the porphyrin is the last deposited material versus the POM. The sign and density of the surface charges may be different, and there are likely differences arising from the hydrophobic porphyrin core versus the hydrophilic POM.

We will have to do further experiments to differentiate the roles of the mobile layer and the surface energetics in the observed currents. (A) The same layer versus current experiments must be done only looking at dipping cycles 8-12 with the porphyrin last and 13-17 with the POM last. If the same trend is observed (slope is greater for layers 8-12 than for layers 13-17) then the differences may be attributed to the mobile layer. (B) If the slope of the current is still much less when the porphyrin is added last in layers 8-12, than when the POM is added last in layers 13-17, then the surface energetic is the likely source of the differences. Note that the CV experiments are done at pH 3, so there may be significant differences in the Stern layer with a net positive charge from the porphyrin compared to the net negative charge from the POM. Therefore there may be a pH dependence.

The electrochemically initiated desorption (or less likely, the irreversible decomposition of the porphyrin) in the initial four scans may leave fewer molecules on the surface and result in smaller than expected increases in the observed CV currents with

each round of deposition. This may indicate that the POM serves to inhibit the desorption of the porphyrin from the electrode, and that the stability of the outermost portion of the film is better when the POM is added last versus when the porphyrin is added last. This interpretation is also consistent with the reports on the increased stability of the porphyrin in the hybrid catalysis systems.[23] Figure 3.5 shows that when the porphyrin is the outermost layer there is no significant increases the porphyrin oxidation peak near 0 V vs Ag/AgCl.

An alternative explanation can be that the observed CV currents also depend on the net surface charge (overall positive when the Por is the last component, and overall negative when the POM is the last component). Since the CV experiments are run at pH 3 with H_2SO_4, the proton mobility through the interfacial layer may be different.[24] This is consistent with the concept of proton coupled electron transfer.[25]

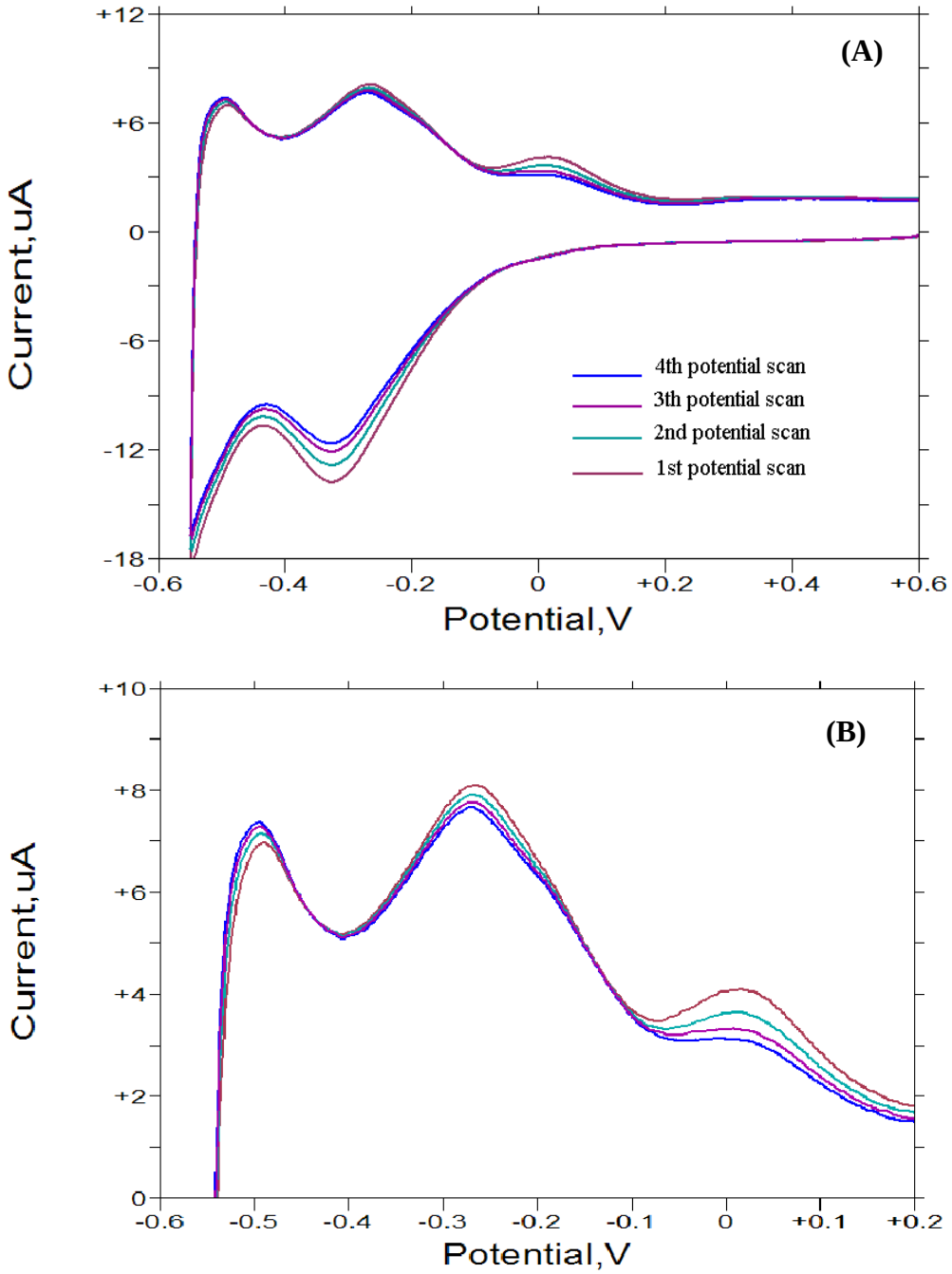

Figure 3.6 (A) Effect of the initial 4 consecutive potential scans on the film built on ITO after 10 deposition cycles with POM as outermost layer. The reduction of the peaks current stops after 4 polarization scans with the fifth scan (not indicated) overlapping the forth one. **(B)** Details of the oxidation peaks. (Potential vs. Ag/AgCl).

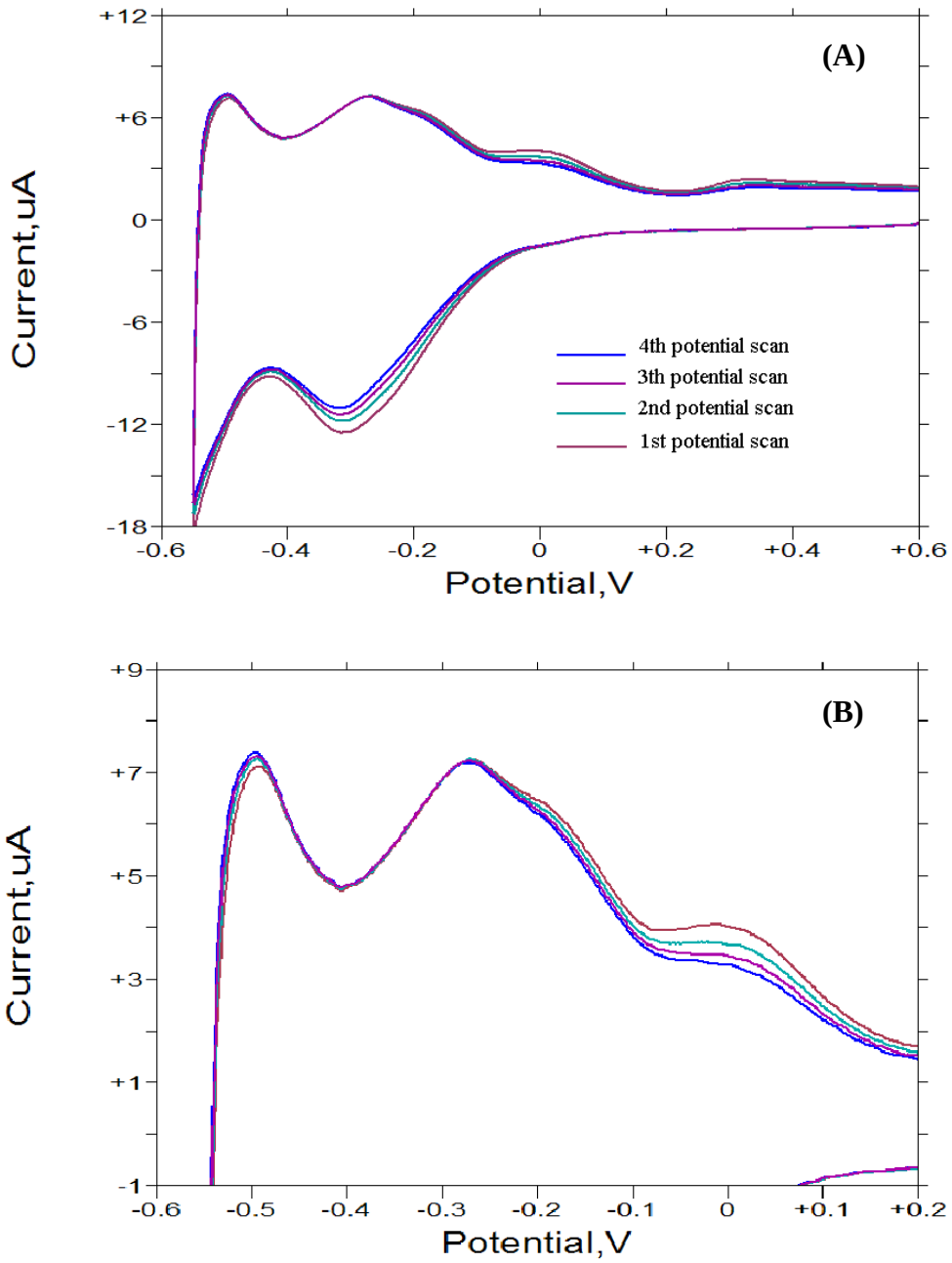

Figure 3.7 (A) Effect of the initial 4 consecutive potential scans on the film built on ITO after 11 deposition cycles with porphyrin as outermost layer. The reduction of the peaks current stops after 4 polarization scans with the fifth scan (not indicated) overlapping the forth one. **(B)** Details of the oxidation peaks. (Potential vs. Ag/AgCl).

3.4 Conclusions

The layer-by-layer deposition process can be successfully adopted for the formation of chemically modified electrodes, without any previous preparation of the electrode surface and using two electroactive small molecules. There is no *a priori* need for either cyclic potential scans or polymeric materials to affect the deposition of thin films consisting of porphyrins and POMs.

The electrochemical responses of the film correspond to the sum of the individual components – the porphyrin and the POM. After the first few deposition cycles necessary to reach a complete coverage of the electrode surface, there is no influence of the film thickness on the electrochemical potentials of the modified electrode. Small increases in the currents are observed for each deposition cycle. This indicates that the electron transfer is still possible in the 0 – 30 nm films. In contrast for electrodes coated with bulk films of redox a polymer, the maximum distance an electron can tunnel is a few angstroms. In order for the electron transfer to go from the electrode to the film surface, a possible electron-hopping mechanism may be involved where electron exchange between neighboring redox sites results in "diffusion" of electrons through the material under the influence of a chemical potential.[26]

These electrochemical experiments are consistent with our previous data in that neither porphyrins nor POMs components result in a uniform, complete layer after a given dipping step and the nanostructured surface has both compounds exposed.

Future work

Electrocatalytic and photoelectrocatalytic properties of the porphyrin/POM film are under investigation. Porphyrins are used as artificial photosensitizers, therefore stimulating the process by light irradiation could change the electrochemical behavior of the film. Catalytic studies on a composite organic/inorganic material formed by association of metalloporphyrins and POMs showed that this material has more efficient catalytic properties than the corresponding metalloporphyrins alone, and that the POMs contributed to the stabilization of the metalloporphyrin against deactivation during the catalytic cycles.[23] Hence, the layer-by-layer method using porphyrin and polyoxometalates can be a very simple and economic technique to fabricate supported catalysts in which catalytically active species are immobilized on the electrode surface, with all the advantages of the heterogeneous catalysis.

Acknowledgement: I wish to thank Mrs. Jing Jing from the laboratory of Prof. Lynn Francesconi for assistance with the CV experiments.

3.5 Chapter 3 References

(1) Bazzan, G.; Smith, W.; Francesconi, L. C.; Drain, C. M. *Langmuir* **2008**, *24*, 3244-3249.

(2) Mitzi, D. B. *Chem. Mater.* **2001**, *13*, 3283-3298.

(3) Kutner, W.; Wang, J.; L'Her, M.; Buck, R. P. *Pure & Appl. Chem.* **1998**, *70*, 1301-1318.

(4) In *Multilayer Thin Films: Sequential Assembly of Nanocomposite Materials*; Decher, G., Schlenoff, J. B., Eds.; Wilei-VCH: 2006.

(5) Meunier, B.; Robert, A.; Pratviel, G.; Bernadou, J. in *The Porphyrin Handbook, Vol. 4* (Eds. Kadish, K.M.; Smith, K.M.; Guilard, R.), Academic Press, San Diego, 2000, pp. 119-188.

(6) Akatsuka, K.; Ebina, Y.; Muramatsu, M.; Sato, T.; Hester, H.; Kumaresan, D.; Schmehl, R. H.; Sasaki, T.; Haga, M. *Langmuir* **2007**, *23*, 6730-6736.

(7) Araki, K.; Wagner, M. J.; Wrighton, M. S. *Langmuir* **1996**, *12*, 5393-5398.

(8) Sun, C.; Zhao, J.; Xu, H.; Sun, Y.; Zhang, X.; Shen, J. *Talanta* **1998**, *46*, 15-21.

(9) Sadakane, M.; Steckhan, E. *Chem. Rev.* **1998**, *98*, 219-238.

(10) Dong, S.; Wang, B. *Electrochim. Acta* **1992**, *37*, 11-16.

(11) Keita, B.; Nadjo, L. *J. Electroanal. Chem.* **1988**, *240*, 325-332.

(12) Keita, B.; Nadjo, L. *J. Electroanal. Chem.* **1987**, *217*, 287-304.

(13) Dong, S.; Wang, B. *Electrochim. Acta* **1992**, *37*, 11-16.

(14) Shiu, K.-K.; Anson, F. C. *J. Electroanal. Chem.* **1991**, *309*, 115-129.

(15) Liu, S.; Kurth, D. G.; Bredenkotter, B.; Volkmer, D. *J. Am. Chem. Soc.* **2002**, *124*, 12279-12287.

(16) Liu, S.; Volkme, D.; Kurth, D. G. *J. Cluster Sci.* **2003**, *14*, 405-419.

(17) Wang, Y.; Hu, C. *Thin Solid Films* **2005**, *476*, 84-91.

(18) Shen, Y.; Liu, J.; Jiang, J.; Liu, B.; Dong, S. *Electroanalysis* **2002**, *14*, 1557-1553.

(19) Shen, Y.; Liu, J.; Jiang, J.; Liu, B.; Dong, S. *J. Phys. Chem. B.* **2003**, *107(36)*, 9744-9748.

(20) Neri, B. P.; Wilson, G. S. *Anal. Chem.* **1972**, *44*, 1002-1009.

(21) Laviron, E. *Electroanalytical Chemistry*; Marcel Dekker: New York, 1983; Vol. 12.

(22) Martel, D.; Gross, M. *J. Solid State Electrochem.* **2007**, *11*, 421-429.

(23) Santos, I. C. M. S.; Rebelo, S. L. H.; Balula, M. S. S.; Martins, R. R. L.; Pereira, M. M. M. S.; Simoes, M. M. Q.; Neves, M. G. P. M. S.; Cavaleiro, J. A. S.; Cavaleiro, A. M. V. *J. Mol. Catal. A: Chem.* **2005**, *231*, 35-45.

(24) Ingersoll, D.; Kulesza, P. J.; Faulkener, L. R. *J. Electrochem. Soc.* **1994**, *141*, 140-147.

(25) Cukier, R. I.; Nocera, D. G. *Annu. Rev. Phys. Chem.* **1998**, *49*, 337.

(26) Laurent, D.; Schlenoff, J. B. *Langmuir* **1997**, *13*, 1552-1557.

Chapter 4

STAMPING PATTERNS OF INSULATED GOLD NANOWIRES WITH SELF-ORGANIZED ULTRATHIN POLYMER FILMS

4.1 Introduction*

The miniaturization of electronics, sensors, displays, and other functional devices has driven intense research and development into new methods to form arrays of nanostructured features on surfaces. Often, these applications require complex patterns of structures with multiple layers and multiple dimensions. There are a variety of lithographic approaches available for the formation of nanostructured materials on surfaces that, similar to those used in the fine arts, can be divided into subtractive and additive methods.[1,2] Subtractive methods are typified by the use of masks or stencils and electromagnetic radiation to systematically etch or chemically alter components of a blank that is comprised of various material layers with appropriate properties for the final nanoscaled device or structure. These subtractive processes are the progeny of photolithographic methods such as blue printing, wherein a mask covers the paper substrate impregnated with two iron complexes and light initiates the formation of an insoluble Prussian blue and water removes the un-reacted salts. Subtractive methods are

* The purpose of this chapter is to provide a brief overview of nanolithographic methods and to describe my contributions to the understanding of the polymer interlayer and capping layers. Adapted from Helt, J. M.; Drain, C. M.; Bazzan, G., Stamping Patterns of Insulated Gold Nanowires with Self-Organized Ultrathin Polymer Films. *J. Am. Chem. Soc.* **2006,** 128, (29), 9371-9377.

well-developed, quite versatile, and are capable of creating structures that are ~10 nm wide to those that are many microns wide. Photolithography is the dominant technique among subtractive methods used commercially, and is the basis for current semiconductor fabrication. As the feature size decreases into the nanometer regime there is a very rapid rise in the costs of manufacturing.

Additive methods are typified by the use of patterned stamps bearing materials, usually on the raised features, which can be transferred to an appropriate substrate by the differences in adhesive forces among the material, the stamp, and the substrate. Exemplary stamping techniques are capable of generating structures down to ca. 10 nm wide but are generally limited to the parallel transfer of one material at a time.[1] Stamps descend from lithography wherein a pattern of an oily ink surrounded by a film of water is transferred to paper by the greater affinity of the ink to the paper than to the limestone, wood, or alumina substrate. Microcontact printing (μCP) belongs to this category, and relies on the use of a polydimethylsiloxane (PDMS) stamp.[3,4]

Many nanofabrication technique use elastomeric materials to fabricate or reproduce patterns, these are grouped under the name of "Soft Lithography."[2,5,6] Among the most common soft lithography techniques there are: replica molding,[7] microtransfer molding,[8] micromolding in capillaries,[9] nanotransfer printing.[10] PDMS is the most common elastomer used because of properties such as chemical stability, optical transparency, thermal stability, reversible deformation. But PDMS also presents a number of technical problems: sagging, shrinking upon curing, and softness that limits the aspect ratio of the microstructures.[11]

In nanoimprint lithography and its variations (see chapter 5) the polymer used is usually thermoplastic or UV/thermally curable.[12] The use of AFM tips to engrave (nanoshaving)[13] and write (dip pen)[14] nanoscaled patterns are also available and are analogous to etching and hand-drawing.

In this chapter we demonstrate that the unique behavior of ultrathin polymer films and polymers at interfaces provides another means to pattern arrays of self-aligned micro- to nanoscaled heterostructures on ceramic surfaces. The thermal nanotransfer of polymer-metal heterostructures detailed here enables direct fabrication of multilayer architectures in a rapid, parallel fashion without employing advanced lithographic tooling or "wet" chemistry for pattern development.

The formation of nanostructured arrays of thermoplastic materials on substrates, using liquid monomers that are later polymerized or solid plastic "inks," has been reported.[2,15-26] Allyl monomers can be used in nanoimprint lithography and heating during the imprint process cures the polymer to form the final structure.[17] Capillary forces can be exploited to place polymer solutions into recessed stamp features,[16] and for nanoimprint methods of thin films.[18,27] The squeezed flow of polymers into cavities has been modeled and demonstrated.[19] Some polymers have been doped with fluorescent dyes to form solid-state dye lasers.[28] Enabled by differential wetting/dewetting, patterns of thin polystyrene (PS) films on chemically patterned substrates has been demonstrated,[20] and the transfer of polymers from molds to substrates has also been discussed.[15] The processes wherein a solid polymer is transferred from the stamp to a substrate have some relevance to the processes described herein in that they both exploit wetting/dewetting dynamics, for example described by de Gennes,[29] and the unique

properties of interfacial polymer films (see below). The use of interfacial forces for nanolithography has been demonstrated by both the soft lithographic transfer techniques[30,31] and in recent developments in technologies for the fabrication of organic display.[32,33]

We demonstrate a nanolithographic method for the formation of polymer insulated gold nanowires in a single processing step that yields a product with three distinct layers: polymer-metal-polymer (PMP structures) with submicrometer dimensions.

4.2 Previous Findings from Prof. C.M. Drain's Lab

A new patterning technique to fabricate polymer-metal-polymer heterostructures was developed by Dr. James Helt, a previous Ph.D. student in the Drain laboratory. A schematic of the multilayer thermal nanotransfer process is illustrated in Figure 4.1. A thermoplastic polymer is coated with a discontinuous thin film of gold, then the coated stamp is compressed against a substrate (mica, glass, silicon, ITO), briefly heated (to temperature within $-45 < T_g < 10$ °C), and subsequently separated from the substrate after cooling. The products are trilayered features formed on the surface, that are composed of a polymer interlayer that binds the feature to the ceramic surface, a thin gold wire, and a capping layer.[34]

The formation of the insulated gold heterostructure is enabled by the physics of ultrathin polymer films and differential adhesion forces originating from polymer reorganization at the stamp-gold interface.[35-41] The general mechanism includes:

(1) The spreading and self-organization of the polymer interlayer. This can be understood in terms of wetting phenomena and surface energetics. The high surface energy of gold ($\gamma \sim 1800$ mN/m at 145 °C)[42] and mica ($\gamma \sim 144$ nN/m)[5] promotes intercalation of the polymeric material into the metal-substrate interface by capillary forces. Intercalation of polymer stamp materials into the metal-substrate interface yields a cohesive polymer layer that binds the metal layer to the substrate (Fig. 4.2).

(2) The formation of a polymer-polymer "interface" between the capping layer and the bulk stamp and the cohesive failure at this "interface." This can be explained by the physical properties of ultrathin polymer films (see chapter 5 for detailed explanations).

Stamps preparation

The stamps were prepared using either commercially available CD and DVD (see chapter 5 for more details), or by compression molding of thermoplastic Lexan® sheets on a patterned silicon wafer master. The polymeric stamps were then coated with a thin film of gold via sputter coating, typically the gold thickness ranged from 3 nm to 25 nm.

Stamping procedure

The gold coated stamps were compressed against the ceramic substrate at ~1 MPa for 1-5 min at $T = -45 < T_g < 10$ °C in a home-built stamping apparatus. The duration of the time at the maximum temperature is referred to as the dwell time and the specific processing parameters are highly dependent on the polymer used in the stamp, the thickness of the gold coating, and the substrate.

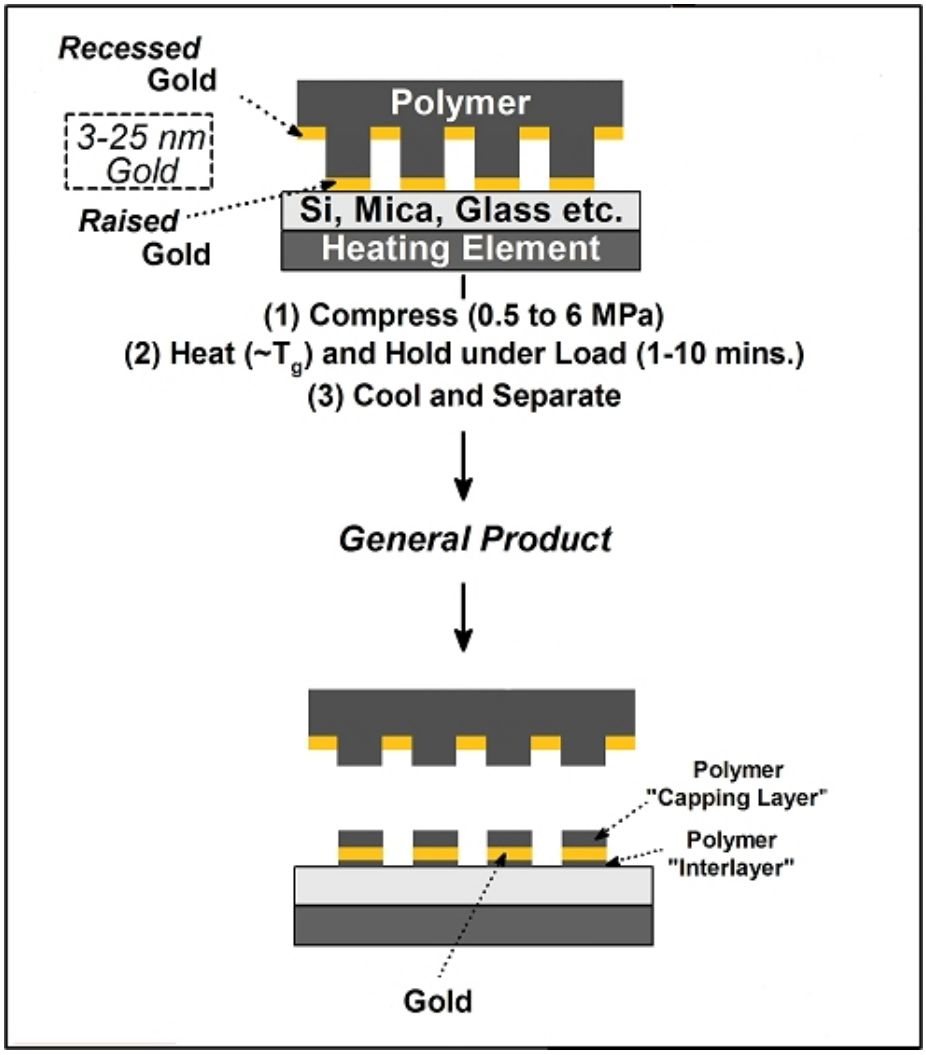

Figure 4.1 Schematic of the multilayer thermal nanotransfer process where polymer-metal heterostructures are fabricated from a bilevel polymer stamp coated with a thin Au film. The coated polymer stamp is brought into compressive contact with a substrate, briefly heated, and subsequently separated from the substrate after cooling. Trilayer structures, comprised of a polymer interlayer, a gold film layer, and a polymer capping layer are formed. Adapted from Ref. 34.

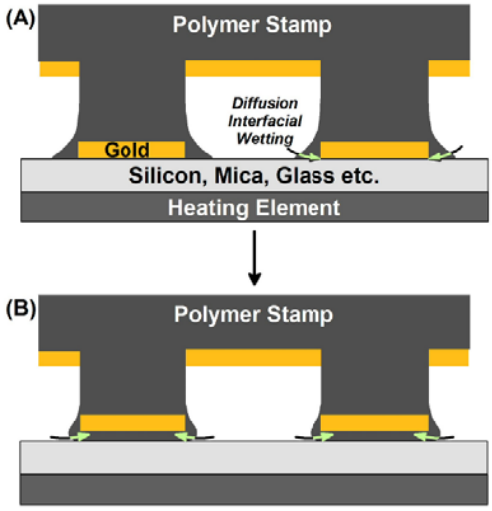

Figure 4.2 Under pressure and heating, polymer flow from the edge (top) and then migrates to the center (bottom) for thick Au films. This process is driven by capillary forces and interfacial energetics. For thin porous Au (< 10nm thick) films diffusion through the pores of the film is likely to occur as well. The relative dimensions of the mobile polymer layer to the stamp features are not drawn to scale. Adapted from Ref. 34.

4.3 Results and Discussion

We focus on the defect structures in the products of this stamping process because these give significant insight into the physical properties of the features and the mechanism of formation. However, large cm^2 areas have been stamped with patterns of the polymer insulated gold nanowires with high fidelity.

The trilayer features fabricated on mica using a CD stamp coated with 15 nm of gold are shown in Figure 4.3. Section analysis of the AFM images reveals a structure height of ~ 27 nm (excluding the prominent polymer edge feature of ~ 85 nm) and the presence of a ledge that is thought to arise from removal of the capping layer from the gold wire during the stamp separation step (by dewetting and/or asymmetric fracture). Assuming that the ledge nominally corresponds to the top of the gold film surface, then the

measured thickness of the capping layer is ~8 nm and the inferred thickness of the polymer interlayer is ~4 nm. This estimated thickness of the interlayer serves as an upper limit, considering that a finite capping layer (perhaps on the order of the Au film RMS roughness ~1.2 nm) may indeed exist on the ledge. This ultrathin polymer interlayer is an integral component of this transfer process as it acts to bind the metal film to the substrate and, therefore, must be sufficiently robust to withstand the tensile forces exerted during stamp-substrate separation.[43]

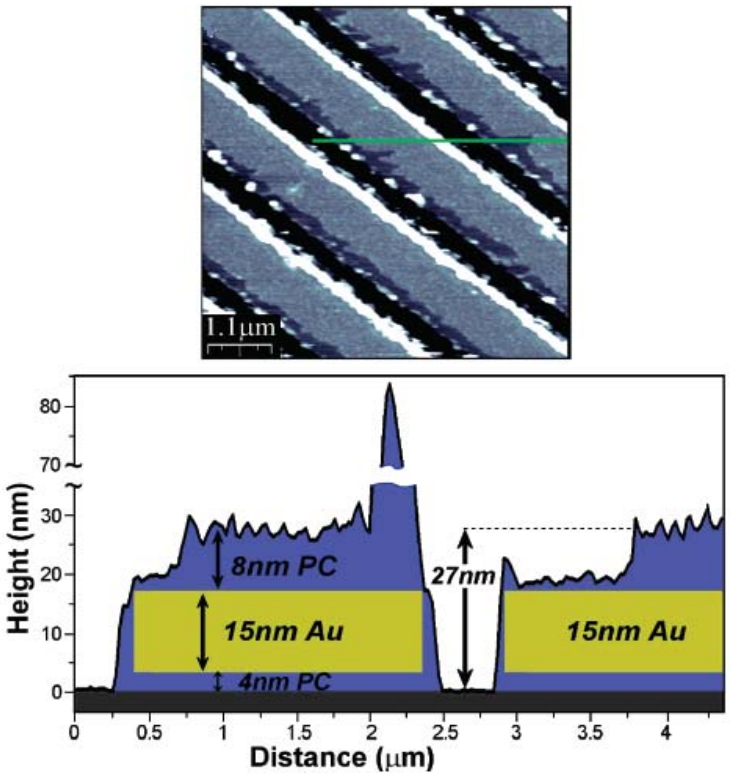

Figure 4.3 AFM topography and section analysis of microstructures fabricated on mica using a bilevel polycarbonate compact disk (CD) stamp coated with 15 nm of Au. Fabrication was conducted at 145 °C for 10 min under an applied pressure of 1.3 MPa. The trilayer structures possess a total height of ~27 nm as illustrated in the AFM topography profile. Incomplete spreading, dewetting, or fracture of the capping layer leads to a ledge in the topography. The capping layer thickness is estimated from this ledge to be h ~8 nm, which provides an upper limit for the thickness of the polymer interlayer (h ~4 nm) considering that a finite capping layer.

Direct Measurement of the Polymer Interlayer Thickness

The thickness of the polymer interlayer film was obtained in two different ways. Direct measurement of the interlayer was done by chemically etching away the gold metal layer which also removes the capping layer. AFM was used to analyze the regions bearing both residual structures and regions where the gold as well as polymer capping layer have been completely removed (Fig. 4.4). AFM enables the polymer interlayer to be directly imaged, and reveals an interlayer thickness of ca. 5 nm (excluding the prominent polymer features) for this stamp geometry and processing conditions (135°C, 10 nm gold layer).

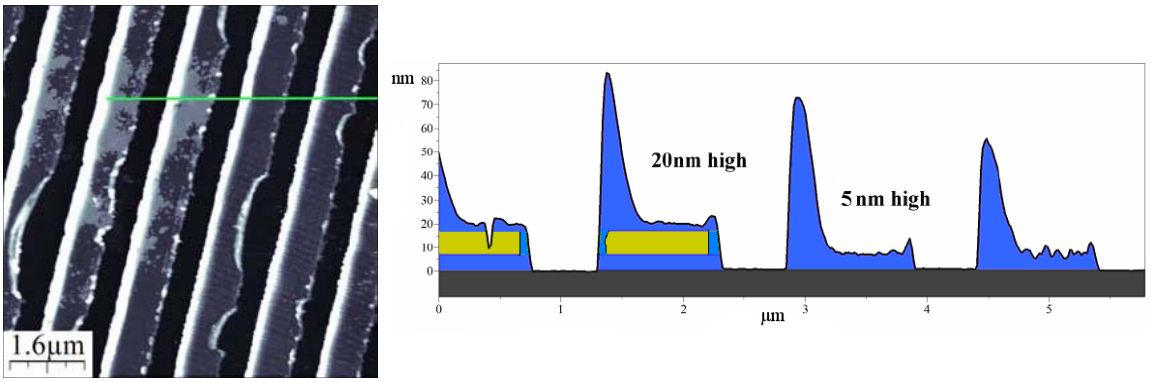

Figure 4.4 AFM topography image (left) of a region of a thermal nanolithograpty of polymer-metal heterostructures product using a CD stamp, with 10 nm Au layer. The left few lines are complete structures and the right few lines are a region wherein the gold has been completely removed via chemical etching. The cross section (right) is filled in to represent the gold (yellow) and polymer (blue) regions. The thickness of the polymer sidewalls are not drawn to scale and are anticipated to be incomplete films.

The polymer interlayer thickness can be obtained also by subtracting from the total thickness of the microstructures, the thickness of the gold layer plus capping layer. The latter can be measure by AFM after either nanoshaving or ozone etching of the capping layer. The three methods to measure the components of the features are generally consistent, with deviations typically on the order of the roughness of the gold layer (ca. 2 nm) and of the substrate.

Figure 4.5 shows the result of a nanoshaving experiment on a pattern fabricated on native silicon oxide, using stamps produced with Lexan® polycarbonate and coated with 20 nm gold film. The stamps had 300 nm tall features with 25 μm wide raised lines and 200 μm pitch. The capping layer is smooth with a height of ~20 nm. Nanoshaving yields to a ~22 nm, inferring a thickness of ca. 2 nm.

Using Lexan® polycarbonate as the thermoplastic polymer stamp results in products with grater coverage, pattern fidelity, and thicker capping layer then the products generated with CDs. The presence of glass fillers in CD stamps and differences in molecular weight can be a reason for these differences. The fabrication of wider structures on silicon oxide (e.g. the 25 μm wide lines in Fig. 4.5) results in a very thin 1-2 nm and incomplete interlayer, but there is still enough polymer intercalated to bind the metal film to the substrate (Fig. 4.6).

Poor contact parallelism during the pattern fabrication leads to the formation of locally asymmetric features. This can be manifested by a sliding of the polymer capping layer during the pattern fabrication (Fig. 4.7), and is only observed when stamping micrometer size features.

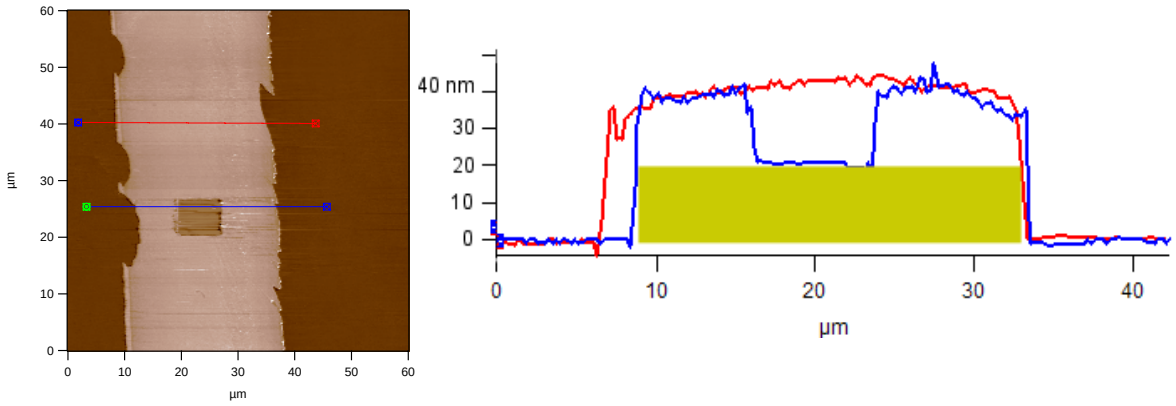

Figure 4.5 Structure fabricated with a Lexan® polycarbonate stamp coated with 20 nm gold. The processing temperature, dwell time and initial contact pressure were 100°C, 2 minutes and 1.3 MPa respectively. The capping layer is symmetric with a height of ~20 nm. Nanoshaving yields a 22 nm height, inferring a ~2 nm interlayer. The thickness of the polymer sidewalls are not drawn to scale and are anticipated to be incomplete films.

Figure 4.6 Schematic representation of wide gold-insulated nanowire (10-25 µm). Because of the large structure the polymer interlayer is incomplete. However enough polymer intercalates between the gold and the substrate to bind the metal film on the surface. The thickness of the polymer sidewalls are not drawn to scale and are anticipated to be incomplete films.

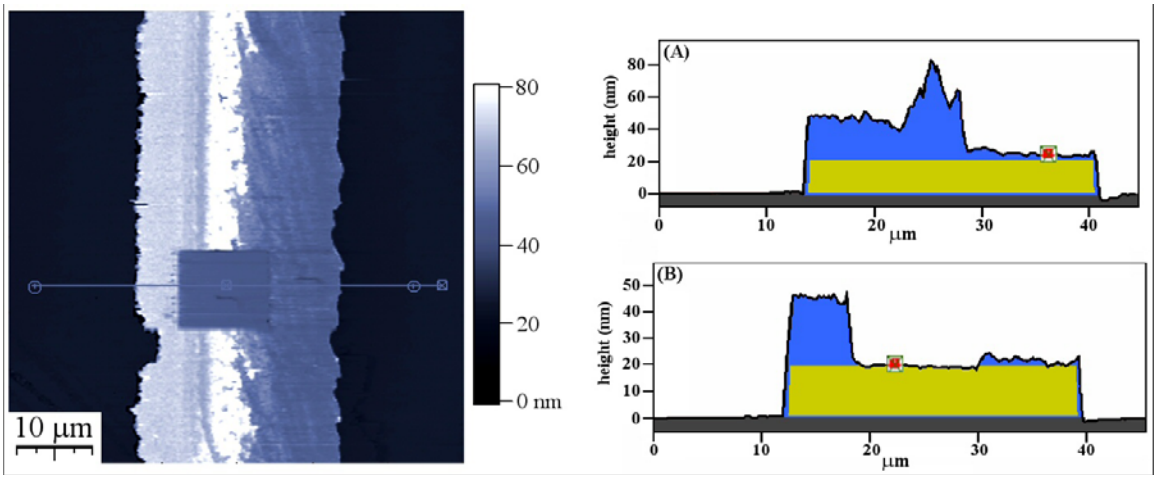

Figure 4.7 Structure fabricated with a Lexan® polycarbonate stamp coated with 20 nm gold. The processing temperature, dwell time and initial contact pressure were 135°C, 2 minutes and 1.3 MPa respectively. (A) AFM imaging (left) reveals the asymmetric capping layer. (B) Removal of the capping layer by nanoshaving down to the gold layer yields a 22 nm height, inferring a ~2 nm interlayer. The thickness of the polymer sidewalls are not drawn to scale and are anticipated to be incomplete films.

4.4 Conclusions

The transfer of insulated submicrometer wide wires from the raised stamp features affords patterns of trilayered PMP structures with uniform wire dimensions. A variety of ceramic substrates, thermoplastic materials, and metals can be used; e.g., inexpensive gold-coated CD or DVD media can be used as stamps, where the combination of materials dictates the relative interfacial forces and the processing parameters. A single processing step yields a product with three distinct layers with nanoscaled dimensions.

The behavior of ultrathin polymer films can be exploited for the fabrication of nanopatterns on ceramic substrates. The fabrication of trilayered nanoscaled structures occurs with greater structural fidelity and greater yield in term of coverage than using than using the same material and conditions to produce micron-scaled features. The polymer insulated gold nanowires may be used in circuitry, electronics or sensors.

4.5 Chapter 4 Reference

(1) *Adv. Mater.* **2004**, *16*, 1245-1377.

(2) Gates, B. D. *Materials Today* **2005**, *8*, 44-49.

(3) Kumar, A.; Whitesides, G. M. *Appl Phys Lett* **1993**, *63*, 2002-2004.

(4) Moran, C. E.; Radloff, C.; Halas, N. J. *Adv. Mater.* **2003**, *15*, 804-807.

(5) Christenson, H. K. *J Phys Chem* **1993**, *97*, 12034-12041.

(6) Xia, Y. N.; Rogers, J. A.; Paul, K. E.; Whitesides, G. M. *Chem Rev* **1999**, *99*, 1823-1848.

(7) Xia, Y.; Whitesides, G. M. *Angew. Chem. Int. Ed.* **1998**, *37*, 550-575.

(8) Zhao, X.-M.; Xia, Y.; Whitesides, G. M. *Adv. Mater.* **1996**, *8*, 837-840.

(9) Kim, E.; Xia, Y. N.; Whitesides, G. M. *Nature* **1995**, *376*, 581-584.

(10) Loo, Y. L.; Willett, R. L.; Baldwin, K. W.; Rogers, J. A. *J. Am. Chem. Soc.* **2002**, *124*, 7654-7655.

(11) Xia, Y.; Whitesides, G. M. *Annu. Rev. Mater. Sci.* **1998**, *28*, 153-84.

(12) Guo, L. J. *J. Phys. D: Appl. Phys.* **2004**, *37*, R123-R141

(13) Liu, G. Y.; Xu, S.; Qian, Y. *Acc. Chem. Res.* **2000**, *33*, 457-466.

(14) Piner, R. D.; Zhu, J.; Xu, F.; Hong, S.; Mirkin, C. A. *Science* **1999**, *283*, 661-663.

(15) Huang, X. D.; Bao, L. R.; Cheng, X.; Guo, L. J.; Pang, S. W.; Yee, A. F. *J. Vac. Sci. Technol. B* **2002**, *20*, 2872-2876.

(16) Salleo, A.; Wong, W. S.; Chabinyc, M. L.; Paul, K. E.; Street, R. A. *Adv. Funct. Mater.* **2005**, *15*, 1105-1110.

(17) Reuther, F.; Kubenz, M.; Schuster, C.; Fink, M.; Vogler, M.; Gruetzner, G.; Grimm, J.; Kaeppel, A. In *Emerging Lithographic Technologies IX*; Mackay, R. S., Ed.; SPIE: San Jose, CA, USA: 2005; Vol. 5751, p pp 976-985.

(18) Kehagias, N.; Zelsmann, M.; Torres, C. M. S. In *Opto-Ireland 2005: Optoelectronics, Photonic Devices, and Optical Networks*; McInerney, J. G., Farrell, G., Denieffe, D. M., Barry, L. P., Gamble, H. S., Hughes, P. J., Moore, A., Eds.; SPIE: Dublin, Ireland: 2005; Vol. Vol. 5825, p pp 654-660.

(19) Bogdanski, N.; Wissen, M.; Ziegler, A.; Scheer, H.-C. *Microelectronic Engineering* **2005**, *78-79*, 598-604.

(20) Zhang, Z.; Wang, Z.; Xing, R.; Han, Y. *Polymer* **2003**, *44*, 3737-3743.

(21) Suh, K. Y.; Langer, R. *Appl. Phys. Lett.* **2003**, *83*, 1668-1670.

(22) Gourdin, S.; Hammond, P.; Crites, T.; Coe, S.; Bulovic, V. In *Materials Research Society Symposium D - Proceedings*; Shur, M. S., Wilson, P. M., Urban, D., Eds.; MRS: 2002; Vol. 736, p pp 271-276.

(23) Meitl, M. A.; Zhu, Z. T.; Lee, K. J.; Nuzzo, R. G.; Rogers, J. A.; Kumar, V.; Adesida, I.; Feng, X.; Huang, Y. Y. *Nat Mater* **2006**, *5*, 33-38.

(24) Rogers, J. A.; Nuzzo, R. G. *Materials Today* **2005**, 50-56.

(25) Nielsen, T.; Pedersen, R. H.; Hansen, O.; Kristensen, A.; Haatainen, T.; Tolkki, A.; Ahopelto, J. In *Technical Digest of the 18th IEEE Conference on Micro Electro Mechanical Systems*; MEMS 2005,: Miami, FL: 2005, p 508-511.

(26) Kee, C. S.; Yoon, K. B.; Choi, C. G. I.; Kim, J. T.; Han, S. P.; Park, S.; Schift, H. J. *Nonlinear Opt. Phys. Mater.* **2005**, *14*, 299-303.

(27) Menard, E.; Bilhaut, L.; Zaumseil, J.; Rogers, J. A. *Langmuir* **2004**, *20*, 6871-6878.

(28) Nilsson, D.; Nielsen, T.; Kristensen, A. *Rev. Sci. Instrum.* **2004**, *75*, 4481-4486.

(29) de Gennes, P. G. *Rev. Mod. Phys.* **1985**, *57*, 827-863.

(30) Ahn, H.; Lee, K. J.; Shim, A.; Rogers, J. A.; Nuzzo, R. G. *Nano Lett.* **2005**, *5*, 2533-2537.

(31) Childs, W. R.; Motala, M. J.; Lee, K. J.; Nuzzo, R. G. *Langmuir* **2005**, *21*, 10096-10105.

(32) Lee, J. Y.; Lee, S. T. *Adv. Mater.* **2004**, *16*, 51-54.

(33) Chin, B. D.; Suh, M. C.; Kim, M. H.; Kang, T. M.; Yang, N. C.; Song, M. W.; Lee, S. T.; Kwon, J. H.; Chung, H. K.; Wolk, M. B.; Bellmann, E.; Baetzoldb, J. P. *J. Information Display* **2003**, *4*, 1-5.

(34) Helt, J. M.; Drain, C. M.; Bazzan, G. *J. Am. Chem. Soc.* **2006**, *128*, 9371-9377.

(35) Ellison, C. J.; Torkelson, J. M. *Nat Mater* **2003**, *2*, 695-700.

(36) Forrest, J. A.; Dalnoki-Veress, K.; Dutcher, J. R. *Physical Review E* **1997**, *56*, 5705.

(37) Forrest, J. A.; Dalnoki-Veress, K.; Stevens, J. R.; Dutcher, J. R. *Phys. Rev. Lett.* **1996**, *77*, 2002–2005.

(38) Fukao, K.; Miyamoto, Y. *Physical Review E* **2000**, *61*, 1743-1754.

(39) Kawana, S.; Jones, R. A. L. *Phys. Rev. E* **2001**, *63*, 021501.

(40) Sharp, J. S.; Teichroeb, J. H.; Forrest, J. A. *Eur. Phys. J. E* **2004**, *15*, 473-487.

(41) Soles, C. L.; Douglas, J. F.; Wu, W. l.; Peng, H.; Gidley, D. W. *Macromolecules* **2004**, *37*, 2890-2900.

(42) Vermaak, J. S.; Kuhlmann-Wilsdorf, D. *J Phys Chem* **1968**, *72*, 4150-4154.

(43) Burkstrand, J. M. *J. Appl. Phys.* **1981**, *52*, 4795-4800.

Chapter 5

POLYMER NANOLITHOGRAPHY BY THERMAL CONTACT NANOTRANSFER

5.1 Introduction

A number of different methods can be used to fabricate nanoscale patterns, and an overview of the conventional patterning technology, such as photolithography and soft lithography, is offered in chapter 4. Among these technologies nanoimprinting lithography (NIL), also known as embossing lithography, has attracted increasing attention in recent years as an inexpensive alternative for nanopattern fabrication. MIT's Technology Review has put NIL as one of 10 emerging technologies that are likely to change the world.[1]

NIL was first introduce by Chou *et al* in 1997.[2] Typically a rigid patterned mold is pressed into a thin thermoplastic polymer film coating a substrate, and heating the polymer to above its glass transition temperature (T_g) allows it to flow into the recessed features of the stamp under an applied pressure. The polymer and mold are then cooled to a temperature below T_g of the polymer, and the mold is separated from the polymer. A thickness contrast is created in the polymer on the surface and the thinner parts of the relief are anisotropically removed by oxygen plasma etching, producing the isolated features on the surface (Fig. 5.1).[3] This leaves a pattern of the polymer and the exposed surface. This lithography has many advantages, for example simple processing and low cost, because it does not require expensive instrumentation and clean room. Further

development of NIL have allowed formation of products with very small lateral resolution[4] to less than 10 nm, high replication fidelity, and high throughput.[5]

NIL relies on viscous polymer flow during the polymer film deformation to create the thickness contrast, hence high temperature (50-100 °C) and pressure (up to 10 MPa) are required to obtain reliable pattern transfer,[6,7] and mold surface treatment or modification is necessary for clean release of the mold from the patterned polymer substrate.[8] Several modifications to NIL have been introduced to overcome or minimize these problems and to further develop the technique, including: (a) low-pressure nanoimprinting[9] that uses a special fluoropolymer film mold; (b) reversal imprinting[10] wherein the polymer is spin coated on the hard mold and then transferred to the substrate; (c) room-temperature imprinting[11] in which the polymeric film coating the substrate is treated with solvent vapor; and (d) step-and-flash imprint lithography[12] (SFIL) that uses a low-viscosity pre-polymer material that is then photocured using UV light transmitted through the transparent mold.

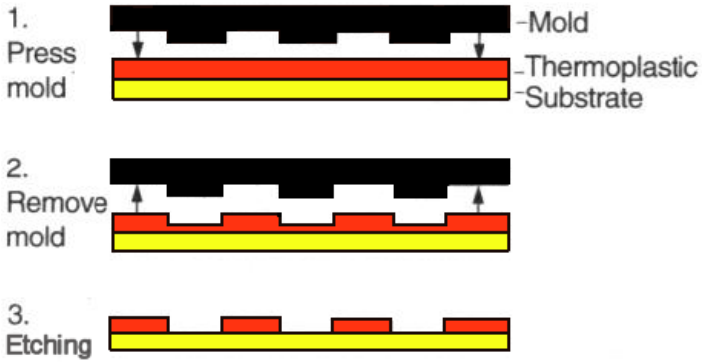

Figure 5.1 Schematic of NIL process. Compression molding is used to create a thickness contrast on the polymer film deposited on the substrate. Anisotropic etching is used to expose the substrate material.

NIL can be applied to a wide range of materials (both inert polymers and functional polymers can be used)[13] which allows the formation of a variety of organic-based optoelectronic devices. In organic optoelectronics, the embossed film consists of materials that either play an active role in a device (e.g. electroluminescent layer) or serve as structures onto which active materials are deposited. Among the devices fabricated using NIL, there are nonlinear optical (NLO) polymer nanostaructures,[14] high resolution organic polymer light-emitting (OLED) pixels,[15] and organic thin-film transistor (TFT).[16]

Herein we describe a new polymer nanolithography technique, based on thermal contact nanotransfer, that results in nano- to micro- scaled patterns of ca. 10 nm thick polymer on ceramic surfaces. The present method evolved from our previous work on the nanofabrication of polymer insulated gold nanowire patterns by self-organization of polymer films on ceramic surfaces,[17] and from our method to fabricated patterns of gold nanowires on polymer surfaces.[18] These three patterning methods exploit the unique physical properties of ultrathin polymer films such as the dynamics of polymers at interfaces.[19,20]

The present stamping method allows multiple stamping processes on a single substrate to afford more complex multilayered patterns, and the polymers can be doped with fluorescent dyes and other functional materials to afford photonic patterns. A significant advantage of the thermal contact nanotransfer method is that inexpensive CDs and DVDs can be used as the stamps and that the method can be affected by an inexpensive, laboratory-built, stamping apparatus. Secondly, this process results in

patterns of films similar to the NIL method, albeit with smaller heights, but obviates the need for the etching step.

There are numerous potential applications of nanopaterns of polymers on surfaces, that range from the masking of the ceramic substrate for chemical modification, deposition of materials on the unmasked substrate, and the further elaboration of nanostructured materials.

5.2 Experimental Procedure

The stamping process has been carried out using a home built stamping apparatus (built by Dr. James Helt, Appendix 5.1). The polymeric nanostructures are formed by the compression of a thermoplastic polymer stamp against a ceramic substrate, the system is than briefly heated, and the stamp is subsequently separated from the substrate after cooling. We used glass and indium-tin oxide (ITO) as substrates. The resulting structures were then characterized with atomic force microscopy (AFM), scanning electron microscopy (SEM), and confocal microscopy.

Atomic force microscope (AFM) measurements were made with an Asylum Research MFP-3D AFM (Santa Barbara, CA). Images were acquired in air using commercial silicon tips (MikroMasch USA, Portland, OR) in AC mode (tapping mode) (NSC15/AlBS) with a typical tip curvature radius of less than 10 nm (NSC15, force constant = 40N/m, resonance frequency = 325 kHz). The z scale was calibrated using commercial calibration grids (MikroMasch USA, Portland, OR). Scanning electron microscopy (SEM) images were obtained with a Carl Zeiss DSM 940. To minimize charging, the typical SEM imaging conditions used an electron beam current at the

sample of ~110 mA with an acceleration voltage of 3.1 kV. A Varian Cary Bio-3 spectrophotometer was used for UV-visible spectroscopy, in double-beam mode. Steady-state fluorescence spectra were taken on a Fluorolog-3, with excitation at the maximum UV-visible absorbance (Soret band). Confocal images were recorded with a Leica TCS SP2 using the 514 nm laser excitation of porphyrin Q-band.

Polymer Stamp Preparation

Recordable compact discs (CD-R) were used as polymer stamps. CD-R generally consist in four layers of material: (1) a a grooved polycarbonate substrate ~1.2 mm thick, (2) a thin layer of organic dye, (3) a few nanometer thick metal layer, (4) a protective coating of lacquer (Fig.5.2). The metal used as reflecting layer can be silver, silver alloy, aluminum, or gold. We used the aluminum coated discs as stamp and passivated gold coated discs as master for preparation of stamps of different polymeric material. Specifically, Imation (5067 149RE 19948), and Delkin Archival Gold (6298 2131 5612) were used. The CD-R were cut in 20x20 mm pieces and immersed in concentrated HNO_3 for 3 minutes, then were rinsed copiously with water, and dried under a stream of N_2 gas.

HNO_3 treatment of the Imation CD-R, which have a metal layer of aluminum,* results in the delamination of the protective lacquer layer and dissolution of the Al layer,[21] leaving a grating structure of polycarbonate with lines ~120 nm deep, ~900 nm wide and a pitch of 1.6 μm (Fig. 5.3). UV-visible analysis of the CD-R after the delaminating process indicates the recording layer containing the dye (usually a phthalocyanine) is removed as well. The samples prepared in this way were then directly used for stamping without further processing.

*Imation technical information see www.imation.com

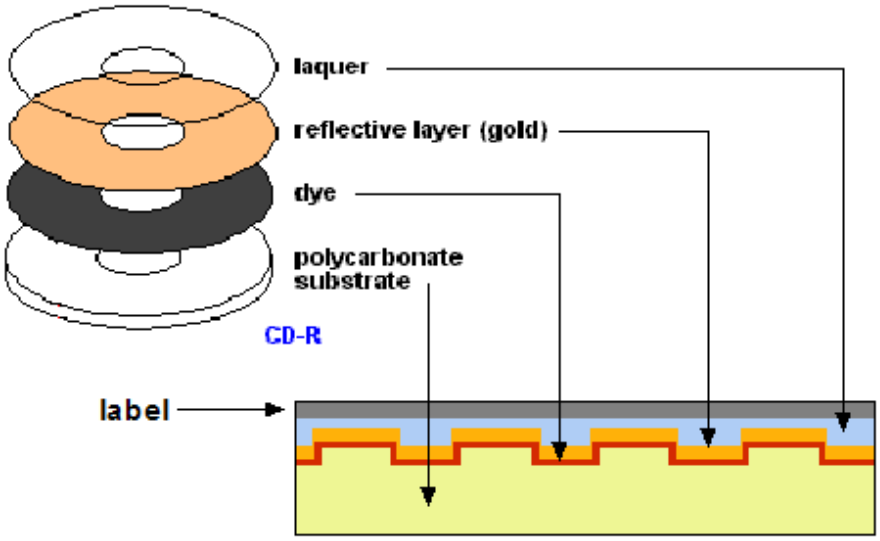

Figure 5.2 Schematic of a recordable compact disc (CD-R) composition. CD-R generally consist of four layers of material: (1) a grooved polycarbonate substrate ~1.2 mm thick, (2) a thin layer of photosensitive organic dye, (3) a nanometer thick metal layer, (4) a protecting coating of lacquer. (Modified from "The computer desktop encyclopedia 1998").

When the Delkin Archival Gold CD-R, with a reflective layer of >92% gold, is treated with HNO_3 only the protective polymer film is removed.[22] The gold coated CD-R have similar feature sizes to the Imation CD-R, with a layer of gold of ~ 50 nm, as estimated by AFM after etching the Au layer with Transene gold etchant type TFA (Danvers, MA) (Fig. 5.4). Self-assembled monolayers (SAMs) of 1-octanethiol were prepared by immersing freshly prepared gold substrates into a dilute solution (1.0 mM) of 1-octanethiol in absolute ethanol for 18-24 h.

The gold substrates modified with SAMs were rinsed sequentially with absolute ethanol and water, and then dried with N_2 gas. The completeness of the film coverage was assayed by observed differences in the water contact angles on the untreated and treated surfaces. Greater contact angles for deionized water on the gold substrate

modified with SAMs are expected due to the hydrophobicity of the hydrocarbon chains compared to the bare gold surface. This quick assay confirms the coverage of the gold surface by the alkanethiols SAM. AFM analysis of the modified gold substrate shows that the passivation with the SAM does not modify the morphology of the gold surface.

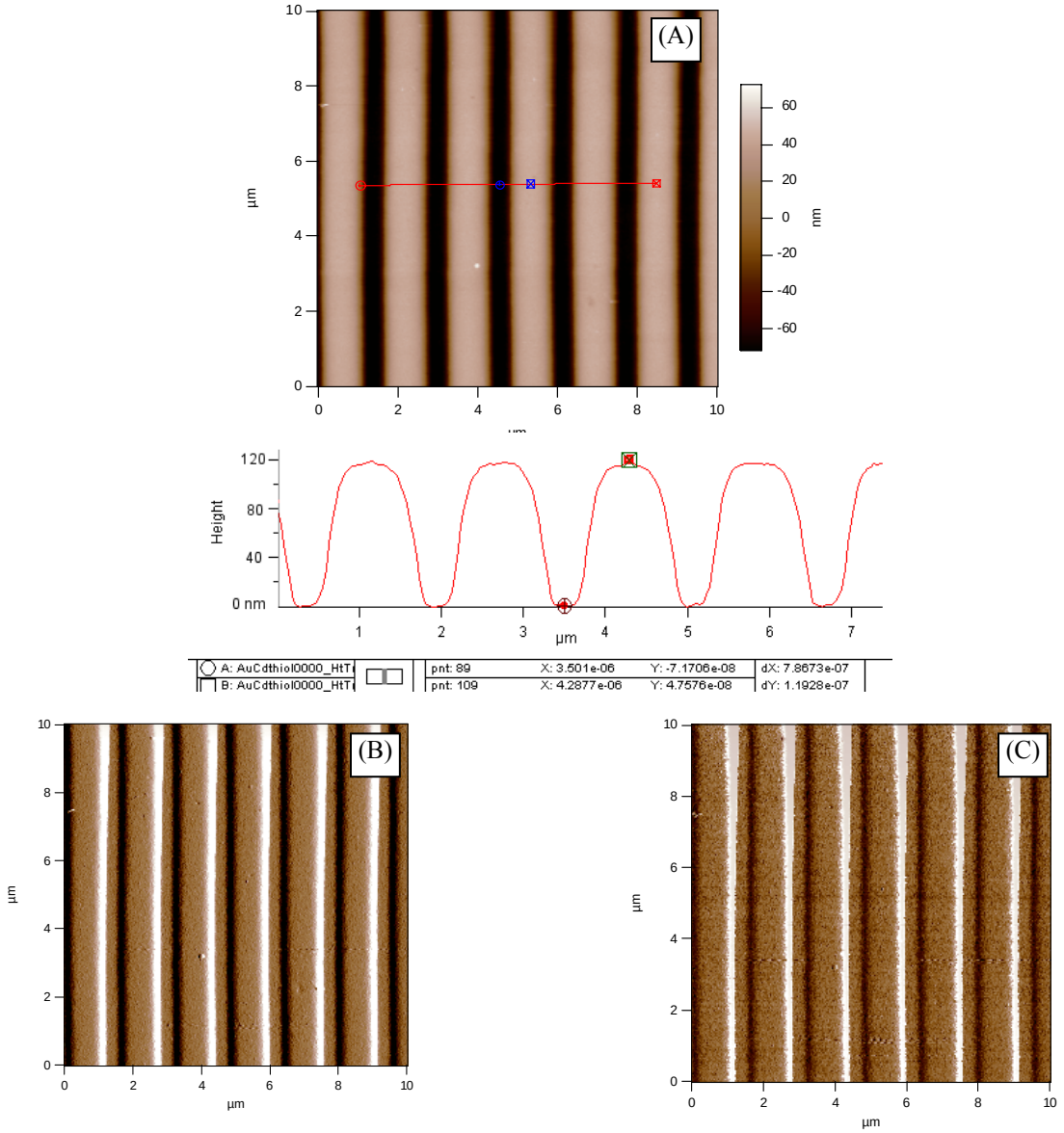

Figure 5.3 AFM images of a Imation CD-R after treatment with conc. HNO_3. (A) Height image, (B) Amplitude Image, (C) Phase Image. The bare polycarbonate grating structure has lines ~120 nm deep,~900 nm wide and a pitch of 1.6 µm

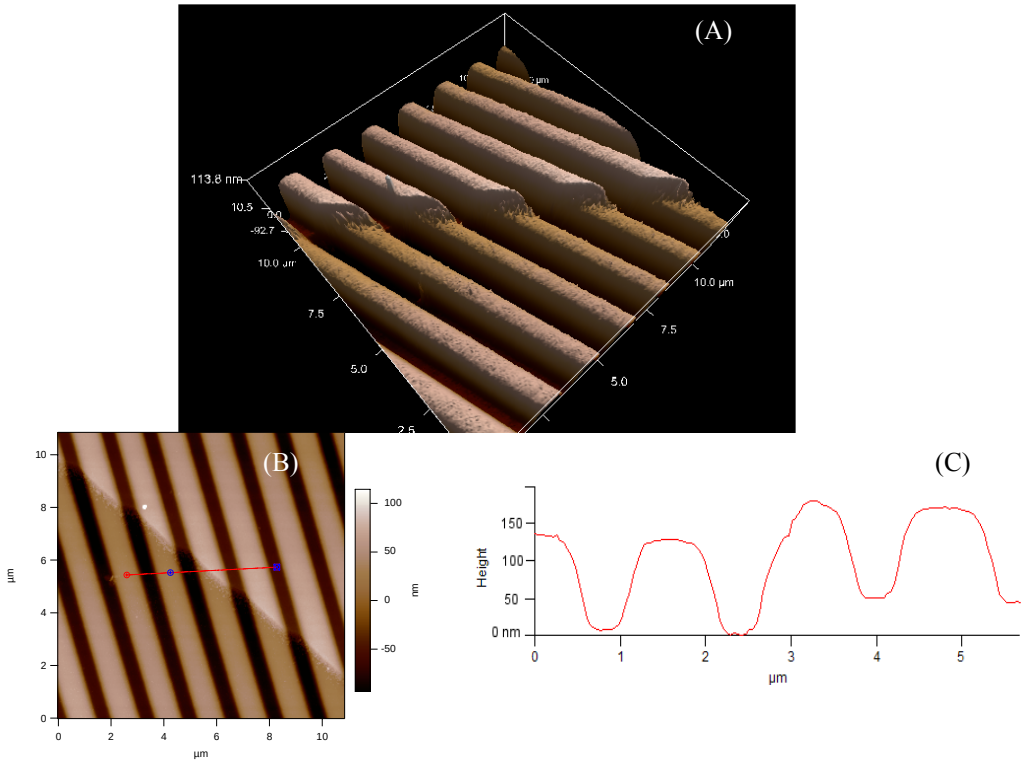

Figure 5.4 AFM images of a Delkin Archival Gold CD-R, after treatment with conc. HNO_3 and etching of part of the layer of gold with Transene gold etchant type TFA (Danvers, MA). The gold thickness is ~50 nm. The CD-R has similar features sizes to the Imation CD-R. (A) - (B) Height images. (C) Line trace.

Doped Polymer Stamps

The stamps can be doped with a fluorescent dye such as porphyrins. As a doping agent we used tetra(4-carboxyphenyl)porphyrin (TCPP). Porphyrins have ~ $2x10^5$ O.D. in the Soret band near 420 nm and ~10% fluorescence quantum yield. Since porphyrin are cheap to synthesize and remarkably stable, they are a good starting point to develop the doping methodd, stamps, and product characterization. The surface doping is accomplished by dipping the polymer stamp into a 1:100 CH_2Cl_2:CH_3CH_2OH solution containing ~0.1 mM of TCPP for 10 seconds, immediately rinsing with copious amounts of water and drying under nitrogen. The doped polycarbonate has been characterized by UV-vis and fluorescence spectroscopy.

5.3 Results and Discussion

Fabrication of polymer patterns

The stamping process is very simple and enables the fabrication of nanoscaled polymeric patterns on ceramic substrates in a one step method. Using a pneumatic press, fitted with a heating-cooling system and a programmable temperature controller, the treated exposed pattern of the CD-R was compressed against a glass or ITO substrate. After heating the stamp-substrate sandwich to less than the glass transition temperature (T_g) of the polymer and cooling it back to room temperature, the substrate was either pried from the stamp using a pair of tweezers, or separated by sonication in water (Fig. 5.5).

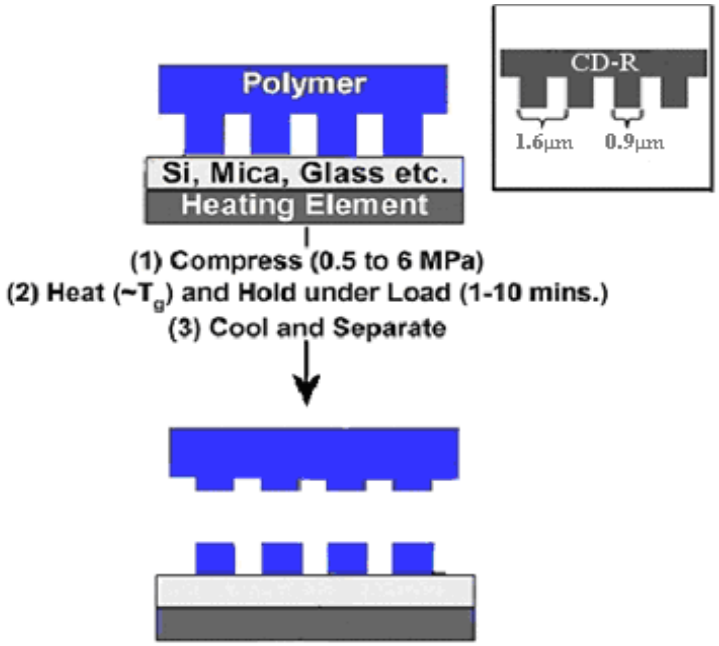

Figure 5.5 (A) Schematic of the stamping process. The polymeric nanostructures are formed by the compression of a thermoplastic polymer stamp against the substrate (glass or ITO), the system is then briefly heated, and subsequently the stamp is separated from the substrate after cooling. **(B)** Depicts the repeat grating structure of commercial CD stamps, which possess a recess depth ~ 150 nm.

The stamping process, usually carried out with a 20x20 mm section of a CD-R on an ozone cleaned ITO substrate, uses a 2-step temperature program (heating/cooling) while the stamp is compressed against the substrate. A typical profile of the temperature program is shown in the appendix. Stamp and substrate are held under a compressive load (contact pressure) of 0.8 MPa at 45 °C for 5 minutes, to let the system reach a thermal equilibrium. The heating ramp represents the maximum heating capacity of the apparatus ~45 °C/min (it takes approximately 2 minutes to reach the dwell temperature). The dwell temperature ranges from 130 °C to 145 °C and the minimum dwell time to obtain structures with high fidelity is 1-2 minutes, and longer dwell times do not increase the quality of the transfer. The system is then allowed to cool (under load) at a rate of ~15 °C/min to room temperature. The applied load is then slowly removed and the stamp is separated from the substrate.

The fabrication of the polymeric features is a consequence of the adhesive failure inside the polymeric material due to formation of a polymer-polymer "interface" and the explanation for this behavior can be found in the studies of the properties of confined polymer films. There is a fairly large literature on the physical properties of ultra-thin polymer films[19,20,23-27] since understanding these properties are important in many applications, including protective and lubricating coatings,[28] adhesives, composite materials, and microelectronics.[13,29] A generally accepted model to explain the behavior of thin polymer films at interfaces is the *three-layer model*, which describes polymer films as possessing three layers with different mobilities and glass transition temperatures. Near the substrate there is a *dead layer* in which the polymer chain mobility, and therefore the T_g, is strongly influenced by interactions with the substrate.

Strong dead layer – substrate interactions reduce the mobility and raise the T_g. At the polymer-air interface there is a *liquid-like* layer with a greater mobility and therefore a lower T_g. Between these two layers there is a *bulk-like* layer which has the same mobility as that of the bulk samples.[30] Thus there are polymer-polymer interfaces that dictate the location of cohesive failure and enable the present stamping method (Fig. 5.6).

This model is attractive because it can address the inhomogeneities that experimental results and theoretical calculations show exist in such supported thin films of polymers. "It is plausible that there are boundary layers between the bulk-like layer and the liquid-like layer and between the bulk-like layer and the dead layer"[31] and this can account for the anisotropic adhesive interactions between the layers. In fact, it has been suggested, from recent modeling of unentangled polycarbonate on a nickel surface, that interfacial polymer segregation could compromise cohesion between the adsorbed ("dead") and adjacent bulk-like macromolecules.[32] For the polymer insulated gold nanowire structures in the previous chapter, the liquid-like layer also resides on the sides of the stamp features, thus enabling it to 'flow' and intercalate in between the gold and the ceramic surfaces. In this case there is no gold-ceramic interface, so the liquid-like layers on the sides of the features likely flow only to a small extent towards the surface.

AFM topography images (Fig. 5.7) show that uniform patterns can be transferred from a CD stamp using a dwell temperature of 130°C and a dwell time of two minutes. The polymeric features on the substrate are well defined with a typical height of 12-15 nm. This is comparable to the *dead layer* persistence lengths (4-13 nm) extracted from recent thin film polycarbonate studies.[33] Consistent with our previous work,[17] the present findings indicate that the intrapolymer interface between the dead and bulk layers forms a

shear plane that allows the patterning of surfaces. The comingled roles of temperature and pressure in the stamp processing increase the polymer interactions with the ceramic substrate to form a well defined dead layer and allow the polymer strands to reorganize to further delineate the boundary with the bulk layer to create a shear plane.

Figure 5.6 Schematic of the *three-layer model* used to describe the behavior of thin polymer films at interfaces. Left: Substrate supported thin film. Right: Film confined between two substrates. Red: *dead layer* which has chain mobility strongly influenced by substrate. Gray: *bulk-like* layer which has the same mobility as that of the bulk samples. Light blue: *liquid-like* layer, at the polymer-air interface, with higher mobility. Dark blue: interfaces between these layers.

The glass transition temperature of polycarbonate is ~150 °C, but T_g depends on molecular weight distribution and on presence of additives (e.g. CD-R contain glass fillers), for the optical recording media it was determined to be 145 °C by differential scanning calorimetry.[17] Thus this polymer nanolithographic technique enables fabrication of structures at temperature well below a polymer's bulk T_g. For the CDs used in this study, the optimal temperature for the stamping process is ~ 130 °C. Patterns have been fabricated with temperature as low as 120 °C, while for temperature closer to T_g there is a decrease in the structural fidelity. The serrated structure of the top of the polymer in the stamped pattern is thought to arise from the dead-layer bulk-layer fracture during the stamp-substrate separation. A better separation technique than prying the stamp from the substrate is needed, preliminary results show that sonication in water may be a promising alternative.

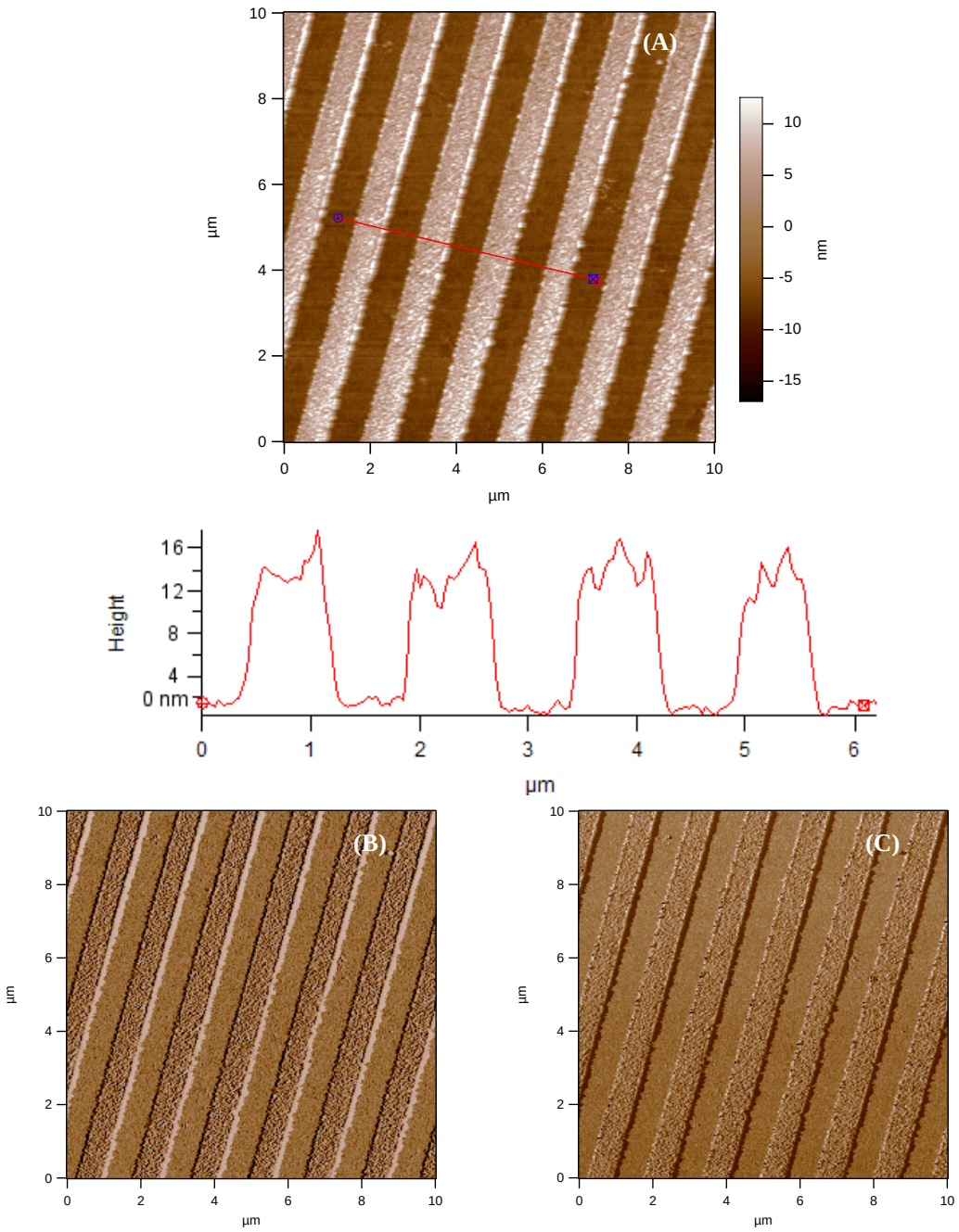

Figure 5.7 ITO patterned with a CD-R stamp using a dwell temperature of 130°C and a dwell time of two minutes. AFM images acquired in tapping mode, (A) height image, (B) amplitude image, (C) phase image. The polymeric features on the substrate are well defined with a typical height of 12-15 nm.

To verify that the polymer is not spreading over the entire substrate surface during the stamping process (i.e. there is no polymer in the grooves of the product), part of the polymer lines have been nanoshaved using a silicon AFM tip during contact mode imaging (Fig. 5.8). Since the minimum height in the cross section analysis of the nanoshaved part does not change compared to the part of the sample with the stamped pattern, we can conclude that the polymer film does not spread over the surface during the heating/compression process. The section analysis in fact has the typical surface roughness profile of the bare ITO surface used in these studies.

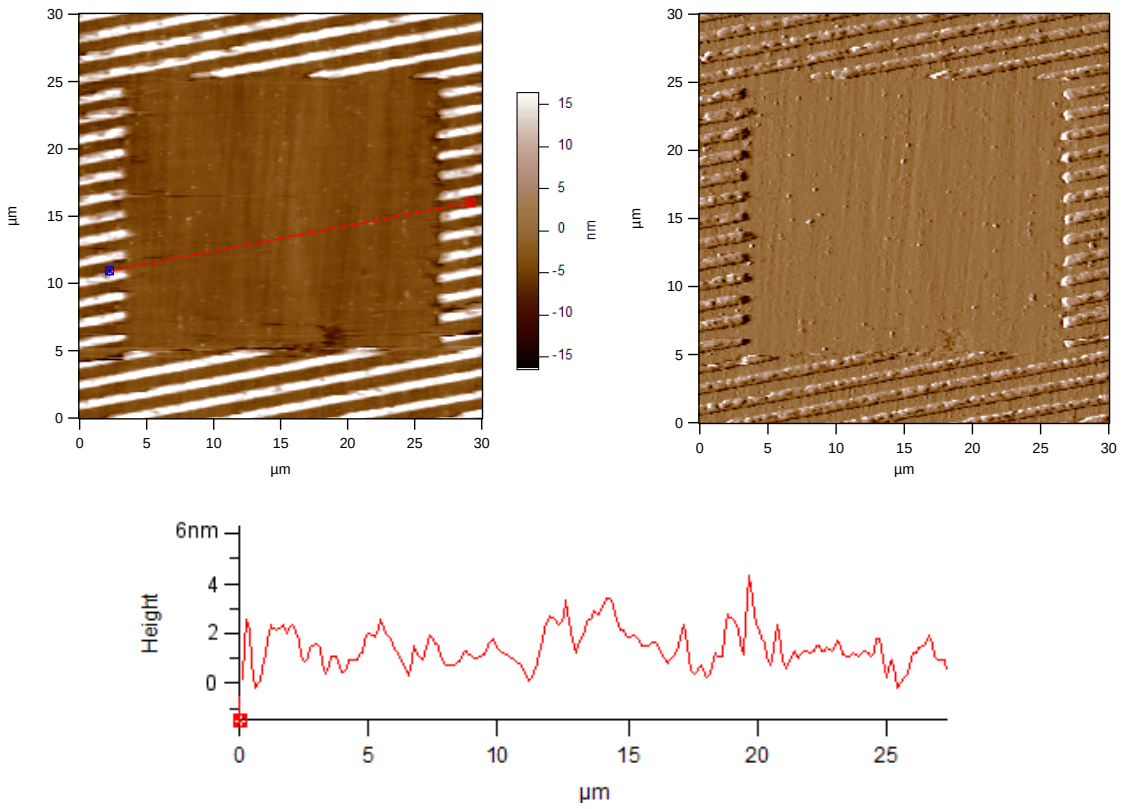

Figure 5.8 AFM images acquired in contact mode after nanoshaving some of the polymer structure. Left: height image. Right: friction image. The section analysis does not show the presence of polymer film and has the typical roughness profile of a bare ITO surface, which confirms that the polymer does not spread over the part of the substrate not in contact with the polymer during the stamping process.

Mechanical and chemical stability of the polymer patterns

The stability of the stamped structures has been evaluated. The polymer features on the ITO and substrates adhere well using a qualitative, but widely used "Scotch® tape peel test,"[34] wherein a piece of Scotch® tape is pressed against the patterned substrate and peeled off. No apparent damage was observed by optical microscopy after removing the Scotch® tape.

Secondly, sonication of the patterned ITO in water leaves the polymer lines in the product surface unchanged with no observable damage to the structures. Notably, sonication in polycarbonate solvents such as toluene or dichloromethane does not completely destroy or remove the patterned polymer, but this treatment does have some effect on the polycarbonate features. This effect is clearly illustrated in the AFM images after sonicating in organic solvents. Figure 5.9A shows a polycarbonate pattern on ITO obtained with two minute dwell time at 135 °C but separated from the stamp at 45°C; the section profile shows the typical ~ 900 nm wide lines with edge features or protrusions that are 15-20 nm. Prominent edge features are in general observed when the system is not allowed to cool to room temperature before separation. Sonication of this stamped product on ITO in CH_2Cl_2 for two minutes removes some polycarbonate, and results in smoothing the prominent edges to leave 5-6 nm thick lines (Fig 5.9B). After two more minutes of sonication in the same solvent the lines are ca. 4 nm high and much smoother (Fig. 5.9C). Treatment of the sample for four more minutes further reduced the height by ca. 1 nm (Fig. 5.9D) to leave ca. 3 nm high features. Thus, the polycarbonate patterns show a remarkable stability against solvent delamination.

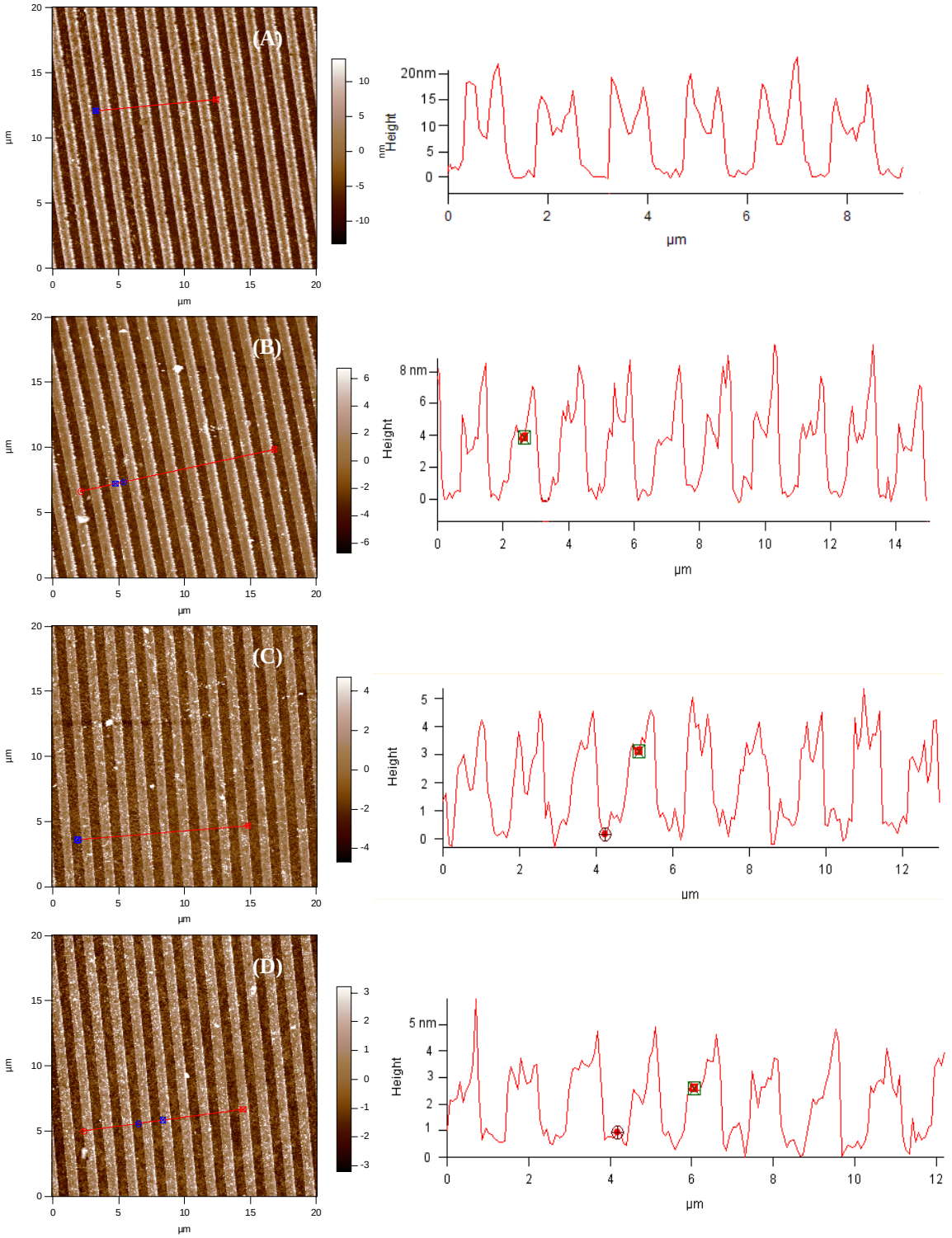

Figure 5.9 Effect of sonication in CH_2Cl_2 of the patterned ITO. **(A)** Pattern on ITO before solvent treatment. **(B)** After two min. sonication in CH_2Cl_2. **(C)** After two more min. (four min. total). **(D)** After four additional min. (eight min. total). The polycarbonate patterns show a remarkable stability against solvent treatment, and this method can actually be used to reduce and smooth the feature thickness.

Moreover, brief sonication in organic solvents can actually be used as part of the processing to further modulate (reduce) the thickness of the polymer patters and to smooth the topology on top of the polymer lines. This secondary step allows formation of patterns with a more uniform height that are only few nanometers thick. This stability can also be exploited to chemical modify or dope the patterned products.

Fabrication of crosshatched lines

Changing the pattern of the polycarbonate stamp will afford different patterns on the ceramic surfaces. It is also possible to fabricate more complicated, 3-dimensional structures on substrates using polymer nanolithography, as demonstrated by the preparation of crosshatched patterns of polycarbonate on ITO. These structures are very easily obtained by successively stamping an ITO substrate with two different CD-R derived stamps. The processing conditions for the first stamping step are the same as describe before, while the best transfer for the second stamping step is achieved using slightly higher dwell temperature (140°C) and contact pressure (1.2 MPa) then those used for the first. AFM images of a characteristic crosshatched pattern obtained in this way are shown in Figure 5.10. The section analysis (Fig. 5.11) shows the usual thickness of ~10 nm for the first lines stamped with typical prominences arising from the separation of the stamp from the substrate. The second set of polycarbonate lines on the bare ITO surface are 25-30 nm thick and have similar roughness, thus the second stamping process deposits lines that are about 2-3 times as thick as the first on the bare ITO substrate. At the intersection where one line is on top of the other, the second set of lines is ca. 20 nm high measured from the top of the first lines The overall feature height for the entire crosshatched pattern is about 30 nm and this likely represents the dead-bulk shear plane

in the polycarobonate at the elevated temperatures and pressures used for the second stamping procedure.

The serrated structure of the polymer pattern is thought to arise from the fracture during the stamp-substrate separation. Figure 5.11 reveals much larger protrusions at the intersection of the polymer lines, and we hypothesize that at this point the polymer stretches more during separation as a consequence of the different interactions with the material underneath, ITO and polycarbonate.

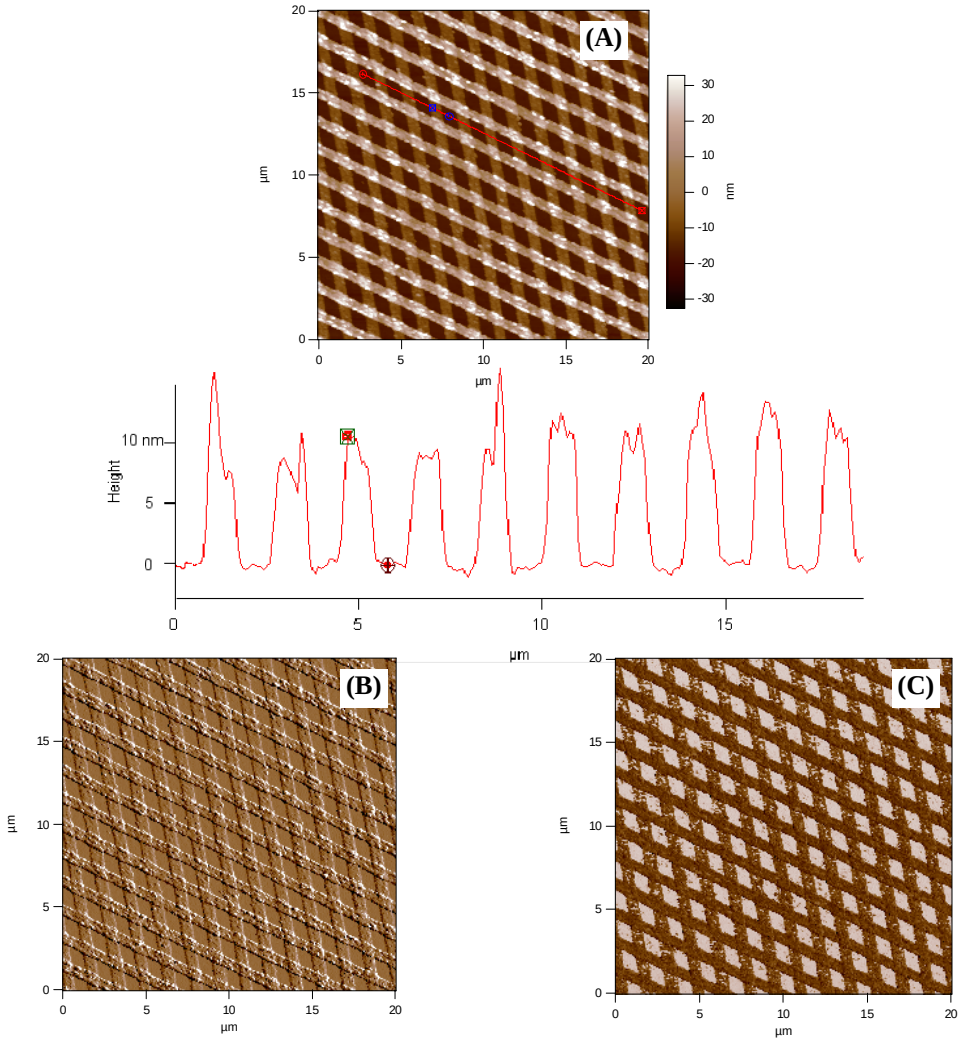

Figure 5.10 ITO patterned with crosshatched lines. AFM images acquired in tapping mode, (A) height image, (B) amplitude image, (C) phase image. The polymeric features on the substrate are well defined.

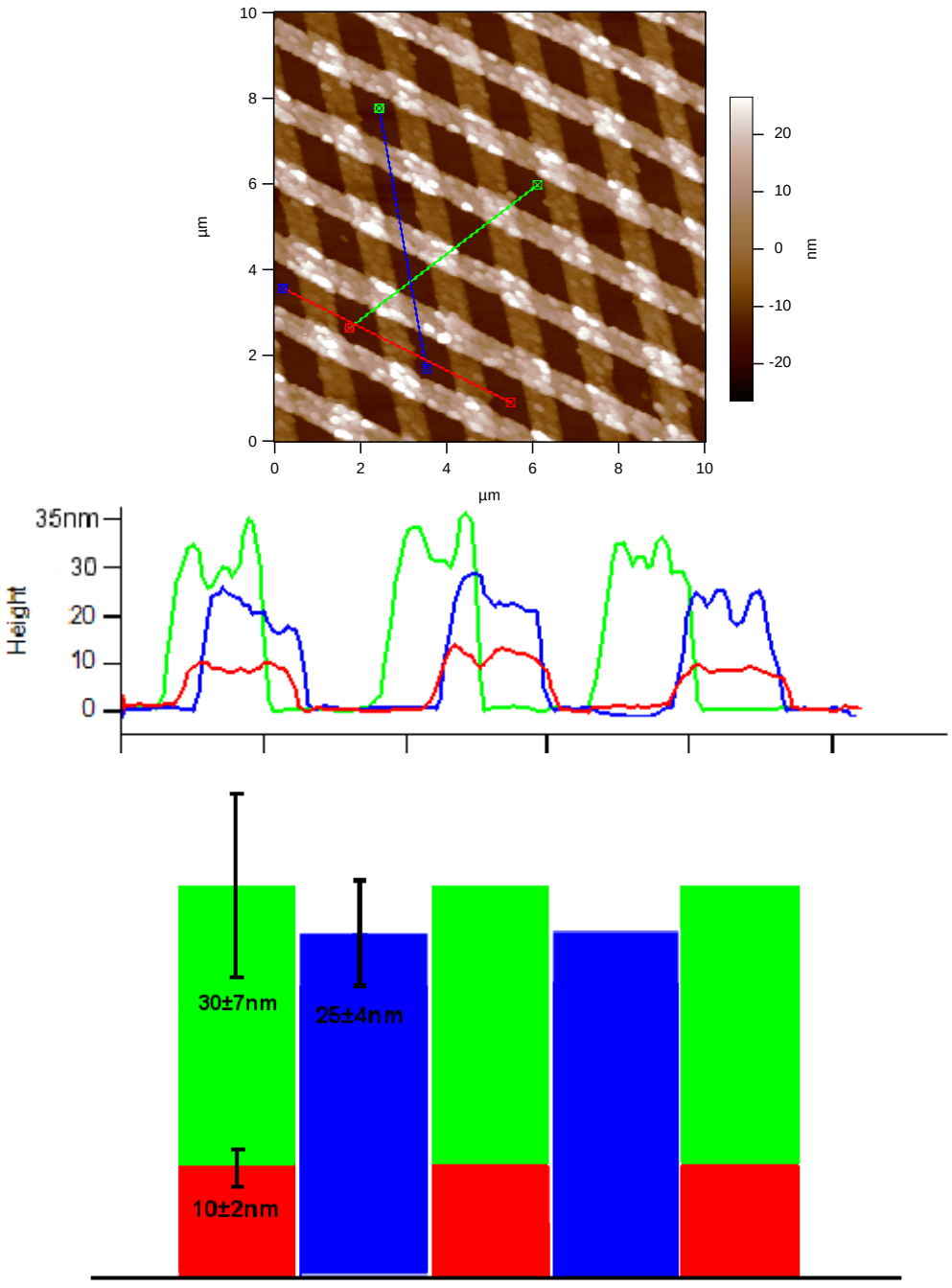

Figure 5.11 Detailed analysis of the crosshatched patterns indicate that under the elevated temperature and pressure of the second stamping step results in features with greater heights to yield a patterns of about 25-30 nm (see text). Bottom: schematic representation of the pattern profile. The colors correspond to the ones in the section analysis: initial stamp product (red), second stamp product on the substrate (blue), and second stamp product on top of the first (green).

The stamping process produces reproducible structures with high fidelity over large areas as shown by AFM images of a 50 μm x 50 μm area (maximum scan size of the instrument, Fig. 5.12A). Scanning electron microscope images also display the quality of the crosshatch pattern over 50 μm x 50 μm area and 300 μm x 300 μm area (Fig 5.12B-C). Optical microscopy indicates good quality structure over much of the substrate with domains of many mm^2. The SEM images were obtained without any previous preparation of the sample, since the polymeric features are only a few nm thick, it is not necessary to coat the sample with a layer of conductive material. The shadows present on Figure 5.12C are due to the previous SEM scans that left the polycarbonate partially charged.

Fabrication of fluorescent patterns

As outlined in the introduction, there are numerous needs for nanoscaled patterns of fluorescent materials such as for OLEDs, sensors, and for other photonics applications. It has been shown that the products of polymer nanolithography can be subsequently modified.[35] Alternatively, the integration of a fluorescent dye into the thermoplastic stamp allows polymer nanolithography of molecularly doped structures.

The stamps can be doped with a fluorescent dye such as TCPP. The doped stamps have the characteristic UV-vis and fluorescence spectra for this molecule, and indicate that TCPP resides in the first few nanometers of the polymer. AFM analysis of the doped stamp shows that the doping treatment does not produce significant changes in the surface morphology of the stamp.

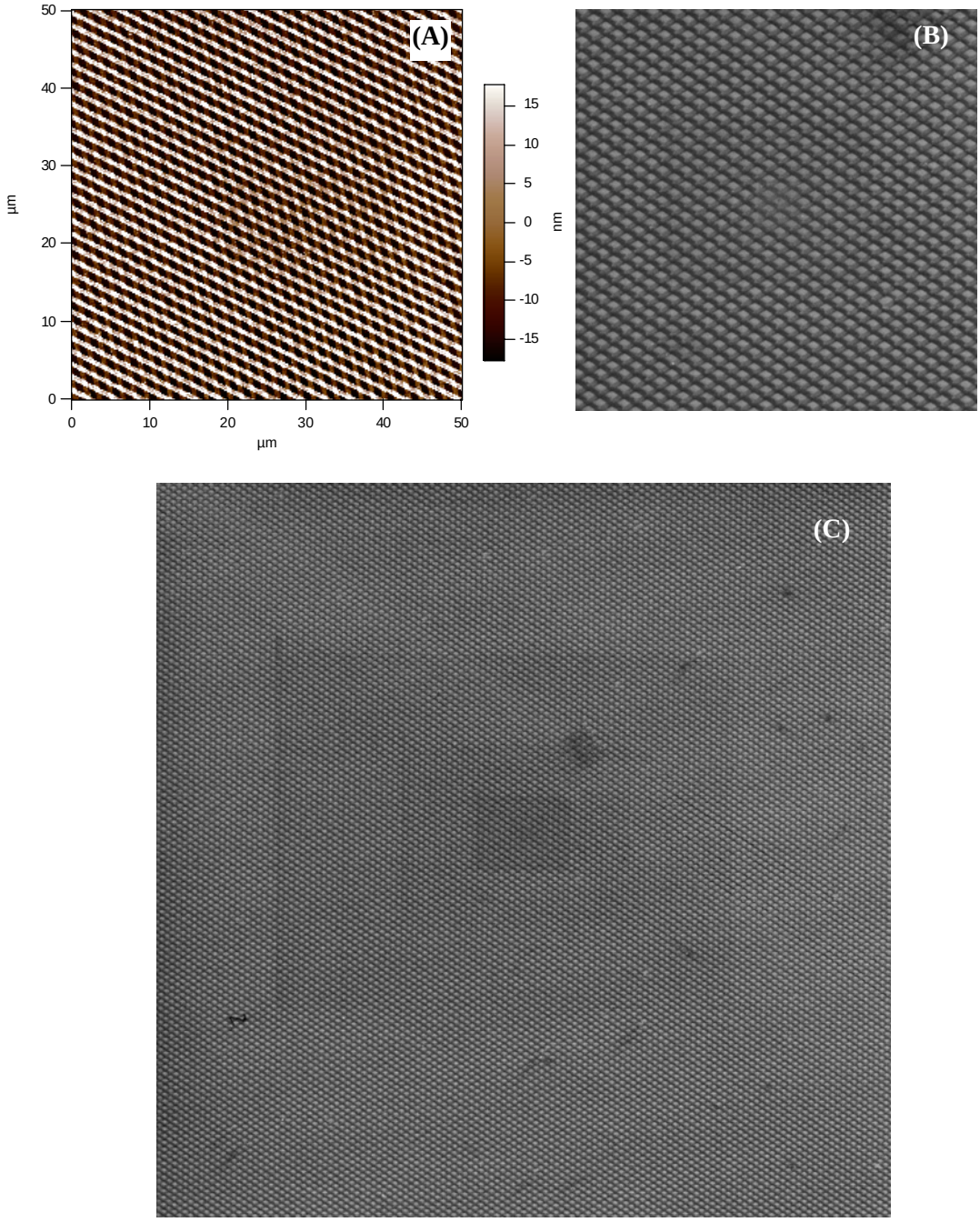

Figure 5.12 Surface coverage and fidelity of the crosshatch pattern. (A) AFM image over a 50 µm x 50 µm area. Scanning electron microscope images of a (B) 50 µm x 50 µm area, and (C) 300 µm x 300 µm area.

The patterns fabricated using these TCPP-doped CD stamps were made under the usual stamping conditions (dwell time = 2 min., dwell temperature = 130°C) on ITO and produced fluorescent lines on the substrate that can be characterized by AFM and confocal microscopy. An example of these patterned fluorescent lines is shown in Figure 5.13, in which an image obtained with the microscope in reflectance mode is compared to the fluorescent image. The images show a part of the ITO with imperfect fabrication to appreciate the details of the fluorescence analysis. The florescent image is obtained using a 514 nm excitation wavelength, therefore exciting the TCPP on the first Q-band. (The confocal microscope does not have a laser at the wavelength of the Soret band.) Therefore even using a dilute solution of the porphyrin, and doping the polycarbonate for only a few seconds, lines with good fluorescence intensity were fabricated.

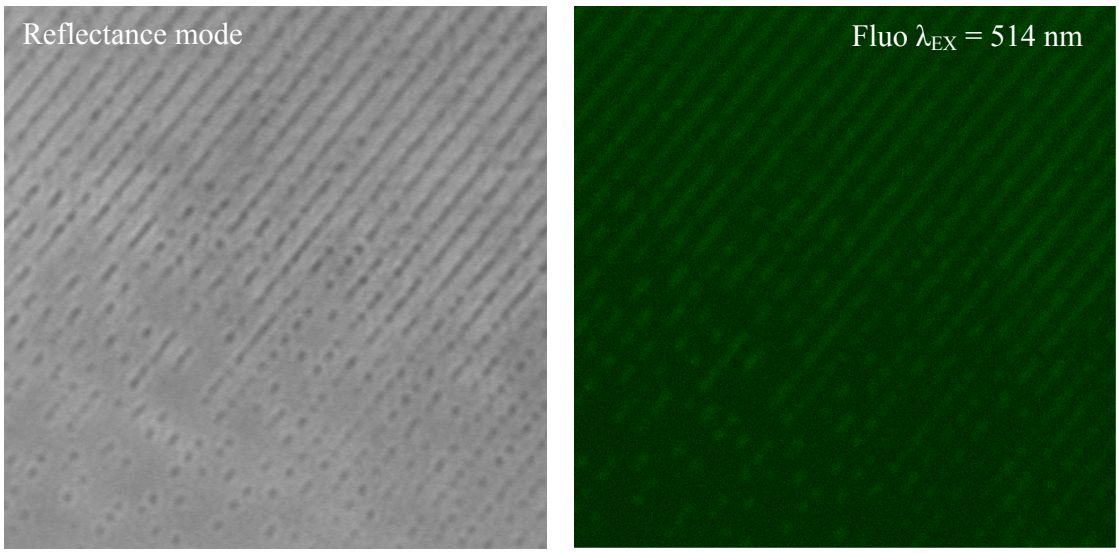

Figure 5.13 Pattern fabrication using a stamp doped with a fluorescent porphyrin produces fluorescent lines on ITO. Left: reflectance image of imperfect sample. Right: the corresponding fluorescent image, obtained using a 514 nm excitation wavelength. Images acquired with a Leica confocal microscope using a 63X objective. Images size: 40 μm x 40 μm.

Passivated Gold-Coated CD-R as template for stamp fabrication

To expand the use of the polymer nanolithography by thermal contact nanotransfer to polymers other than polycarbonate (CD-R) it is necessary to fabricate patterned polymer samples to use as a stamp. The simplest and most commonly used methods to replicate patterns, such as molding and embossing, utilize hard molds that are mostly made of Si or SiO_2, fabricated with traditional photolithography or related techniques. These masters can be quite expensive and difficult to find. Since we were interested in developing the methods rather than the exact topography of the stamp, we decided to use the gold-coated CD-R for this purpose. To avoid sticking of the molded polymeric material on the gold surface during the stamp preparation, a low surface tension coating to the gold was prepared. Treatment with an alkanethiol forms a low surface energy SAMs on the gold limiting the strong tendency of adhesion of the polymer with the mold.

The covalently bonded SAMs are chemically and thermally stable, and this allowed the passivated gold-coated CD-R to be used multiple times for stamp preparation. The use of these gold-CD-R master is limited by the thermal plastic properties of the polycarbonate (T_g = 145°C), so stamps can be prepared only using polymeric materials with a T_g below the polycarbonate T_g. We have successfully prepared stamp of polystyrene (PS) (T_g = 100°C) by compression molding of PS sheets at 115°C for 15 minutes under an applied pressure of 0.92 MPa (Fig. A5.4). This yelds a stamp that is a replica of the CD-R features with lines that are ~ 100 nm high. Preliminary results show that is possible to fabricate polystyrene patterns on ITO using these stamps but the stamping conditions still need to be optimized.

5.4 Conclusions

A new polymer nanolithography technique has been presented. For certain applications, this fabrication process can be an alternative or complementary to other successful and widely used methods such as nanoimprint lithography. The numerous studies and many potential applications discussed in the introduction show the importance of fabrication of polymer nanopatterns and that each method has an array of advantages that are applications and materials dependent. The polymer thermal-contact nanotransfer demonstrated here can make nanofabrication accessible to many researchers without requiring special equipment, complex masters, or multistep processing, in contrast to many previously developed soft nanolithographic techniques. To make this method available to a broad cross section of the scientific community, it was designed such that readily available nanopatterned materials (e.g. CD and DVD) could be used as the stamp.

With this method polymer patterns can be fabricate in a very fast way (two minutes dwell time, ~15 total time process) using temperature 20-30 °C below T_g (while conventional NIL uses temperature 50-100 °C above T_g) and at relatively low pressure. Moreover, the fabrication of multilevel patterns has been demonstrated to yield a simple means of fabricating three-dimensional polymer nanostructures. This latter aspect of the present method indicates that it can be use to stamp polymeric features on polymer substrate that possess higher T_g than the patterned polymer – thus allowing the fabrication of flexible samples.

We have focused on the formation of patterned lines on simple ceramic substrates created from commercial CD stamps to enable polymer nanolithography to be done

routinely by almost any lab, but other patterns from polycarbonate are feasible, as are other substrates such as mica. More studies are necessary to evaluate the effect of the polymer molecular weight and the substrate on the thickness of the polymer patterns. The maximum thickness of the features is a limiting factor for this method as it is dictated by the thickness of the dead layer to ca. 5 – 20 nm for the polycarbonate used, but solvent treatment post fabrication allows the formation of structures that are just few nanometer thick, and removed polymer can, in principle be recovered and recycles.

Future work will focus on the fabrication of patterned arrays of other polymers such as polystyrene, polyester, and conducting polymers. The used of dye-doped polymers or polymers containing other functional molecules can be used by this polymer thermal nanotransfer method. It remains to be seen if polymer blends, and block co-polymers can be used.

5.5 Appendix 5.1

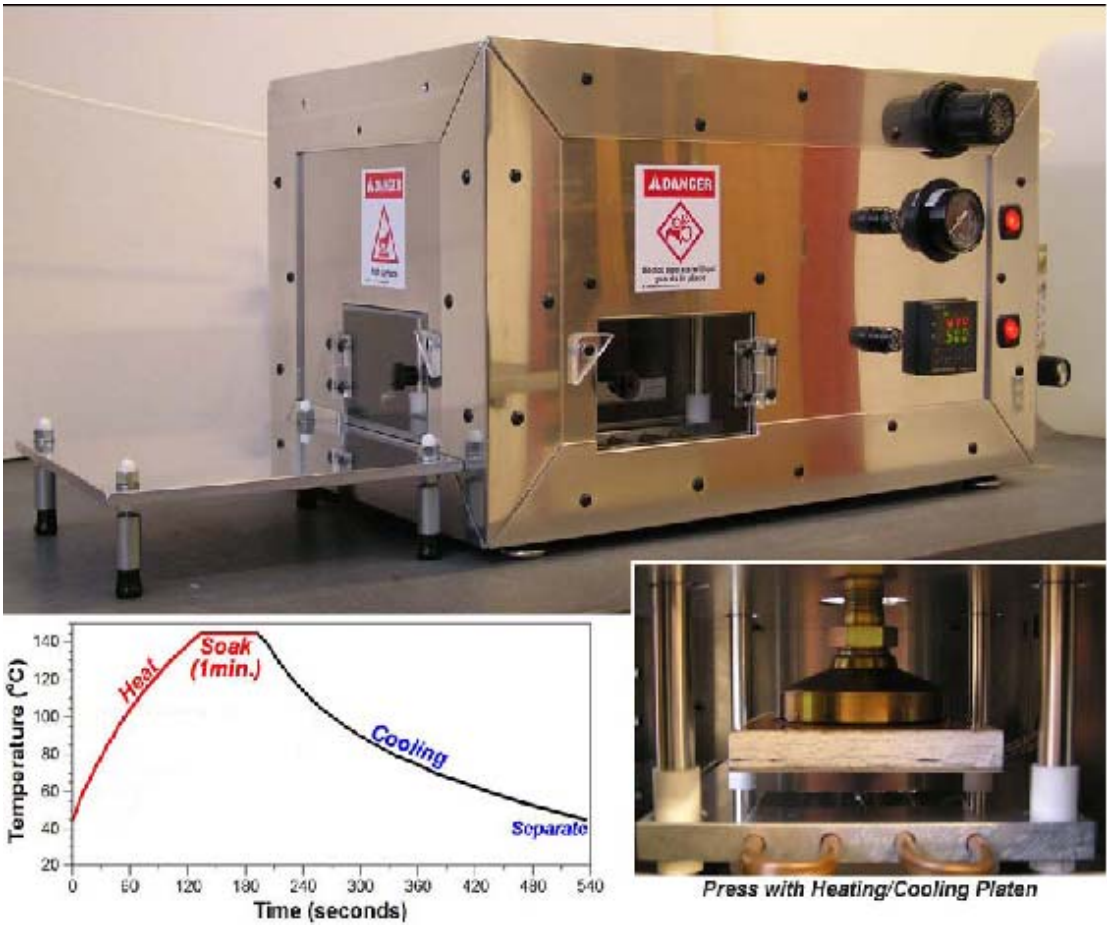

Figure A5.1 Top and right are photos of the home-built stamping apparatus. The right shows the pressure cell and heating platen. Bottom left: the graph of a typical temperature program used during thermal nanotransfer fabrication, showing 1 minute of dwell time. (Taken from Ref. 17)

Specifications for the custom pneumatic press used for the thermal synthesis and transfer of materials to and from polymers are provided in Table A5.1. A picture of the press is also provided in Figure A5.1.

Table A5.1 Specifications for Heated Pneumatic Press

Property	**Value**
Maximum compressive load	8,200 N
Wafer diameter capacity	100 mm
PID controlled programmable temperature segments	16
Heating Platen Power	1000 watts
Maximum operating temperature *(20 minutes)*	185°C
Maximum Heating Rate with Coolant flow >10 GPH	46°C/min
Dwell temperature overshoot during initial ramp	0.4 - 1.2°C
Critical cooling rate with coolant flow >10 GPH (21°C Water Coolant)	28°C/min
Strike Plate Insulating Capacity (*Contacting 100°C Platen*)	0.7°C/min

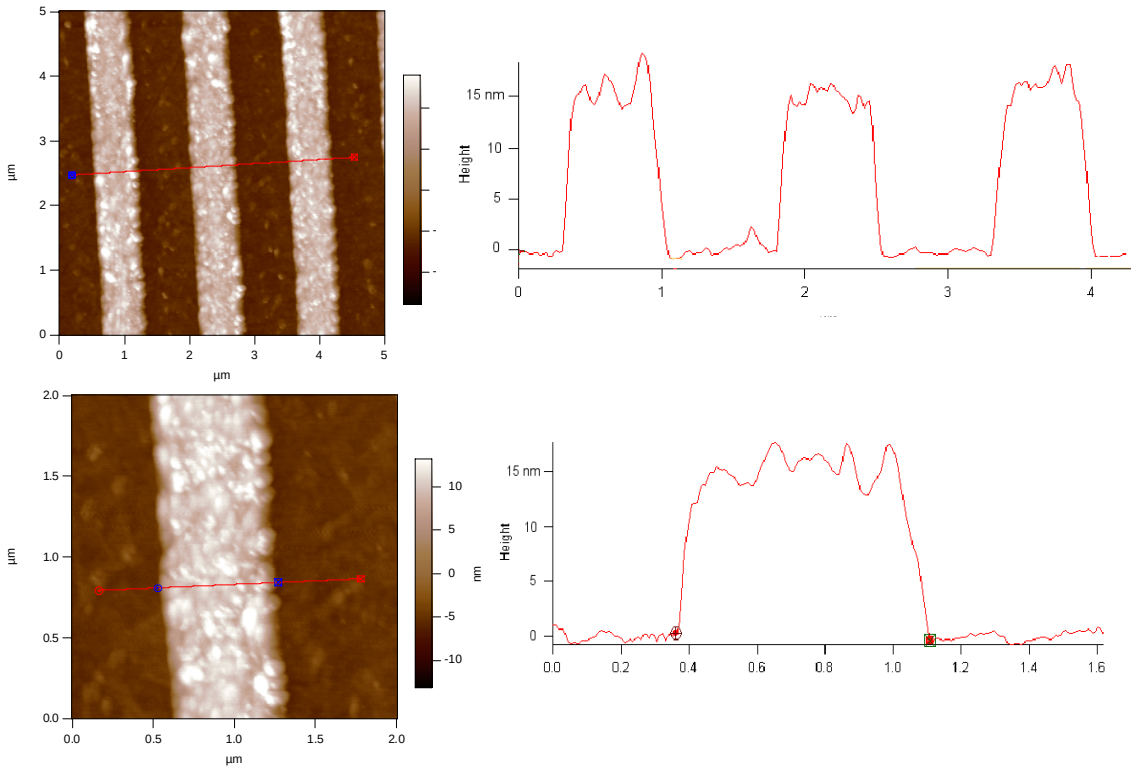

Figure A5.2 Details of the polymer lines fabricated on ITO using a CD-R stamp (dwell temperature of 130°C and a dwell time of 2 minutes). AFM images acquired in tapping mode, height image and section analysis. The polymeric features on the substrate are well defined with a typical height of 12-15 nm.

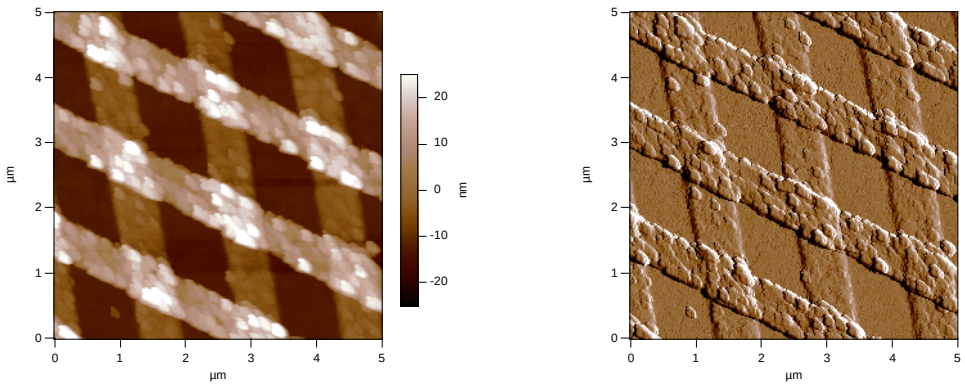

Figure A5.3 Details of the crosshatched polymer lines fabricated on ITO using a CD-R stamp (dwell temperature of 130°C and a dwell time of 2 minutes). AFM images acquired in tapping mode. Left: height image. Right: amplitude image.

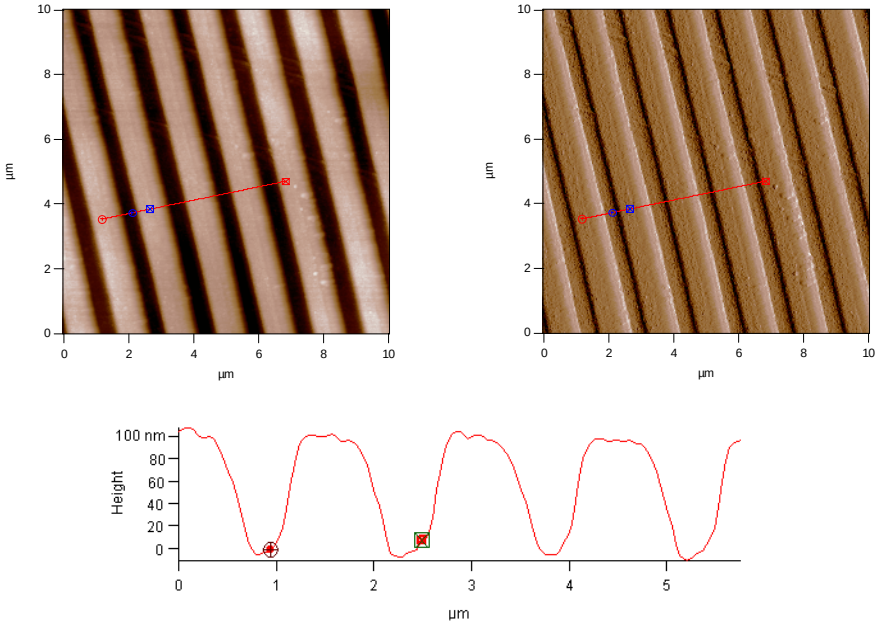

Figure A5.4 AFM images of polystyrene stamp prepared using passivated gold-coated CD-R as template formed by compression molding of PS sheets at 115°C for 15 minutes under an applied pressure of 0.92 MPa. Left: height image. Right: amplitude image.

5.6 Chapter 5 References

(1) Special; Report *Technol. Rev.* **2003**, *106*, 36.

(2) Chou, S. Y.; Krauss, P. R.; Renstrom, P. J. *Science* **1996**, *272*, 85-87.

(3) Stephen Y. Chou, P. R. K. P. J. R. *Appl Phys Lett* **1995**, *67*, 3114-3116.

(4) Michael, D. A.; Haixiong, G.; Wei, W.; Mingtao, L.; Zhaoning, Y.; Wasserman, D.; Lyon, S. A.; Stephen, Y. C. *Appl Phys Lett* **2004**, *84*, 5299-5301.

(5) Dahl-Young, K.; Hong, H. L. *Appl Phys Lett* **1999**, *75*, 2599-2601.

(6) Heyderman, L. J.; Schift, H.; David, C.; Gobrecht, J.; Schweizer, T. *Microelectronic Engineering* **2000**, *54*, 229-245.

(7) Zankovych, S.; Hoffmann, T.; Seekamp, J.; Bruch, J. U.; Torres, C. M. S. *Nanotechnology* **2001**, *12*, 91-95.

(8) Jung, G. Y.; Li, Z.; Wu, W.; Chen, Y.; Olynick, D. L.; Wang, S. Y.; Tong, W. M.; Williams, R. S. *Langmuir* **2005**, *21*, 1158-1161.

(9) Khang, D. Y.; Kang, H.; Kim, T. I.; Lee, H. H. *Nano Lett.* **2004**, *4*, 633-637.

(10) Huang, X. D.; Bao, L. R.; Cheng, X.; Guo, L. J.; Pang, S. W.; Yee, A. F. *J. Vac. Sci. Technol. B* **2002**, *20*, 2872-2876.

(11) Dahl-Young, K.; Hong, H. L. *Appl Phys Lett* **2000**, *76*, 870-872.

(12) Baily, T.; Choi, B. J.; Colburn, M.; Meissl, M.; Shaya, S.; Ekerdt, J. G.; Sreenavasan, S. V. *J. Vac. Sci. Technol. B* **2000**, *18*, 3572-3577.

(13) Menard, E.; Meitl, M. A.; Sun, Y.; Park, J. U.; Shir, D. J. L.; Nam, Y. S.; Jeon, S.; Rogers, J. A. *Chem. Rev.* **2007**, *107*, 1117-1160.

(14) Guo, L. J.; Cheng, X.; Chao, C. Y. *Journal of Modern Optics* **2002**, *49*, 663-673.

(15) Cheng, X.; Hong, Y. T.; Kanicki, J.; Guo, L. J. *J. Vac. Sci. Technol. B* **2002** *20*, 2877-2880.

(16) Austin, M. D.; Chou, S. Y. *Appl Phys Lett* **2002**, *81*, 4431-4433.

(17) Helt, J. M.; Drain, C. M.; Bazzan, G. *J. Am. Chem. Soc.* **2006**, *128*, 9371-9377.

(18) Helt, J. M.; Drain, C. M.; Batteas, J. D. *J. Am. Chem. Soc.* **2004**, *126*, 628-634.

(19) Forrest, J. A.; Dalnoki-Veress, K.; Dutcher, J. R. *Physical Review E* **1997**, *56*, 5705.

(20) Keddie, J. L.; Jones, R. A. L.; Cory, R. A. *Faraday Discuss* **1994**, 219-230.

(21) Rice, R. W.; Sarode, D. V. *Ind. Eng. Chem. Res.* **2001**, *40*, 1872-1878.

(22) Yu, H. Z. *Anal. Chem.* **2001**, *73*, 4743-4747.

(23) *Eur. Phys. J. E* **2002**, *8*, 101-261.

(24) Fryer, D. S.; Nealey, P. F.; de Pablo, J. J. *Macromolecules* **2000**, *33*, 6439-6447.

(25) Ranjeet, S. T.; David, S. F.; Silvia, P.; Martha, F. M.; Juan, J. d. P.; Paul, F. N. *Journal of Chemical Physics* **2001**, *115*, 9982-9990.

(26) Yamamoto, S.; Tsujii, Y.; Fukuda, T. *Macromolecules* **2002**, *35*, 6077-6079.

(27) Fryer, D. S.; Peters, R. D.; Kim, E. J.; Tomaszewski, J. E.; de Pablo, J. J.; Nealey, P. F.; White, C. C.; Wu, W. l. *Macromolecules* **2001**, *34*, 5627-5634.

(28) *Springer Handbook of Nanotechnology*; 1 ed.; Bhushan, B., Ed.; Springer: Berlin, 2004.

(29) Durig, U.; Cross, G.; Despont, M.; Drechsler, U.; Haberle, W.; Lutwyche, M. I.; Rothuizen, H.; Stutz, R.; Widmer, R.; Vettiger, P.; Binnig, G. K.; King, W. P.; Goodson, K. E. *Tribol Lett* **2000**, *9*, 25-32.

(30) DeMaggio, G. B.; Frieze, W. E.; Gidley, D. W.; Zhu, M.; Hristov, H. A.; Yee, A. F. *Phys Rev Lett* **1997**, *78*, 1524-1527.

(31) Fukao, K.; Miyamoto, Y. *Physical Review E* **2000**, *61*, 1743-1754.

(32) Abrams, C. F.; Site, L. D.; Kremer, K. *Physical Review E (Statistical, Nonlinear, and Soft Matter Physics)* **2003**, *67*, 021807.

(33) Soles, C. L.; Douglas, J. F.; Wu, W. l.; Peng, H.; Gidley, D. W. *Macromolecules* **2004**, *37*, 2890-2900.

(34) Araki, K.; Wagner, M. J.; Wrighton, M. S. *Langmuir* **1996**, *12*, 5393-5398.

(35) Beinhoff, M.; Appapillai, A. T.; Underwood, L. D.; Frommer, J. E.; Carter, K. R. *Langmuir* **2006**, *22*, 2411-2414.

Bibliography

Chapter 1

(1) Ball, P. *Nature* **2001**, *409*, 413-416.

(2) Alivisatos, A. P.; Barbara, P. F.; Castleman, A. W.; Chang, J.; Dixon, D. A.; Klein, M. L.; McLendon, G. L.; Miller, J. S.; Ratner, M. A.; Rossky, P. J.; Stupp, S. I.; Thompson, M. E. *Adv. Mater.* **1998**, *10*, 1297-1336.

(3) Fox, M. A. *Acc. Chem. Res.* **1999**, *32*, 201-207.

(4) Aviram, A.; Ratner, M. *Ann. N.Y. Acad. Sci.* **1998**, *852*, 1-21.

(5) Reed, M. A. *MRS Bull.* **2001**, *26*, 113-120.

(6) Lehn, J.-M. *Angew. Chem.* **1990**, *102*, 1347-1362.

(7) Lehn, J.-M. *Angew. Chem. Int. Ed.* **1990**, *29*, 1304-1319.

(8) Lindsey, J. S. *New J. Chem.* **1991**, *15*, 153-180.

(9) Stang, P. J.; Olenyuk, B. *Acc. Chem. Res.* **1997**, *30*, 502-518.

(10) Krische, M. J.; Lehn, J.-M.; Melendez, R. E.; Carr, A. J.; Linton, B. R.; Hamilton, A. D.; Zimmerman, S. C.; Corbin, P. S.; Kato, T.; Fujita, M. *Molecular Self-Assembly Organic versus Inorganic Approaches*; Springer-Verlag Berlin Heidelberg, 2000; Vol. 96.

(11) Drain, C. M.; Mauzerall, D. *Bioelectrochem. Bioenerg.* **1990**, *24*, 263-266.

(12) Drain, C. M.; Christensen, B.; Mauzerall, D. C. *Proc. Natl. Acad. Sci., USA* **1989**, *86*, 6959-6962.

(13) Drain, C. M. *Proc. Natl. Acad. Sci., USA* **2002**, *99*, 5178-5182.

(14) Drain, C. M.; Smeureanu, G.; Batteas, J.; Patel, S. In *Encyclopedia of Nanoscience and Nanotechnology*; Schwartz, J. A., Contescu, C. I., Putyera, K., Eds.; Marcel Dekker, Inc.: New York, 2004; Vol. 5, p 3481-3502.

(15) Drain, C. M.; Chen., X. In *Encyclopedia of Nanoscience & Nanotechnology*; Nalwa, H. S., Ed.; American Scientific Press: New York, 2004; Vol. 9, p 593-616.

(16) Milic, T.; Garno, J. C.; Smeureanu, G.; Batteas, J. D.; C. M. Drain *Langmuir* **2004**, *20*, 3974-3983.

(17) Milic, T. N.; Chi, N.; Yablon, D. G.; Flynn, G. W.; Batteas, J. D.; Drain, C. M. *Angew. Chem., Int. Ed.* **2002**, *41*, 2117-2119.

(18) Bruce, D. W.; Wali, M. A.; Wang, Q. M. *Chem. Commun.* **1994**, 2089-2090.

(19) Wang, Q. M.; Bruce, D. W. *Angew. Chem. Int. Ed. Engl.* **1997**, *36*, 150-152.

(20) Drain, C. M.; Lehn, J.-M. *Chem. Commun.* **1994**, 2313-2315 (correction 1995, p503).

(21) Drain, C. M.; Russel, K. C.; Lehn, J.-M. *Chem. Commun.* **1996**, 337-338.

(22) Drain, C. M.; Fischer, R.; Nolen, E.; Lehn, J. M. *Chem. Commun.* **1993**, 243-245.

(23) Drain, C. M.; Hupp, J. T.; Suslick, K. S.; Wasielewski, M. R.; Chen, X. *J. Porph. Phthal.* **2002**, *6*, 241-256.

(24) Shmilovits, M.; Diskin-Posner, Y.; Vinodu, M.; Goldberg, I. *Crystal Growth & Design* **2003**, *3*, 855-863.

(25) Latterini, L.; Blossey, R.; Hofkens, J.; Vanoppen, P.; De Schryver, F. C.; Rowan, A. E.; Nolte, R. J. M. *Langmuir* **1999**, *15*, 3582-3588.

(26) Drain, C. M.; Nifiatis, F.; Vasenko, A.; Batteas, J. D. *Angew. Chem. Int. Ed.* **1998**, *37*, 2344-2347.

(27) Slone, R. V.; Hupp, J. T. *Inorg. Chem.* **1997**, *36*, 5422-5423.

(28) Merlau, M. L.; Mejia, M. d. P.; Nguyen, S. T.; Hupp, J. T. *Angew. Chem. Int. Ed.* **2001**, *40*, 4239-4242.

(29) Drain, C. M.; Batteas, J. D.; Flynn, G. W.; Milic, T.; Chi, N.; Yablon, D. G.; Sommers, H. *Proc. Natl. Acad. Sci., USA* **2002**, *99*, 6498-6502.

(30) Liu, G.-Y.; Xu, S.; Qian, Y. *Acc. Chem. Res.* **2000**, *33*, 457-466.

(31) Gong, X.; Milic, T.; Xu, C.; Batteas, J. D.; Drain, C. M. *J. Am. Chem. Soc.* **2002**, *124*, 14290-14291.

(32) Fujita, M.; Kwon, Y. J.; Washizu, S.; Ogura, K. *J. Am. Chem. Soc.* **1994**, *116*, 1151-1152.

(33) Slone, R. V.; Hupp, J. T.; Stern, C. L.; Albrecht-Schmitt, T. E. *Inorg. Chem.* **1996**, *35*, 4096-4097.

(34) Linton, B.; Hamilton, A. D. *Chem. Rev.* **1997**, *97*, 1669-1680.

(35) Yuan, H.; Thomas, L.; Woo, L. K. *Inorg. Chem.* **1995**, *35*, 2808-2817.

(36) Stang, P. J.; Fan, J.; Olenyuk, B. *Chem. Commun.* **1997**, 1453-1454.

(37) Hunter, C. A.; Sanders, J. K. M. *J. Am. Chem. Soc.* **1990**, *112*, 5525-5534.

(38) Chou, J. H.; Nalwa, H. S.; Kosal, M. E.; Rakow, N. A.; Suslick, K. S. *Applications of porphyrins and metalloporphyrins to materials chemistry*; Academic Press: New York, 2000; Vol. 6.

(39) Chambron, J.-C.; Heitz, V.; Sauvage, J.-P. In *The Porphyrin Handbook*; Kadish, K. M., Smith, K. M., Guilard, R., Eds.; Academic Press: New York, 2000; Vol. 6, p 1-42.

(40) Dagani, R. In *C & E News* 1998; Vol. 76 p1-32.

(41) Qi, L.; Colfen, H.; Antonietti, M. *Nano Lett.* **2001**, *1*, 61-65.

(42) Maiti, N. C.; Mazumdar, S.; Periasamy, N. *J. Phys. Chem. B* **1998**, *102*, 1528-1538.

(43) Kano, K.; Minamizono, H.; Kitae, T.; Negi, S. *J. Phys. Chem. A* **1997**, *101*, 6118-6124.

(44) Purrello, R.; Monsu' Scolaro, L.; Bellacchio, E.; Gurrieri, S.; Romeo, A. *Inorg. Chem.* **1998**, *37*, 3647-3648.

(45) Delamarche, E.; Bernard, A.; Schmid, H.; Bietsch, A.; Michel, B.; Biebuyck, H. *J. Am. Chem. Soc.* **1998**, *120*, 500-508.

(46) In *ACS Symp. Ser. 928*; Schubert, U. S., Newkome, G. R., Manners, I., Eds.; American Chemical Society: 2006, p 168-183.

(47) Helt, J. M.; Drain, C. M.; Batteas, J. D. *J. Am. Chem. Soc.* **2004**, *136*, 628-634.

(48) Lindsey, J. S. In *The Porphyrin Handbook*; Kadish, K. M., Smith, K. M., Guilard, R., Eds.; Academic Press: New York, 2000; Vol. 1, p 45-118.

(49) Drain, C. M.; Gong, X. *Chem. Commun.* **1997**, 2117-2118.

Chapter 2

(1) Izquierdo, A.; Ono, S. S.; Voegel, J. C.; Schaaf, P.; Decher, G. *Langmuir* **2005**, *21*, 7558-7567.

(2) Schlenoff, J. B.; Dubas, S. T. *Macromolecules* **2001**, *34*, 592-598.

(3) Maruccio, G.; Cingolania, R.; Rinaldia, R. *J. Mater. Chem.* **2004**, *14*, 542-554.

(4) Wei Zhao, J.-J. X. H.-Y. C. *Electroanalysis* **2006**, *18*, 1737-1748.

(5) Ozin, G. A.; Arsenault, A. C. *Nanochemistry - A Chemical Approach to Nanomaterials*; Royal Society of Chemistry: London, 2005.

(6) Ariga, K.; Hill, J. P.; Ji, Q. *Phys. Chem. Chem. Phys.* **2007**, 2319-2340.

(7) Drain, C. M.; Chen., X. In *Encyclopedia of Nanoscience & Nanotechnology*; Nalwa, H. S., Ed.; American Scientific Press: New York, 2004; Vol. 9, pp 593-616.

(8) Drain, C. M.; Smeureanu, G.; Batteas, J.; Patel, S. In *Dekker Encyclopedia of Nanoscience and Nanotechnology*; Schwartz, J. A., Contescu, C. I., Putyera, K., Eds.; Marcel Dekker, Inc.: New York, 2004; Vol. 5, pp 3481-3502.

(9) Drain, C. M.; Bazzan, G.; Milic, T.; Vinodu, M.; Goeltz, J. C. *Isr. J. Chem.* **2005**, *45*, 255-269.

(10) Drain, C. M.; Goldberg, I.; Sylvain, I.; Falber, A. *Top. Cur. Chem.* **2005**, *245*, 55-88.

(11) Drain, C. M.; Fischer, R.; Nolen, E.; Lehn, J. M. *Chem. Commun.* **1993**, 243-245.

(12) Drain, C. M.; Kirmaier, C.; Medforth, C. J.; Nurco, D. J.; Smith, K. M.; Holten, D. *J. Phys. Chem.* **1996**, *100*, 11984-11993.

(13) Drain, C. M.; Shi, X.; Milic, T.; Nifiatis, F. *Chem. Commun.* **2001**, 287-288 (Adendum 1418).

(14) Shi, X.; Barkigia, K. M.; Fajer, J.; Drain C. M. *J. Org. Chem.* **2001**, *66*, 6513-6522.

(15) Drain, C. M.; Nifiatis, F.; Vasenko, A.; Batteas, J. D. *Angew. Chem., Int. Ed.* **1998**, *37*, 2344-2347.

(16) Drain, C. M.; Lehn, J.-M. *Chem. Commun.* **1994**, 2313-2315 (correction 1995, p503).

(17) Drain, C. M.; Christensen, B.; Mauzerall, D. C. *Proc. Natl. Acad. Sci., U.S.A.* **1989**, *86*, 6959-6962.

(18) Drain, C. M.; Mauzerall, D. C. *Biophys. J.* **1992**, *63*, 1544-1555.

(19) Drain, C. M.; Mauzerall, D. C. *Biophys. J.* **1992**, *63*, 1556-1563.

(20) Yamase, T. *Chem. Rev.* **1998**, *98*, 307-326.

(21) Katsoulis, D. E. *Chem. Rev.* **1998**, *98*, 359-388.

(22) Geletii, Y. V.; Hill, C. L.; Atalla, R. H.; Weinstock, I. A. *J. Am. Chem. Soc.* **2006**, *128*, 17033-17042.

(23) Fang, X.; Hill, C. L. *Angew. Chem. Int. Ed* **2007**, *46*, 3877-3880.

(24) Santos, I. C. M. S.; Rebelo, S. L. H.; Balula, M. S. S.; Martins, R. R. L.; Pereira, M. M. M. S.; Simoes, M. M. Q.; Neves, M. G. P. M. S.; Cavaleiro, J. A. S.; Cavaleiro, A. M. V. *J. Molecular Catalysis A: Chemical* **2005**, *231*, 35-45.

(25) Hagrman, D.; Hagrman, P. J.; Zubieta, J. *Angew. Chem., Int. Ed.* **1999**, *38*, 3165-3168.

(26) Qian, D. J.; Nakamura, C.; Miyake, J. *Chem. Commun.* **2001**, *22*, 2312-2313.

(27) Massari, A. M.; Gurney, R. W.; Wightman, M. D.; Huang, C.-H. K.; Nguyen, S. T.; Hupp, J. T. *Polyhedron* **2003**, *22*, 3065-3072.

(28) Lee, S. J.; Hupp, J. T. *Coord. Chem. Rev.***2006**, *250*, 1710-1723.

(29) Araki, K.; Wagner, M. J.; Wrighton, M. S. *Langmuir* **1996**, *12*, 5393-5398.

(30) Mayer, I.; Nakamura, M.; Toma, H. E.; Araki, K. *Electrochim. Acta* **2006**, *52*, 263-271.

(31) Sun, Y.; Zhang, X.; Sun, C.; Wang, Z.; Shen, J.; Wang, D.; Li, T. *Chem. Commun.* **1996**, 2379-2380.

(32) Jiang, L.; Chang, Q.; Ouyang, Q.; Liu, H.; Wang, Y.; Zhang, X.; Song, Y.; Li, Y. *Che.l Phys.* **2006**, *324*, 556-562.

(33) Jiang, L.; Lu, F.; Li, H.; Chang, Q.; Li, Y.; Liu, H.; Wang, S.; Song, Y.; Cui, G.; Wang, N.; He, X.; Zhu, D. *J. Phys. Chem. B.* **2005**, *109*, 6311-6315.

(34) Huang, M.; Shao, Y.; Sun, X.; Chen, H.; Liu, B.; Dong, S. *Langmuir* **2005**, *21*, 323-329.

(35) Han, B. H.; Manners, I.; Winnik, M. A. *Chem. Mater.* **2005**, *17*, 3160-3171.

(36) Akatsuka, K.; Ebina, Y.; Muramatsu, M.; Sato, T.; Hester, H.; Kumaresan, D.; Schmehl, R. H.; Sasaki, T.; Haga, M. *Langmuir* **2007**, *23*, 6730-6736.

(37) Shen, Y.; Liu, J.; Jiang, J.; Liu, B.; Dong, S. *J. Phys. Chem. B.* **2003**, *107*, 9744-9748.

(38) Shen, Y.; Liu, J.; Jiang, J.; Liu, B.; Dong, S. *Electroanalysis* **2002**, *14*, 1557-1553.

(39) Martel, D.; Gross, M. *J. Solid State Electrochemistry* **2007**, *11*, 421-429.

(40) Xu, L.; Wang, E.; Li, Z.; Kurth, D. G.; Du, X.; Zhang, H.; Qin, C. *New J. Chem.* **2002**, *26*, 782-786.

(41) Pasternack, R. F.; Francesconi, L.; Raff, D.; Spiro, E. *Inorg. Chem.* **1973**, *12*, 2606-2610.

(42) Zhang, C.; Howell, R. C.; Scotland, K. B.; Perez, F. G.; Todaro, L.; Francesconi, L. C. *Inorg. Chem.* **2004**, *43*, 7691-7701.

(43) Helt, J. M.; Drain, C. M.; Bazzan, G. *J. Am. Chem. Soc.* **2006**, *128*, 9371-9377.

(44) Troupis, A.; Hiskia, A.; Papaconstantinou, E. *Applied Catalysis B: Environmental* **2003**, *42*, 305-315.

(45) Milic, T.; Garno, J. C.; Batteas, J. D.; Smeureanu, G; Drain, C. M. *Langmuir* **2004**, *20*, 3974-3983.

(46) Koenig, J.-F.; Martel, D. *Thin Solid Films* **2007**, in press (corrected proof doi:10.1016/j.tsf.2007.07.137).

(47) Rojas, O. J.; Ernstsson, M.; Neuman, R. D.; Claesson, P. M. *J. Phys. Chem. B* **2000**, *104*, 10032-10042.

(48) Radeva, R.; Radeva, T. *Physical Chemistry of Polyelectrolytes;* Marcel Dekker: New York, 2001; Vol. 99.

(49) Ostrovskaya, L.; Perevertailo, V.; Ralchenko, V.; Dementjev, A.; Loginova, O. *Diamond Relat. Mate.* **2002**, *11*, 845-850.

(50) Smay, G. L. *J. Am. Ceram. Soc.* **1988**, *71*, C-217-C-219.

(51) Zhong, Z.; Zhong, Y.; Liu, C.; Yin, S.; Zhang, W.; Shi, D. *Phys. Stat. Sol. (A)* **2003**, *198*, 197-203.

(52) Pasternack, R. F.; Huber, P. R.; Boyd, P.; Engasser, G.; Francesconi, L.; Gibbs, E.; Fasella, P.; Cerio Venturo, G.; Hinds, L. deC. *J. Am. Chem. Soc.* **1972**, *94*, 4511-4517.

Chapter 3

(1) Bazzan, G.; Smith, W.; Francesconi, L. C.; Drain, C. M. *Langmuir* **2008**, *24*, 3244-3249.

(2) Mitzi, D. B. *Chem. Mater.* **2001**, *13*, 3283-3298.

(3) Kutner, W.; Wang, J.; L'Her, M.; Buck, R. P. *Pure & Appl. Chem.* **1998**, *70*, 1301-1318.

(4) In *Multilayer Thin Films: Sequential Assembly of Nanocomposite Materials*; Decher, G., Schlenoff, J. B., Eds.; Wilei-VCH: 2006.

(5) Meunier, B.; Robert, A.; Pratviel, G.; Bernadou, J. in *The Porphyrin Handbook, Vol. 4* (Eds. Kadish, K.M.; Smith, K.M.; Guilard, R.), Academic Press, San Diego, 2000, pp. 119-188.

(6) Akatsuka, K.; Ebina, Y.; Muramatsu, M.; Sato, T.; Hester, H.; Kumaresan, D.; Schmehl, R. H.; Sasaki, T.; Haga, M. *Langmuir* **2007**, *23*, 6730-6736.

(7) Araki, K.; Wagner, M. J.; Wrighton, M. S. *Langmuir* **1996**, *12*, 5393-5398.

(8) Sun, C.; Zhao, J.; Xu, H.; Sun, Y.; Zhang, X.; Shen, J. *Talanta* **1998**, *46*, 15-21.

(9) Sadakane, M.; Steckhan, E. *Chem. Rev.* **1998**, *98*, 219-238.

(10) Dong, S.; Wang, B. *Electrochim. Acta* **1992**, *37*, 11-16.

(11) Keita, B.; Nadjo, L. *J. Electroanal. Chem.* **1988**, *240*, 325-332.

(12) Keita, B.; Nadjo, L. *J. Electroanal. Chem.* **1987**, *217*, 287-304.

(13) Dong, S.; Wang, B. *Electrochim. Acta* **1992**, *37*, 11-16.

(14) Shiu, K.-K.; Anson, F. C. *J. Electroanal. Chem.* **1991**, *309*, 115-129.

(15) Liu, S.; Kurth, D. G.; Bredenkotter, B.; Volkmer, D. *J. Am. Chem. Soc.* **2002**, *124*, 12279-12287.

(16) Liu, S.; Volkme, D.; Kurth, D. G. *J. Cluster Sci.* **2003**, *14*, 405-419.

(17) Wang, Y.; Hu, C. *Thin Solid Films* **2005**, *476*, 84-91.

(18) Shen, Y.; Liu, J.; Jiang, J.; Liu, B.; Dong, S. *Electroanalysis* **2002**, *14*, 1557-1553.

(19) Shen, Y.; Liu, J.; Jiang, J.; Liu, B.; Dong, S. *J. Phys. Chem. B.* **2003**, *107(36)*, 9744-9748.

(20) Neri, B. P.; Wilson, G. S. *Anal. Chem.* **1972**, *44*, 1002-1009.

(21) Laviron, E. *Electroanalytical Chemistry*; Marcel Dekker: New York, 1983; Vol. 12.

(22) Martel, D.; Gross, M. *J. Solid State Electrochem.* **2007**, *11*, 421-429.

(23) Santos, I. C. M. S.; Rebelo, S. L. H.; Balula, M. S. S.; Martins, R. R. L.; Pereira, M. M. M. S.; Simoes, M. M. Q.; Neves, M. G. P. M. S.; Cavaleiro, J. A. S.; Cavaleiro, A. M. V. *J. Mol. Catal. A: Chem.* **2005**, *231*, 35-45.

(24) Ingersoll, D.; Kulesza, P. J.; Faulkener, L. R. *J. Electrochem. Soc.* **1994**, *141*, 140-147.

(25) Cukier, R. I.; Nocera, D. G. *Annu. Rev. Phys. Chem.* **1998**, *49*, 337.

(26) Laurent, D.; Schlenoff, J. B. *Langmuir* **1997**, *13*, 1552-1557.

Chapter 4

(1) *Adv. Mater.* **2004**, *16*, 1245-1377.

(2) Gates, B. D. *Materials Today* **2005**, *8*, 44-49.

(3) Kumar, A.; Whitesides, G. M. *Appl Phys Lett* **1993**, *63*, 2002-2004.

(4) Moran, C. E.; Radloff, C.; Halas, N. J. *Adv. Mater.* **2003**, *15*, 804-807.

(5) Christenson, H. K. *J Phys Chem* **1993**, *97*, 12034-12041.

(6) Xia, Y. N.; Rogers, J. A.; Paul, K. E.; Whitesides, G. M. *Chem Rev* **1999**, *99*, 1823-1848.

(7) Xia, Y.; Whitesides, G. M. *Angew. Chem. Int. Ed.* **1998**, *37*, 550-575.

(8) Zhao, X.-M.; Xia, Y.; Whitesides, G. M. *Adv. Mater.* **1996**, *8*, 837-840.

(9) Kim, E.; Xia, Y. N.; Whitesides, G. M. *Nature* **1995**, *376*, 581-584.

(10) Loo, Y. L.; Willett, R. L.; Baldwin, K. W.; Rogers, J. A. *J. Am. Chem. Soc.* **2002**, *124*, 7654-7655.

(11) Xia, Y.; Whitesides, G. M. *Annu. Rev. Mater. Sci.* **1998**, *28*, 153-84.

(12) Guo, L. J. *J. Phys. D: Appl. Phys.* **2004**, *37*, R123-R141

(13) Liu, G. Y.; Xu, S.; Qian, Y. *Acc. Chem. Res.* **2000**, *33*, 457-466.

(14) Piner, R. D.; Zhu, J.; Xu, F.; Hong, S.; Mirkin, C. A. *Science* **1999**, *283*, 661-663.

(15) Huang, X. D.; Bao, L. R.; Cheng, X.; Guo, L. J.; Pang, S. W.; Yee, A. F. *J. Vac. Sci. Technol. B* **2002**, *20*, 2872-2876.

(16) Salleo, A.; Wong, W. S.; Chabinyc, M. L.; Paul, K. E.; Street, R. A. *Adv. Funct. Mater.* **2005**, *15*, 1105-1110.

(17) Reuther, F.; Kubenz, M.; Schuster, C.; Fink, M.; Vogler, M.; Gruetzner, G.; Grimm, J.; Kaeppel, A. In *Emerging Lithographic Technologies IX*; Mackay, R. S., Ed.; SPIE: San Jose, CA, USA: 2005; Vol. 5751, p pp 976-985.

(18) Kehagias, N.; Zelsmann, M.; Torres, C. M. S. In *Opto-Ireland 2005: Optoelectronics, Photonic Devices, and Optical Networks*; McInerney, J. G., Farrell, G., Denieffe, D. M., Barry, L. P., Gamble, H. S., Hughes, P. J., Moore, A., Eds.; SPIE: Dublin, Ireland: 2005; Vol. Vol. 5825, p pp 654-660.

(19) Bogdanski, N.; Wissen, M.; Ziegler, A.; Scheer, H.-C. *Microelectronic Engineering* **2005**, *78-79*, 598-604.

(20) Zhang, Z.; Wang, Z.; Xing, R.; Han, Y. *Polymer* **2003**, *44*, 3737-3743.

(21) Suh, K. Y.; Langer, R. *Appl. Phys. Lett.* **2003**, *83*, 1668-1670.

(22) Gourdin, S.; Hammond, P.; Crites, T.; Coe, S.; Bulovic, V. In *Materials Research Society Symposium D - Proceedings*; Shur, M. S., Wilson, P. M., Urban, D., Eds.; MRS: 2002; Vol. 736, p pp 271-276.

(23) Meitl, M. A.; Zhu, Z. T.; Lee, K. J.; Nuzzo, R. G.; Rogers, J. A.; Kumar, V.; Adesida, I.; Feng, X.; Huang, Y. Y. *Nat Mater* **2006**, *5*, 33-38.

(24) Rogers, J. A.; Nuzzo, R. G. *Materials Today* **2005**, 50-56.

(25) Nielsen, T.; Pedersen, R. H.; Hansen, O.; Kristensen, A.; Haatainen, T.; Tolkki, A.; Ahopelto, J. In *Technical Digest of the 18th IEEE Conference on Micro Electro Mechanical Systems*; MEMS 2005,: Miami, FL: 2005, p 508-511.

(26) Kee, C. S.; Yoon, K. B.; Choi, C. G. I.; Kim, J. T.; Han, S. P.; Park, S.; Schift, H. J. *Nonlinear Opt. Phys. Mater.* **2005**, *14*, 299-303.

(27) Menard, E.; Bilhaut, L.; Zaumseil, J.; Rogers, J. A. *Langmuir* **2004**, *20*, 6871-6878.

(28) Nilsson, D.; Nielsen, T.; Kristensen, A. *Rev. Sci. Instrum.* **2004**, *75*, 4481-4486.

(29) de Gennes, P. G. *Rev. Mod. Phys.* **1985**, *57*, 827-863.

(30) Ahn, H.; Lee, K. J.; Shim, A.; Rogers, J. A.; Nuzzo, R. G. *Nano Lett.* **2005**, *5*, 2533-2537.

(31) Childs, W. R.; Motala, M. J.; Lee, K. J.; Nuzzo, R. G. *Langmuir* **2005**, *21*, 10096-10105.

(32) Lee, J. Y.; Lee, S. T. *Adv. Mater.* **2004**, *16*, 51-54.

(33) Chin, B. D.; Suh, M. C.; Kim, M. H.; Kang, T. M.; Yang, N. C.; Song, M. W.; Lee, S. T.; Kwon, J. H.; Chung, H. K.; Wolk, M. B.; Bellmann, E.; Baetzoldb, J. P. *J. Information Display* **2003**, *4*, 1-5.

(34) Helt, J. M.; Drain, C. M.; Bazzan, G. *J. Am. Chem. Soc.* **2006**, *128*, 9371-9377.

(35) Ellison, C. J.; Torkelson, J. M. *Nat Mater* **2003**, *2*, 695-700.

(36) Forrest, J. A.; Dalnoki-Veress, K.; Dutcher, J. R. *Physical Review E* **1997**, *56*, 5705.

(37) Forrest, J. A.; Dalnoki-Veress, K.; Stevens, J. R.; Dutcher, J. R. *Phys. Rev. Lett.* **1996**, *77*, 2002–2005.

(38) Fukao, K.; Miyamoto, Y. *Physical Review E* **2000**, *61*, 1743-1754.

(39) Kawana, S.; Jones, R. A. L. *Phys. Rev. E* **2001**, *63*, 021501.

(40) Sharp, J. S.; Teichroeb, J. H.; Forrest, J. A. *Eur. Phys. J. E* **2004**, *15*, 473-487.

(41) Soles, C. L.; Douglas, J. F.; Wu, W. l.; Peng, H.; Gidley, D. W. *Macromolecules* **2004**, *37*, 2890-2900.

(42) Vermaak, J. S.; Kuhlmann-Wilsdorf, D. *J Phys Chem* **1968**, *72*, 4150-4154.

(43) Burkstrand, J. M. *J. Appl. Phys.* **1981**, *52*, 4795-4800.

Chapter 5

(1) Special; Report *Technol. Rev.* **2003**, *106*, 36.

(2) Chou, S. Y.; Krauss, P. R.; Renstrom, P. J. *Science* **1996**, *272*, 85-87.

(3) Stephen Y. Chou, P. R. K. P. J. R. *Appl Phys Lett* **1995**, *67*, 3114-3116.

(4) Michael, D. A.; Haixiong, G.; Wei, W.; Mingtao, L.; Zhaoning, Y.; Wasserman, D.; Lyon, S. A.; Stephen, Y. C. *Appl Phys Lett* **2004**, *84*, 5299-5301.

(5) Dahl-Young, K.; Hong, H. L. *Appl Phys Lett* **1999**, *75*, 2599-2601.

(6) Heyderman, L. J.; Schift, H.; David, C.; Gobrecht, J.; Schweizer, T. *Microelectronic Engineering* **2000**, *54*, 229-245.

(7) Zankovych, S.; Hoffmann, T.; Seekamp, J.; Bruch, J. U.; Torres, C. M. S. *Nanotechnology* **2001**, *12*, 91-95.

(8) Jung, G. Y.; Li, Z.; Wu, W.; Chen, Y.; Olynick, D. L.; Wang, S. Y.; Tong, W. M.; Williams, R. S. *Langmuir* **2005**, *21*, 1158-1161.

(9) Khang, D. Y.; Kang, H.; Kim, T. I.; Lee, H. H. *Nano Lett.* **2004**, *4*, 633-637.

(10) Huang, X. D.; Bao, L. R.; Cheng, X.; Guo, L. J.; Pang, S. W.; Yee, A. F. *J. Vac. Sci. Technol. B* **2002**, *20*, 2872-2876.

(11) Dahl-Young, K.; Hong, H. L. *Appl Phys Lett* **2000**, *76*, 870-872.

(12) Baily, T.; Choi, B. J.; Colburn, M.; Meissl, M.; Shaya, S.; Ekerdt, J. G.; Sreenavasan, S. V. *J. Vac. Sci. Technol. B* **2000**, *18*, 3572-3577.

(13) Menard, E.; Meitl, M. A.; Sun, Y.; Park, J. U.; Shir, D. J. L.; Nam, Y. S.; Jeon, S.; Rogers, J. A. *Chem. Rev.* **2007**, *107*, 1117-1160.

(14) Guo, L. J.; Cheng, X.; Chao, C. Y. *Journal of Modern Optics* **2002**, *49*, 663-673.

(15) Cheng, X.; Hong, Y. T.; Kanicki, J.; Guo, L. J. *J. Vac. Sci. Technol. B* **2002** *20*, 2877-2880.

(16) Austin, M. D.; Chou, S. Y. *Appl Phys Lett* **2002**, *81*, 4431-4433.

(17) Helt, J. M.; Drain, C. M.; Bazzan, G. *J. Am. Chem. Soc.* **2006**, *128*, 9371-9377.

(18) Helt, J. M.; Drain, C. M.; Batteas, J. D. *J. Am. Chem. Soc.* **2004**, *126*, 628-634.

(19) Forrest, J. A.; Dalnoki-Veress, K.; Dutcher, J. R. *Physical Review E* **1997**, *56*, 5705.

(20) Keddie, J. L.; Jones, R. A. L.; Cory, R. A. *Faraday Discuss* **1994**, 219-230.

(21) Rice, R. W.; Sarode, D. V. *Ind. Eng. Chem. Res.* **2001**, *40*, 1872-1878.

(22) Yu, H. Z. *Anal. Chem.* **2001**, *73*, 4743-4747.

(23) *Eur. Phys. J. E* **2002**, *8*, 101-261.

(24) Fryer, D. S.; Nealey, P. F.; de Pablo, J. J. *Macromolecules* **2000**, *33*, 6439-6447.

(25) Ranjeet, S. T.; David, S. F.; Silvia, P.; Martha, F. M.; Juan, J. d. P.; Paul, F. N. *Journal of Chemical Physics* **2001**, *115*, 9982-9990.

(26) Yamamoto, S.; Tsujii, Y.; Fukuda, T. *Macromolecules* **2002**, *35*, 6077-6079.

(27) Fryer, D. S.; Peters, R. D.; Kim, E. J.; Tomaszewski, J. E.; de Pablo, J. J.; Nealey, P. F.; White, C. C.; Wu, W. l. *Macromolecules* **2001**, *34*, 5627-5634.

(28) *Springer Handbook of Nanotechnology*; 1 ed.; Bhushan, B., Ed.; Springer: Berlin, 2004.

(29) Durig, U.; Cross, G.; Despont, M.; Drechsler, U.; Haberle, W.; Lutwyche, M. I.; Rothuizen, H.; Stutz, R.; Widmer, R.; Vettiger, P.; Binnig, G. K.; King, W. P.; Goodson, K. E. *Tribol Lett* **2000**, *9*, 25-32.

(30) DeMaggio, G. B.; Frieze, W. E.; Gidley, D. W.; Zhu, M.; Hristov, H. A.; Yee, A. F. *Phys Rev Lett* **1997**, *78*, 1524-1527.

(31) Fukao, K.; Miyamoto, Y. *Physical Review E* **2000**, *61*, 1743-1754.

(32) Abrams, C. F.; Site, L. D.; Kremer, K. *Physical Review E (Statistical, Nonlinear, and Soft Matter Physics)* **2003**, *67*, 021807.

(33) Soles, C. L.; Douglas, J. F.; Wu, W. l.; Peng, H.; Gidley, D. W. *Macromolecules* **2004**, *37*, 2890-2900.

(34) Araki, K.; Wagner, M. J.; Wrighton, M. S. *Langmuir* **1996**, *12*, 5393-5398.

(35) Beinhoff, M.; Appapillai, A. T.; Underwood, L. D.; Frommer, J. E.; Carter, K. R. *Langmuir* **2006**, *22*, 2411-2414.